Piezoelectric-Based In-Situ Damage Detection of Composite Materials for Structural Health Monitoring Systems

by

Seth Stovack Kessler

S.M. Aeronautics and Astronautics
Massachusetts Institute of Technology, 2/2000

S.B. Aeronautics and Astronautics
Massachusetts Institute of Technology, 6/1998

Submitted to the Department of Aeronautics and Astronautics in Partial Fulfillment of the Requirements for the Degree of

DOCTORATE OF PHILOSOPHY IN AERONAUTICS AND ASTRONAUTICS
AT THE
MASSACHUSETTS INSTITUTE OF TECHNOLOGY
FEBRUARY 2002

Signature of Author……..…….
Department of Aeronautics and Astronautics
Massachusetts Institute of Technology
January 28th, 2002

Certified by……..……...……..
S. Mark Spearing
Associate Professor of Aeronautics and Astronautics
Massachusetts Institute of Technology
Thesis Committee Chairman

Certified by……..…….....
Carlos E. S. Cesnik
Associate Professor of Aerospace Engineering
The University of Michigan
Thesis Committee Member

Certified by……..…….
Mauro J. Atalla
Research Engineer, United Technologies Research Center
Thesis Committee Member

Certified by……..…….
Marthinus van Schoor
President, Midé Technology Corporation
Thesis Committee Member

Accepted by……..…….
Wallace E. Vander Velde
Professor of Aeronautics and Astronautics
Massachusetts Institute of Technology
Chair, Committee on Graduate Students

[This page intentionally left blank]

PIEZOELECTRIC-BASED IN-SITU DAMAGE DETECTION OF COMPOSITE MATERIALS FOR STRUCTURAL HEALTH MONITORING SYSTEMS

by

Seth Stovack Kessler

Submitted to the Department of Aeronautics and Astronautics
on January 28th, 2002 in partial fulfillment of the
requirements for the Degree of Doctorate of Philosophy in
Aeronautics and Astronautics

ABSTRACT

Cost-effective and reliable damage detection is critical for the utilization of composite materials. This thesis presents the conclusions of an analytical and experimental survey of candidate methods for in-situ damage detection in composite materials. Finite element results are presented for the application of modal analysis and Lamb wave techniques to quasi-isotropic graphite/epoxy test specimens containing representative damage. These results were then verified experimentally by using piezoelectric patches as actuators and sensors for both sets of experiments. The passive modal analysis method was reliable for detecting small amounts of global damage in a simple composite structures. By comparison, the active Lamb wave method was sensitive to all types of local damage present between the sensor and actuator, provided useful information about damage presence and severity, and presents the possibility of estimating damage type and location. Analogous experiments were also performed for more complex built-up structures such as sandwich beams, stiffened plates and composite cylinders. These techniques have proven suitable for structural health monitoring applications since they can be applied with low power conformable sensors and can provide useful information about the state of a structure during operation. Piezoelectric patches could also be used as multipurpose sensors to test using a variety of methods such as modal analysis, Lamb wave, acoustic emission and strain based methods simultaneously by altering driving frequencies and sampling rates. Guidelines and recommendations drawn from this research are presented to assist in the design of a structural health monitoring system for a vehicle, and provides a detailed example of a SHM system architecture. These systems will be an important component in future designs of air and spacecraft to increase the feasibility of their missions.

Thesis Supervisor: S. Mark Spearing
Title: Associate Professor of Aeronautics and Astronautics

ACKNOWLEDGMENTS

There are many people I would like to recognize for their help and support with my research. Without them, I would not have been able to accomplish this milestone so quickly with such satisfying results. I would like to thank my advisor Prof. Mark Spearing; he has always believed in my abilities and provided whatever advice and resources necessary for me to accomplish my goals. The rest of my thesis committee, Prof. Carlos Cesnik, Dr. Mauro Atalla and Dr. Tienie van Schoor, each spent countless hours meeting with me to discuss aspects of my research and working revisions of my various publications. While not officially a member of my thesis committee, Prof. Costas Soutis provided as much support as anyone else during the past few years, and added much more meaning to my work.

Next, I would like to acknowledge everyone who provided technical support for this project. Thanks to Al Supple for teaching me almost everything I know about composite manufacturing, and John Kane, Don Weiner for provided invaluable assistance with testing and machining throughout my the project. A special thanks goes to Dave Robertson, who spent much of his free time assisting me with electrical components for my experiments. Prof. Paul Lagace, Prof. John Dugundji and Prof. S.C. Wooh have also provided me with valuable advice.

Many co-workers contributed to this work by helping with research, analysis, writing and providing support. Thank you DJ, Torrey, Chris, Jeremy Mark, Barb and Dennis from TELAC, Erin from GTL, and Kevin, Chris and Dave from AMSL who have given me wonderful advice, inspiration and friendship over the years. A special thanks goes to all of my UROP's: Ricky Watkins, Michelle Park, Joel Torres.

Lastly, I need to thank my loving family—Dad, Mom, Bree and Moira—who have always given me their support. I love you all.

Table of Contents

List of Figures

List of Tables

CHAPTER 1

INTRODUCTION

Structural Health Monitoring (SHM) has been defined in the literature as the "acquisition, validation and analysis of technical data to facilitate life-cycle management decisions." [1] More generally, SHM denotes a system with the ability to detect and interpret adverse "changes" in a structure in order to improve reliability and reduce life-cycle costs. The most fundamental challenge in designing a SHM system is knowing what "changes" to look for and how to identify them. The characteristics of damage in a particular structure plays a key role in defining the architecture of the SHM system. The resulting "changes," or damage signature, will dictate the type of sensors that are required, which in-turn determines the requirements for the rest of the components in the system.

The present research project focuses on the relationship between various sensors and their ability to detect "changes" in a material or structure's behavior. Dozens of sensor types have been cited throughout the literature such as optical fibers, resistive foil gauges and shape memory alloys, which detect damage through a variety of techniques—some more effectively than others. Piezoelectric sensors have become of particular interest in this thesis due to their versatility, conformability, low power consumption and high bandwidth. Several of these sensors and sensing methods will be described in detail in future chapters.

Of all the broad applications for SHM, currently the aerospace industry has one of the highest payoffs since damage can lead to catastrophic (and expensive) failures, and the vehicles

involved undergo regular costly inspections. Currently 27% of an average aircraft's life cycle cost, both for commercial and military vehicles, is spent on inspection and repair; a figure that excludes the opportunity cost associated with the time the aircraft is grounded for scheduled maintenance [2]. These commercial and military vehicles are increasingly using composite materials to take advantage of their excellent specific strength and stiffness properties, fatigue performance, as well their ability to reduce radar cross-section and "part-count". However, composite materials present challenges for design, manufacturing, maintenance and repair over metallic parts since they tend to fail by distributed and interacting damage modes [3, 4]. Furthermore, damage detection in composites is more difficult than in metallic structures due to the anisotropy of the material, the conductivity of the fibers, the insulating properties of the matrix, and the fact that much of the damage often occurs beneath the top surface of the laminate and is therefore not readily detectable (the threshold of detectablity is often termed barely visible impact damage, or BVID). Currently successful composite non-destructive testing (NDT) techniques for small laboratory specimens, such as X-radiographic detection (penetrant enhanced X-ray) and hydro-ultrasonics (C-scan), are impractical for in service inspection of large components and integrated vehicles. Inspection specifications for in-service composite airframes are published by the FAA, however the listed methods such as eddy-current and single-sided ultrasound are expensive, time-consuming and can be unreliable when applied to composites by comparison to techniques used for metals. It is clear that new reliable approaches for damage detection in composites need to be developed to ensure that the total cost of ownership of critical structures does not become a limiting factor for their use.

This thesis explores the use of piezoelectric sensors as a means to detect common forms of damage in graphite/epoxy composite structures. Analytical procedures were used to predict

the effectiveness of various testing methods, and to help design and optimize appropriate testing procedures. Subsequently, these experiments were performed commencing at the narrow coupon level and building up through representative structural elements. The two primary damage detection methods explored in the present research were frequency response methods and Lamb wave techniques. Frequency response methods rely on loss in stiffness in a structure causing a noticeable shift in the natural frequencies and a corresponding change in the normal mode shapes. These methods are easily applied and fairly sensitive to damage, however they are often more practical in detecting global loss of stiffness than localizing the degraded region. Conversely, Lamb waves, which are a traveling elastic perturbation, can detect small regions of local damage by observing the wave speed changing due to differences in stiffness in the damaged zone. The disadvantage of Lamb wave methods is that they require an active driving mechanism to propagate the waves. Acoustic emission and strain-based methods are also considered during the course of this work. The overall goal of this project is to create analytical tools and procedures that are validated by experimentation, in order to make knowledgeable decisions in designing a reliable SHM system for composite structures using piezoelectric sensors.

Chapter 2 of this thesis discusses the history of damage detection in structures, assesses current FAA standard detection practices, and continues to explain the motivations behind incorporating a structural health monitoring system into a vehicle. In Chapter 3, the fundamentals of frequency response methods are described, and analytical, computational and experimental results are presented for the application of these techniques to graphite/epoxy composite laminates. Similarly, Chapter 4 focuses on Lamb wave methods, introducing their derivation, finite element solutions and experimental results on simple coupons and built up

structures. Both of these chapters discuss the role of their respective methods in future designs for structural health monitoring systems. Chapter 5 presents two other means of detecting damage via piezoelectric sensors, and describes experiments performed during the current research with acoustic emission and strain monitoring methods using PZT piezoceramic sensors. The cumulative knowledge generated by the previous chapters is then connected in Chapter 6, which discusses the components of a structural health monitoring system, and then makes recommendations and provides trade studies to assist in designing a successful in-situ damage detection system. Finally Chapter 7 provides a summary of the work performed, along with recommendations for future work in developing SHM systems for composite structures.

Chapter 2

BACKGROUND

This chapter presents a survey of damage detection methods for composite materials. Composite materials are gaining acceptance and demand in several commercial markets including sporting goods, construction and transportation. For many of these applications however, such as aircraft, without a reliable damage detection approach, the total cost of ownership may become a limiting factor for the structure's use. Several non-destructive evaluation techniques are compared on the basis of their strengths and weaknesses for in-service testing of composite materials. Current inspection regulations and practices for composite components in commercial aircraft are also presented. This chapter concludes with a discussion of the motivations behind implementing a structural health monitoring system, and background for various applications presented in the literature.

2.1 Non-Destructive Evaluation (NDE) in Composite Materials

There are several inherent difficulties in detecting damage in composite materials as opposed to traditional engineering materials such as metals or plastics. One reason is due to its inhomogeneity and anisotropy; most metals and plastics are formed by one type of uniformly isotropic material with very well known properties. Laminated composite materials on the other hand can have a widely varying set of material properties based on the chosen fibers, matrix and

manufacturing process. This makes modeling composites complex, and often non-linear. Another obstacle to many detection techniques is the fact that composites are often a mix between materials with widely differing properties, such as a very good conducting fiber in an insulating matrix. A last difficulty is that damage in composite materials often occurs below the surface, which further prevents the implementation of several detection methods. The importance of damage detection for composite structures is often accentuated over that of metallic or plastic structures because of their load bearing requirements. Typically unreinforced plastics are not used in load critical members; since their properties are predictable and are usually simple and inexpensive to manufacture, they are often designed to be replaceable safe-life parts. Similarly, metals are generally well understood and easy to model, thus they are frequently designed using damage tolerant methodologies. The behavior of composite material on the other hand is much less well understood, and an unexpected failure of the composite part could prove catastrophic to a vehicle. These materials are still often used in many structures however, mostly for applications where high specific strength and stiffness are required. Therefore, the development of reliable damage detection methods is critical to maintain the integrity of these vehicles. The following sections provide descriptions of various non-destructive techniques that have been developed for the detection of damage in composite materials [5].

2.1.1 Visual inspection methods

Perhaps the most natural form of evaluating composite materials is by visual inspection [6]. Several variants of this method exist at various levels of sophistication from the use of a static optical or scanning electron microscope to optical examination by eye over the structure.

While microscopy can be a useful method to obtain detailed information such as micro-crack counting or delamination area, it can only be used in the laboratory since a section must be removed from the larger structure. Visual inspection of a vehicle is perhaps the simplest and least expensive method described in this section, however often damage in composite materials occurs below the surface, so it is not easy to identify by the unassisted eye. Also, the eye alone can determine little detail about the damage mechanism or its severity. While this method can potentially provide some useful data for damage detection, on a large-scale structure this process would prove inefficient and ineffective.

2.1.2 X-radiography methods

X-radiographic techniques rely on recording the difference in x-ray absorption rates through the surface of a structure. These methods can be implemented in real-time digitally, or by taking static radiographs, whereas areas of different permeability or density are differentiated by the magnitude of x-ray exposure to the media on the opposite side of the surface after a predetermined excitation time. To accentuate damaged regions with cracks or delamination, often a liquid penatrant is applied to the area to be examined. While these techniques are relatively inexpensive and simple to implement and interpret, they require large and costly equipment that is difficult to use on large structural components without removing them from the vehicle. The greatest challenge to using x-radiography in a vehicle application however, is that all of these methods require access to both sides of the surface in order to emit and collect the X-ray radiation, which is often not practical.

2.1.3 Strain gauge methods

Strain gauge methods are perhaps currently the most common way to monitor damage in composite materials on in-service vehicles [7]. A voltage applied across a foil gauge is capable of measuring strain by the change in resistance due to deformation. These devices are relatively small, light and inexpensive making them simple to implement, and their results are easily interpreted. They are capable of monitoring local strain to detect time-history overloads and deformations. A disadvantage to this technique is that the results from a single gauge can only cover a small area of the surface accurately, so a large quantity of them would be necessary to monitor an entire vehicle, yielding a complex system with many wires. In order to avoid this situation the gauges can only be placed in a few select predicted problem areas.

2.1.4 Optical fiber methods

In order to cover more area on a structure for strain measurement, another technique that has evolved is the use of embedded small-diameter optical fibers, which can be multiplexed to record measurements over large regions [8]. A comprehensive collection of distributed optical fiber sensing can be found in a review article by Rogers [9]. In using this method of detection, pulses of polarized laser light are transmitted along an optical fiber, and gratings are placed in various locations to reflect a portion of the light at a certain wavelength. By recording the time of flight of the beam, the length of that segment of fiber can be easily deduced; if a strain has been applied to that segment of fiber, the time of flight would change. Active areas of research in optical fiber techniques include analytical modeling of the fibers for predictive purposes, experimentally determining the effects of the finite diameters of these fibers, and the

manufacturing issues of producing small diameter fiber and bonding optical fibers into composite materials and sandwich structures [10-16]. Opponents of optical fiber methods claim that there is a large shear-lag effect due to the cladding, coating and adhesion layers surrounding the optical core that makes it impossible to take accurate measurements, and furthermore that these fibers introduce weak points in a laminate as potential crack and delamination initiation sites [17]. Regardless, optical fibers are still widely used for large civil structure applications since they can be easily multiplexed over long distance.[14].

2.1.5 Ultrasonic methods

Another commonly implemented NDE technique is ultrasonic testing, most often referred to as A, B and C-scans. These tests are usually conducted with two coupled water-jet heads moving in tandem on either side of the specimen surface, sending ultrasonic waves through the water stream on one side, and collecting the transmitted acoustic waves on the opposite side. An A-scan refers to a single point measurement of density, a B-scan measures these variations along a single line, and a C-scan is a collection of B-scans forming a surface contour plot. The C-scan has been common practice in the aerospace industry since the introduction of composite parts to this field, since its results are widely understood and can be used to scan a large area of structure in a relatively short time period. Typically water is used as a couplant, however newer non-contact techniques have been attempted that use air as a couplant, which have not been able to achieve as accurate results. Beyond the size and cost of the equipment, there also is the problem that access is required to both sides of the structure, so parts must often be disassembled for testing. Single-sided ultrasonic reflective methods are in development to remedy this problem, however the quality of their results is still not acceptable for inspection purposes.

2.1.6 Eddy current methods

The use of eddy-currents is another valuable strain-based technique for metallic structures. These methods are the second most commonly used for in-service vehicle inspection next to ultrasonic methods. Eddy currents methods function by detecting changes in electromagnetic impedance due to strain in the material [18]. Much work has been recently done at MIT, JENTEK Sensors Inc., and General Dynamics in this field, sensing strains and cracks in short specimens and around holes with conformable sensors. This field is not as mature for composite materials as it is for metals however, due to the insulative properties of the epoxy matrix [19-26]. Eddy-current methods are often used because they are simple to implement and do not require much equipment, however their disadvantage is they require large amounts of power and that the data they produce is among the most complicated to interpret, and the analysis involves solutions of an elaborate inverse problem to deduce the presence of damage.

2.1.7 Vibration-based methods

Most vibration-based damage detection techniques for composite materials have focused on modal response. Structures can be excited by ambient energy, an external shaker, or embedded actuators, and the dynamic response is then recorded. Embedded strain gauges or accelerometers can be used to calculate the resonant frequencies. Changes in normal modes can be correlated with loss of stiffness in a structure, and usually analytical models or response-history tables are used to predict the corresponding location of damage. These methods are implemented easily within existing infrastructure of a vehicle at a low cost, however the data

they produce can be complicated to interpret. This technique holds much potential for NDE within composite materials, and will be presented in further depth in Chapter 3. Another popular vibration measurement technique in composites is acoustic emission (AE). Changes in material properties can be deduced using resonant beam sensors, accelerometers, piezoelectrics, or microphones to record energy being released by matrix cracking or fibers fracturing [27, 28]. This method has the advantage of being able to use an array of multiple sensors to triangulate the location of damage by the signal time of flight [29]. Recent advances in this field include the development of micro-electro-mechanical systems (MEMS) technology to manufacture extremely small, inexpensive, conformable and accurate AE sensors that are embeddable in composite materials [30-32]. Again, the data from this method can be complicated to interpret, but holds much potentially useful information for the detection of damage in composite materials. Acoustic emission techniques employing piezoelectric sensors will be discussed further in Chapter 5.

Active variants of vibration methods exist that use embedded or surface mounted actuators to excite a structure ultrasonically to produce various types of elastic waves which propagate over large distances, and complementary embedded sensors to detect reflected and transmitted waves [33]. Examples of these include Rayleigh waves in thick structures, shear (SH) waves and Lamb waves. Lamb waves have been found to be particularly effective in detecting the presence and location of damage in composite materials, with all the same advantages of the previously mentioned vibration techniques of small and lightweight sensors, as well as the disadvantage of complicated results. The use of Lamb wave methods and the interpretation of their data will be explored in Chapter 4 of this thesis [34].

2.1.8 Other methods

Another technique that has been investigated for NDE is the concept of "smart-tagged" composites. Using this method, either the matrix of the composite material is magnetically doped to measure the induced electro-magnetic field due to deformation, or alternatively the resistance of the fibers can be measured [35]. This technique is challenging to implement and interpret, and thus is currently not very well understood. A creative method that has been developed for mechanically-fastened joints, is the "smart-bolt" concept, which uses phase-changing bolts to create a magnetic field in regions that have been overloaded [36]. Several variants of this method are under development at various companies and universities that use surface mounted magnetostrictive and magnetoelastic sensor to measure over-stresses and strains in composite materials [37-40]. Still, there are several other more exotic methods that are being explored, which use creative means such as triboluminescent materials that give off light when they are strained, measure the resistance of thermoplastic films, and use optical surface reflection techniques [41-46]. All of these techniques have exhibited much potential for detecting specific types of damage in composite materials, however none of them are mature enough to be used for inspection currently. Most likely a combination of several types of the methods described in this section would have to be used to capture arbitrary forms of damage successfully in composite materials, expounding on both their strength and weaknesses.

2.2 Current Inspection Regulations and Practices

There are several documents issued by the Federal Aviation Administration (FAA) that regulate how aircraft may be design and inspected. The FAR 25 lists the acceptable engineering

design criteria for the damage tolerant design of an aircraft, which will be discussed further in the SHM motivation section [47]. The Code of Federal Regulations (CFR) Title 14 Part 145 requires that all maintenance be performed using methods prescribed by Advisory Circular (AC) 43.13-1B [48]. The certified techniques include visual inspection, liquid penetrant inspection, magnetic particle inspection, eddy current inspection, ultrasonic inspection, radiography, acoustic emission, and thermography. For each of these methods, a section is written in the AC that specifies the accepted procedure for each of these methods, along with detailed diagrams, checklists and reporting formats. For each certified commercial aircraft, an Aircraft Maintenance Manual (AMM) is created by the manufacturer in conjunction with the FAA CFR Title 14 Part 39 that lists each component to be inspected, the inspection interval, the type of damage to be concerned about, and the suggested methods to be used for the inspection.

One example is the airworthiness directive for the Boeing model 747 series airplanes, 14-CFR-39-9807. It specifies an inspection to detect disbonding, corrosion or cracking on a specific fuselage skin panel to be performed prior to the accumulation of 2,000 total flight cycles using liquid penetrant, magnetic particle or eddy current inspection techniques, and then repeated inspections every subsequent 150 flight cycles [48]. Similar instructions can be found in this extensive document for each component to be inspected in that family of aircraft, often grouping parts that have the same requirements. For most composite components in commercial applications, currently only visual inspections are required. The aircraft is designed to be able to survive with any invisible damage, and there is a condition that such damage not grow over the period of two inspection intervals as determined by an instrumented coin tap test. For the planned Airbus A3XX, it has been reported in the literature that the design service goal is 24,000 flights, with general visual inspections every 24 months, and a detailed tear-down inspection for

crack and corrosion via ultrasonic and eddy current techniques every 6,000 flights after the first 12,000 flights [49]. While an A3XX under traditional practice would not undergo a thorough inspection in the first half of its expected life, one using a SHM system would be constantly monitored without interruption of service. This would enable the operator to discover premature damage that could potentially lead to failure, which may have been overlooked during a visual inspection. It could also reduce the lifecycle cost by allowing the vehicle to safely exceed its original design life. While there is currently no specific provision in any of the published directives for a structural health monitoring system, one could be implemented under the current regulations since it still could use the same sensing methods such as ultrasonic or eddy current-based methods; the SHM system would just monitor the vehicle more frequently. Other motivations for implementing a SHM system will be presented in the following section.

2.3 Structural Health Monitoring

Structural health monitoring essentially involves the embedding of an NDE system (or a set of NDE systems) into a structure to allow continuous remote monitoring for damage. There are several advantages to using a SHM system over traditional inspection cycles, which are presented in the following motivation section. A variety of SHM systems have been implemented in many industries, ranging from industrial machinery to spacecraft. Some of these systems are executed in-situ, such as with rotor bearings on gas turbine generators which are constantly monitored for changes in their characteristic frequencies, and others collect data for post-operation processing such as with black boxes on commercial airplanes. As companies strive to lower their operational costs, many of these SHM systems have been developed for use on particular systems. Several universities and research institutes have also attempted to devise

strategies for generic SHM systems for a wide range of applications. This section also provides an account of currently implemented SHM systems that are described in the literature.

2.3.1 Motivations for SHM

Structural health monitoring is an emerging technology lending to the development of systems capable of continuously monitoring structures for damage with minimal human intervention [7]. The goals of SHM systems are to improve reliability and safety while reducing maintenance costs, to minimize the overall cost of ownership of a vehicle. There are several components required to design a successful and robust SHM system, which include sensor power systems, communications and algorithms to interpret the large amounts of data. This thesis focuses on the sensors and sensing techniques used to detect the damage, a component which is crucial to the flow down of requirements to the development of the rest of the SHM system; an overview of the other essential components will be described in Chapter 6. The purpose of this section is to demonstrate the economic and structural integrity motivations for structural health monitoring.

When a new vehicle is built, the choice of the design methodology is what drives the inspection requirement of the components. There are three major methodologies currently employed for aerospace vehicle design: safe-life, damage tolerant, and condition-based maintenance. Each of the three methods offers structural and financial benefits as well as carrying potential shortcomings. Safe-life design was adopted in early vehicle design, and used a statistical approach to predict the operational life of a component that would then be replaced, eliminating the need for inspection. Currently, most vehicles are designed using the damage tolerant approach, which uses models to predict the critical flaw size for a component, and then

set inspection intervals based upon that prediction to detect and repair the part prior to failure. This method has suited the aerospace industry for many years to detect damage reliably, however the frequent and elaborate inspection cycles are inefficient. The suggested approach for future vehicles has been condition-based maintenance, which possess the advantages of both the methods mentioned previously. By using an in-situ structural health monitoring system to continuously monitor the structure, components would remain in operation without regularly scheduled maintenance until the SHM system reported that a repair was necessary, at which point it would be serviced. This section further describes the advantages and disadvantages of each of these design methodologies, and then provides the economic benefits of introducing a condition-based maintenance system along with a SHM system.

The safe-life approach was an early design methodology for aircraft components proposed by Miner in 1945 [50]. In this approach to design, components are analyzed and tested on the basis of a typical in-service cyclic load spectra, and a fatigue life is then estimated. This life is then modified by a factor of safety, usually between 2 and 4, to ensure a "safe-life" of operation at which point the part is then retired [51]. Advantages of safe-life methodology include a very simple model to design from after testing, and reduction in inspection time and costs. This second point is especially important in the case where a component is difficult to access for inspection, or particularly challenging to repair, as it is often the case with composites. The disadvantages of safe-life however, are that there is no provision to ensure that a good part is not discarded, and the components designed by this method generally have weight and cost penalties due to the relatively arbitrary factor of safety [52]. Also, by the nature of safe-life design, it is not possible to furnish a measure of quantitative safety. There can be a large difference in median and minimum life values, as seen in several examples in the literature,

which bring into question whether median life S-N curves are appropriate for design applications [50, 53-57].

One paper in the literature relays how in a study by Jacoby, the predicted lives of 100 out of 300 different types of structures erred on the non-conservative side, and data from the American Helicopter Society showed scatter in fatigue life of one common component ranged from 9 to 2,600 hours [50]. A second example is found as a case study in a fatigue textbook to illustrate the benefits of switching from a safe-life design to a damage-tolerant one [51]. The study focused on USAF gas turbine disks, where it was estimated that only 1 out of every 1000 disks that were retired actually had a significant crack in it. It was shown that for the F100 engine, by using eddy current monitoring at regular intervals to test the integrity of the disks instead of discarding them, up to $1.7 billion could be saved in the course of 20 years. Based on extensive studies of service history, the safe-life methodology has been proven a safe approach for fatigue design in rotating components however. While almost all fixed-wing craft in the past 20 years have been designed according to damage-tolerant criteria, most current rotorcraft still use safe-life components, which has been successful due to the accountable and repeatable loads seen by these rotating components [58]. This trend is changing now however, as helicopter manufacturers aim to achieve better weight and cost margins, by spending more time designing more accurate models for damage-tolerant designs [52].

For the reasons presented above, most of the aerospace community has determined it is more economically efficient and structurally deterministic to rely on a damage-tolerant design approach. In fact, according to the FAA requirements in FAR/JAR 25.571, now only landing gear and engine components can be designed using safe-life [47, 49, 59]. Damage-tolerant design is based on the principle that through operation cycles the strength of the material in an

airplane degrades over time, so inspection intervals should be specified to be able to recognize and repair this damage before it becomes critical. The basic requirements state that the critical areas on the aircraft structure must be identified and verified to be able to survive the applicable loading spectra and environmental conditions through a series of analyses and tests. Prior data from similar aircraft are admissible as long as the differentiating characteristics between the aircraft are investigated. An appropriate inspection schedule must then be specified to ensure a damage tolerant design; this usually is chosen as half the time it would take the largest crack previously detected or, in the case that no damage has been found, the largest crack that cannot be detected to grow to its critical length. The only other major requirement is for the structure to be reasonably survivable (i.e. to be able to complete the remainder of the current flight cycle) after suffering a bird or fan blade strike. Several papers can also be found in the literature that specifically address the requirement of composites as specified in AC 20-107a [60-62]. Aside from the original requirements, these documents specify that a composite structure must measure the residual strength at several points, post-damage, to determine its damage tolerant characteristics. They also state that if the laminate is thought to be fatigue resistant, a no-growth validation must be performed up to a statistically significant portion of the anticipated number of usage cycles. There is a window of opportunity to inspect for cracks in metallic structures prior to catastrophic failure between where a crack becomes measurable and where it grows to its critical size, however even though composites require much longer inspection intervals, an impact event in a composite laminate can reduce its residual strength instantaneously to a value below its design strength [60].

To further improve upon the benefits gained from a traditional damage-tolerant design, several papers in the literature have claimed as much as a 25-33% decrease in total life costs by

using continuous condition-based maintenance methodologies [63-65]. Using this methodology, instead of setting a regular inspection and maintenance interval, the structure would be continuously monitored allowing the aircraft to forgo predetermined regular inspections intervals traditionally required by a damage-tolerant design. Condition-based maintenance combines many of the advantages of the safe-life design principles with those of damage-tolerant design, in that the structure is relied upon in service for much longer using predictive models, however there still are provisions for maintenance and repair when needed. The disadvantage of this method is that the reliability of the structure is now dependant on the accuracy and accountability of the monitoring system. This is where the need for dependable structural health monitoring systems is introduced. Once research has been performed that thoroughly demonstrates the performance of various SHM system configurations for certain materials, these systems can be implemented on aircraft and other structures to replace regularly scheduled overhauls and inspection cycles, and only repair parts when needed. Not only does drastically reducing or altogether eliminating regular inspections save expense, but there is much opportunity cost gained in being able to operate the vehicle when it would have been otherwise detained for scheduled inspections. Many of these inspections involve the tear-down of larger components, and can take more than a day before the plane is back in service. Needless to say, there is additionally the potential of a huge investment cost savings if the SHM system can detect damage before a catastrophic failure in time to salvage it.

Current commercial aircraft are designed for at least 20-25 years of service and up to 90,000 flights (75,000 flights for 737's, 20,000 flights for 747's, and 50,000 flights for 757 and 767's), while future designs are sure to require at least this endurance [49]. In recent years, the average major airline has spent 12% of its total operating expenses on maintenance and

inspection amounting to an industry total of almost $9 billion a year [66]. For smaller and regional airlines this percentage averages nearly 20% a year totaling almost another $1 billion in costs. Using these figures, a FAA requirement to implement SHM system with a condition-based maintenance philosophy has the potential of saving the airline industry alone $2.5-3 billion a year. To be able to use these systems with confidence though, much more research still needs to be performed to assess the capabilities of SHM systems to facilitate the inspection reliably, analysis and interpretation of the physical condition of critical structural components. This thesis is a piece of the developmental puzzle needed to validate the true potential of SHM systems. It presents a thorough overview of several candidate sensors and sensing techniques, as well as how they would be implemented in a SHM system, and proceeds to describe their limitations in certain materials as well. The requirements of other components of a SHM system are also described, along with potential system level schemes and design principles for a successful structural health monitoring to be used for composite materials.

2.3.2 General SHM applications

In recent years, several attempts have been made to implement SHM systems in operation applications. While some effort has been placed towards infrastructure and civil engineering applications such as bridges and highways, aerospace structures have one of the highest payoffs for SHM applications, and thus most of the examples found in the literature deal with the implementation of SHM strategies in air and space-craft. New military fighter-craft such as the Eurofighter, the Joint Strike Fighter and the F-22 all incorporate Health Usage Monitoring Systems (HUMS), which record peak stress, strain and acceleration experienced in key components of the vehicle [67]. While these systems do continuously and autonomously

monitor the condition of various components of these vehicles, they are essentially extensions of the "black-box" in that their data is not used to make decisions during normal operation and typically would only be accessed during a scheduled inspection or after a crash.

Several papers in the literature have proposed SHM strategies for aerospace applications, however the trend in these papers has been to elaborate on the damage detection mechanism and they neglect to describe how it would be applied to a vehicle in flight or define the other components of the system. In a collection of papers written by Zimmerman, he suggests that an algorithmic approach could be used to enhance the model correlation and health monitoring capabilities using frequency response methods [68]. Minimum rank perturbation theory is used to address the problem of incomplete measurements in collecting data in a SHM system. This is a problem that is often overlooked by researchers studying frequency response techniques, that a true structure does not conform to ideal conditions, and data can be missing from measurements taken which must be replaced using probabilistic theories along with models. Other researchers have developed algorithms to attempt to correlate modal response under arbitrary excitation to models using a probabilistic sub-space based approach [69]. Again, these are crucial considerations for the implementation of frequency response in a SHM system. A few papers in the literature have been dedicated to the use of Lamb waves in SHM systems. Giurgiutiu used Lamb wave techniques to compare changes in thin aluminum aircraft skins after various levels of usage to detect changes, and used finite element techniques to attempt to predict the level of damage with some success [33]. More detailed work was done by Cawley's group at Imperial College, who used Lamb waves to experimentally examine representative metallic aircraft components such as lap joints, painted sections and tapered thickness [70]. The paper concludes that these methods present good sensitivity to localized damage sites, however the responses are

often complicated to interpret, and many limitations exist for the implementation of these methods over large areas.

Two techniques that have been realized in flight vehicles are acoustic emission and eddy current methods. Honeywell and NASA have been working in a collaborative project since the mid-1990's to introduce an acoustic emission-based SHM system into critical military aircraft components [71, 72]. This program, which involved the monitoring of T-38 and F/A-18 bulkheads, is one of the most thorough examples of a SHM system to date. Beyond the development of their sensing technique, they also worked on the other hardware components necessary for on-board processing and communication, as well as vehicle conformity issues. These experiments were able to demonstrate successfully the collection of fatigue data and triangulation of some cracks from metallic components while in flight, which could then be analyzed post-flight to make decisions about flight-readiness. In another program Northrop had similar success using AE to monitor small aircraft, and presented a paper in the literature discussing the limitations of these methods for on-line testing [29]. They suggested using between 100 and 1000 sensors to implement this system in a larger aircraft depending on whether the entire structure is being monitored or just critical components. Lastly, work has been done by Jentek Sensor in the implementation of conformable eddy current sensors to the monitoring of aerospace vehicles [19, 73]. Their technology has proven successful for the monitoring of fatigue growth in metallic components such as gas turbine engine blades and aircraft propellers. Damage is detected by solving the inverse problem for the material properties based upon the electrical conductivity and complex permeability captured by meandering winding magnetometers.

2.3.3 SHM in composite structures

The progression of SHM systems within composite structures has virtually paralleled that of metallic structures since these technologies have only recently begun to be implemented. The additional complexity introduced by composite materials is in the fact that the materials are not homogeneous or isotropic, so many of the analytical models previously produced are difficult to use. In Zou's review of frequency response methods for damage identification in composite structures, several analytical procedures are described that attempt to model the response of composite materials to damage in various frequency spectra [74]. One particularly successful method used by Zhang is the introduction of transmittance functions to correlate modal data with a database of finite element solutions for a composite structure [75]. Recently, Boeing has been exploring the use of frequency response methods in SHM systems for composite helicopter blades [76]. Their system, which is called Active Damage Interrogation (ADI), uses piezoelectric actuators and sensors in various patterns to produce transfer functions in components that are compared to baseline "healthy" transfer functions to detect damage. While this system is incapable of locating specific areas of damage, it has been proven effective for monitoring the development of progressive damage in small composite components.

The use of Lamb waves for SHM of composites has been proposed in many papers in the literature. These methods are at a much less mature stage than frequency response methods in terms of real life applications, however in recent years attention has been given to key factors of their implementation. A few researchers have pursued analytical methods for the evaluation of the data received by Lamb wave techniques, most of which have focused on wavelet decomposition or time of flight comparison using finite element techniques [77-79]. Other important preliminary experimentation has been performed by ONERA to evaluate the effects of

testing composite sandwich structures, however their results published to date have proven inclusive [80]. Lastly, much work has been done by Soutis's group at Imperial College to investigate the effects of finite width on Lamb wave propagation experimentally, and attempt to use these techniques to calculate the size, depth and location of delaminations [81, 82]. However, to date no Lamb wave research in the literature has demonstrated their use in conjunction with other SHM components or on an operational structure.

2.3.4 Goals for SHM

As explained in the previous motivation section, the primary goal of SHM is to be able to replace current inspection cycles with a continuously monitoring system. This would reduce the downtime of the vehicle, and increase the probability of damage detection prior to catastrophic failure. The remainder of this section presented the current state of SHM within the aerospace industry. Several parts of SHM systems have been developed and tested successfully, however much work remains before these systems can be implemented reliably in an operational vehicle. The present research attempts to fill some of the gaps remaining in SHM technologies. NDE techniques with the highest likelihood of success were thoroughly examined, including frequency response methods in Chapter 3, Lamb wave methods in Chapter 4, and acoustic emission and strain monitoring methods in Chapter 5. For each of these methods, an analytical and experimental procedure was followed to optimize the testing parameters and data interpretation. Their strength, limitations and SHM implementation potential were evaluated, and suggested roles for each are presented. The requirement of the other components necessary in an SHM system are described in Chapter 6, and recommendations are offered for a structural health monitoring system architecture based on the results presented in this thesis.

Chapter 3

FREQUENCY RESPONSE METHODS

In this chapter, experimental results are presented for the application of modal analysis techniques applied to graphite/epoxy specimens containing representative damage modes. The specimens were excited using a piezoelectric patch, and changes in natural frequencies and modes were found by comparing the structures' responses using a scanning laser vibrometer. Finite element models were created using 2-D shell elements for comparison with these experimental results, which accurately predicted the response of the specimens at low frequencies, but coalescence of higher frequency modes makes mode-dependent damage detection difficult for structural applications. The frequency response method was found to be reliable for detecting even small amounts of damage in a simple composite structure, however the potentially important information about damage type, size, location and orientation were lost using this method since several combinations of these variables can yield identical response signatures.

3.1 Background

Several techniques have been researched for detecting damage in composite materials, many of them focusing on modal response [83-88]. These methods are among the earliest and most common, principally because they are simple to implement on any size structure. Structures can be excited by ambient energy, an external shaker or embedded actuators, and

embedded strain gauges or accelerometers can be used to monitor the structural dynamic responses [89-99]. Changes in normal vibrational modes can be correlated to loss of stiffness in a structure, and usually analytical models or experimentally determined response-history tables are used to predict the corresponding location of damage [74]. The difficulty, however, comes in the interpretation of the data collected by this type of system. There are also detection limitations imposed by the resolution and range of the individual sensors chosen, and the density with which they are distributed over the structure. There have been many different approaches described in the literature that use modal evaluation techniques to locate damage in everything from small specimens to full components. The two major categories that will be described in detail in the following sections are model-dependent and model-independent methods.

3.1.1 Model-based frequency response methods

One of the most thorough reports on frequency response methods can be found in a recently published paper by Zou *et al*. [74], which presents a review of vibration-based techniques that rely on models for identification of delamination in composite structures. The authors suggest that model-dependent methods are capable of providing both global and local damage information, as well as being cost-effective and easily operated. All of the methods they assessed use piezoelectric sensor and actuators along with finite element analysis results to locate and estimate damage events by comparing changes in dynamic responses. The paper compares the merits of four different dynamic response parameters: modal analysis, frequency domain, time domain and impedance domain. Modal analysis-based methods utilize input from several modal parameters including frequency, mode shape and damping ratio to detect damage. Frequency domain techniques attempt to detect damage by only using the frequency response of

the structure. In using time domain methods, damage is estimated by using time histories of inputs and their vibration responses. Lastly, impedance domain techniques use changes in electrical impedance to measure damage in the structure. The authors recommended modal analysis methods on account of their global nature, low cost, and flexibility to select measurement points, however they indicated that they lack the ability to localize damage and require large data storage capacity for comparisons. They claimed that frequency domain methods alone were incapable of detecting the location of damage, however when combined with time domain methods they can detect damage events both globally and locally. Lastly, the impedance domain techniques were described as suitable for detecting most delaminations reliably, unless the layers above the defect are very thin compared to the remaining laminate.

Several other papers have documented the use of a combination of the modal analysis and frequency domain methods to detect various damage types with piezoelectric actuators and sensors coupled with finite element or analytical models. Banks and Emeric [100] investigated changes in particular modes up to 1 kHz using the Galerkin method on cantilevered aluminum beams with notches, and a similar experiment was performed by Mitchell *et al.* [101] to detect changes in the first mode of a specimen. In addition they demonstrated wireless data transfer. One of the few examples in the literature of damage detection in a more complicated geometry was investigated by Purekar and Pines [102], who used this technique to search for delamination in composite rotorcraft flexbeams. Again, finite element models were built to help locate the sources of experimental changes in the transfer functions of their specimens.

3.1.2 Model independent frequency response methods

Zhang *et al*. [75] investigated the use of transmittance functions for health monitoring, a technique which does not require the use of analytical models. A system of piezoelectric patches were placed on a structure, where some were used as sensors and others as actuators, and responses at certain sensor locations due to broadband actuation were recorded for the healthy structure to be later compared to a potentially damaged structure. Changes in curvature were used in this case to detect, locate and assess damage to the structure. One significant finding was that the optimal frequency range to actuate their structure was between 10-20 kHz, however they found that only frequencies less than 5 kHz (200-1800 Hz in most cases) were practical to collect experimental data. Lastly, Valdes and Soutis [103] detected delamination in composite laminates using piezoceramic patches and piezoelectric film sensors, again without the use of models. Frequency sweeps between 8-14 kHz were used to induce vibrations on the structure, and clear reductions in modal frequencies were found as the delamination area in the test specimen was increased.

The present research investigates the feasibility of modal evaluation techniques in detecting damage for health monitoring of composite structures. Characteristics examined include these methods' ability to detect various types of damage, their precision in determining the damage location, and their sensitivity to sensor density. Conformability, or the ability of a sensing system to be integrated easily into an existing vehicle's structure and infrastructure, is also assessed. A similar procedure is followed by several of the papers presented above to evaluate these methods. Finite element models were created to predict the natural frequencies of simple narrow coupons with various forms of damage, and to perform trade-studies to evaluate the efficiency and utility of model-dependent versus model-independent methods. Subsequently,

experiments were performed to validate these models, by attempting to detect the damage with different sensor systems including a laser vibrometer and piezoelectric-based impedance meter.

3.2 Analytical Procedures

Prior to experimentation, analytical models were produced to better understand what results were to be expected from the testing, and to set the test parameters correctly. Simple beam theory was used to obtain initial values for natural frequencies of the narrow coupon specimens that were to be tested, which were followed by finite element solutions. These finite element models were created in I-DEAS, and could accurately predict the natural frequencies for even complex geometries, as well as plot their mode shapes for comparison between control models and ones with simulated damage.

3.2.1 Simple beam theory

The equations for the natural frequencies of simple beams are well understood, and the derivations are available in several textbooks [104, 105]. As with most mechanics problems, the unit element is analyzed by force and moment balances to provide the characteristic equation:

$$m\ddot{w} - (Tw')' + (EIw'')'' = f_z \tag{3.1}$$

with boundary conditions:

$$\begin{aligned} w = w' = 0 \quad & \text{Fixed end (no deflection or slope condition)} \\ EIw'' = (EIw'')' = 0 \quad & \text{Free end (no moment or shear force condition)} \end{aligned} \tag{3.2}$$

and solutions are in the form of:

$$f = A\sinh \lambda x + B\cosh \lambda x + C\sin \lambda x + D\cos \lambda x \tag{3.3}$$

where m is the mass of the beam per unit length, w is the vertical deflection, EI is the bending stiffness and x is the position along the length of the beam. T and f represent possible forces on the beam, either an applied tension or a distributed load respectively. When these equations are solved for the fixed-free case with no applied loads or pre-tensions, the equation for the natural frequencies *f* is (this is only an approximation for n<5, see Blevins [105]):

$$f_n = \frac{(2n-1)^2 p}{8L^2}\sqrt{\frac{EI}{m}} \quad \text{for n} = 1,2,3... \tag{3.4}$$

where *f* is the natural frequency in hertz. The values of these natural frequencies for the particular case examined in the present research can be found in the results section.

3.2.2 Finite element modeling

A 2-D finite element analysis was performed in I-DEAS™ to determine the frequency response of simple graphite/epoxy composite specimens. Eight-node quadrilateral shell elements were used (500 in total) to model a standard 250 x 50 x 1 mm tensile coupon. A convergence study was performed to determine that 6 mm square elements were optimal to solve for the normal modes of the system, with a change in resonant frequencies of less than 0.1% by decreasing the element size by 1 mm^2. To simulate a clamped boundary condition, the 25 mm of nodes on one end of the specimen were constrained in all of their degrees of freedom. A Classical Laminated Plate Theory (CLPT) code was written in MATLAB™ to calculate the composite elastic matrices for a $[90/\pm45/0]_s$ quasi-isotropic laminate of AS4/3501-6 (E_1 = 142 GPa, E_2 = 9.8 GPa, G_{12}= 5.4 GPa, ν_{12}= 0.3), which were then entered into a material property card in I-DEAS™ [106]. The "Simultaneous Vector Iteration" method was used to calculate the natural frequencies of the system up to 20 KHz, and their corresponding mode shapes [107].

Several types of damage were also simulated in various models, as represented in **Figure 3.1**. One simple variation of the control model had a hole modeled into it. Other models had altered extension and bending stiffness matrices either in specific regions or across the entire model, which simulated reduction in axial stiffness due to distributed damage caused by either static or fatigue loading as suggested by the literature [108]. For transverse ply cracks in a quasi-isotropic laminate caused by a static load, the results the literature showed that the axial stiffness is reduced asymptotically to 90-95% of its original value as the crack density in the specimen reaches saturation [109]. These same studies found that the laminate modulus is affected more by fatigue-induced cracks for the same crack density, achieving about 80% of its original value. The most challenging damage to model was a delaminated area in the specimen. First, a separate set of elastic matrices were computed using the MATLAB™ code for the two half laminates in the delaminated area, and these properties were entered into I-DEAS™ as separate material property cards. Next, the elements in the delamination region were copied, and each half laminate was assigned the appropriate new properties, as seen in **Figure 3.2**. Finally the outlining nodes of both groups were tied together by constraining all of their degrees of freedom.

3.3 Experimental Procedures

Two sets of experiments were performed to evaluate the merits of frequency response methods. The first one used a laser vibrometer to measure and record the displacements versus time of several points across specimens in a finely meshed grid, which could then be used to calculate natural frequencies and mode shapes for a certain range of frequencies. The second test used an impedance meter to record the frequencies of resonance of the sensors attached to the specimens, however provided no information of mode shape. The following sections will also

describe the manufacturing procedure used to fabricate these specimens with representative forms of damage, which were consistently reused for each set of experimentation in this thesis.

3.3.1 Specimen fabrication

Four graphite/epoxy panels were manufactured according to a standard procedure [110] using AS4/3501-6. A $[90/\pm45/0]_s$ quasi-isotropic laminate was selected for these experiments, and the specimens were cut to 250 x 50 x 1 mm using a continuous diamond grit cutting wheel. Next, various types of damage were introduced to the specimens. In the first group, 6.4 mm diameter holes were drilled into the center of each specimen using a silicon-carbide core drill to minimize damage during the drilling process. The next group was hit with a hammer in a 25 x 25 mm square region to simulate low velocity impact damage. The third group was loaded in a 4-point bending fixture until audible damage was heard, and the fourth was cyclically loaded in the same fixture for 2000 cycles at 80% of this load with an R ratio of −1. The next two groups of specimens were delamination specimens. Two methods were used to introduce the delamination: one used a thin utility blade to cut a 50 x 20 mm slot in one side, and the other with a Teflon strip cured into the center of the laminate. In both cases the delamination was at the center mid-plane of the laminate. The final group consisted of the control specimens. After the damage was introduced into each specimen, an x-ray radiograph was taken using a die-penetrant to help document the type, degree and location of the damage as shown in **Figure 3.3**.

3.3.2 Laser vibrometer tests

In order to deduce the natural frequencies and mode shapes of the specimens, a Polytec™ scanning laser vibrometer system was used. The clamped boundary condition simulating a cantilever beam was found to be the most sensitive factor in the experiments, so the specimens were clamped to a pre-specified load of 9 N-m in a vice using a torque wrench. The specimens were excited using two square 13 mm PZT wafers which were temporary adhered with thin double-sided tape to the base of the specimens. Experimentation demonstrated that thicker tape affected the modal results, however this thin tape applied with thumb pressure was sufficient to reproduce results from adhesively bonded wafers. The PZT was actuated out of phase by an 8V sine chirp signal (fast repeated sine sweep [111]), which was sent to the actuators through a function generator to drive them between 0 Hz and 20 kHz. A separate set of tests was also performed using an external shaker to excite the specimens with this same chirp signal. The laser was set to scan through a fine mesh of points along each specimen's surface recording the velocity response at that grid position. This data along with complimentary data from a stationary control laser were used to produce frequency/response plots and mode shapes.

3.3.3 Impedance tests

The accuracy of the frequency responses found from the vibrometer was validated by a second test that was performed using an impedance meter. This test used a similar set-up to that of the vibrometer test, using the same boundary conditions and specimens, however in this case one PZT wafer was used to actuate, and the other to sense. Segments of 1V sine sweeps were generated by the impedance meter in 1000 Hz increments to excite the actuator, and the

frequency dependent impedance response was captured by the second piezoelectric sensor. The advantage of using this method is that it is more sensitive to higher frequencies than the vibrometer system, and it is more representative of a potentially surface-mounted SHM sensor system. The disadvantage however, is that mode shapes cannot be extracted.

3.4 Results

The following sections present the analytical and experimental results for the frequency response methods that were being examined. The analytical solutions include results of a simple beam theory approach, however mostly focus on the finite element results. The experimental results highlight the laser vibrometer results, as they are most easily compared to the finite element solutions, although also present the results from the impedance readings. All of these results are compared and placed into context in the discussion section that follows.

3.4.1 Analytical results

There are three sets of results that are presented in this section that were generated by I-DEAS™ for each model. The first is a list of natural frequencies converged to a specified number of significant figures for the frequency range requested. The second is a series of plots of the mode shapes that correspond to these natural frequencies. The final result is a transfer function plot for the velocity magnitude response to the frequency spectrum. As suggested by the literature, all of these results were obtained in the range 0-20 kHz, and the transfer function plot for this range is shown in **Figure 3.4**. From this plot it was apparent that not much data could be visually extracted from such a broad frequency range, so the rest of the data presented

here are for the modes below 500 Hz with an explanation of this decision in the discussion section. A table comparing the first six natural frequencies and mode-shapes of each specimen can be found in **Table 3.1**. Also seen in this table are the results from the simple beam theory calculations. A few graphical samples of their mode-shapes can be seen in **Figure 3.5**. The most relevant set of results found from the analytical part of this research was the transfer function plot, as shown in **Figure 3.6**. This plot compares a control model with one that had the simulated damage of a 25 x 50 mm delamination located in the mid-plane of the specimen along the free edge, and was modeled as described previously. Similar trends were observed for the other damaged models, all yielding similar trends. The significance of these plots will be delineated in the discussion section.

3.4.2 Experimental results

There were three sets of outputs for each test on the vibrometer: the velocity magnitude response, the normal mode maximum peaks and corresponding deformation shapes as computed by the vibrometer software. The impedance meter tests resulted in only transfer functions between the actuating and sensing PZT wafers, which were used to identify modes that had not been captured by the vibrometer due to the fact that it was averaging the transfer functions across the entire specimen. Again the dynamic responses were found between 0-20 kHz, a sample of which for the vibrometer results of a control specimen is shown in **Figure 3.7** and for the impedance results of a control and delaminated specimen is shown in **Figure 3.8**. A table comparing the first six natural frequencies and mode-shapes of a control specimen and several other damaged specimens (as described in the experimental setup) can be found in **Table 3.2**. A few selected mode shapes from the vibrometer display are presented in **Figure 3.9** to be later

contrasted to the predicted shapes. Lastly, **Figure 3.10** displays the velocity magnitude response to a frequency range below 500 Hz for all of the tested specimens. From this plot conclusions regarding the true effect of various damage types on the frequency response of a system can be extracted.

3.5 Discussion

This section provides a discussion of the results presented in the previous section. Overall, good correlation was observed between the analytical and experimental results, and these methods appeared to be relatively sensitive to even small amounts of damage. The discussion is completed with an evaluation of the possible roles of these frequency response methods within the framework of a structural health monitoring system.

3.5.1 Effect of damage on frequency response

For both the numerical (FE) and experimental results it is evident that all the forms of damage investigated in this study caused detectable changes in the natural frequencies of a simple coupon. These changes are present in each of the lower normal frequencies, and become more pronounced at higher frequencies to a degree that corresponding modes between the control and damaged specimens become indiscernible. This frequency reduction can be explained by classical structural dynamics [104]. Natural frequencies are determined by the boundary conditions of a system through the variable λ^2, which is determined by the characteristic equation of the structure, and is multiplied by the ratio $(EI/m)^{½}$ (for beam like structures), where E is the Young's modulus, I is the 2^{nd} moment of area and m is the mass.

When damage is introduced to a specimen by one of a variety of mechanisms, the resulting local loss of stiffness directly affects this ratio, thereby affecting the natural frequencies of the structure. The delaminated specimens have a region that effectively behaves as two separate laminates with reduced stiffness, and the set with one edge delaminated has an even more prominent change in the torsion modes due to its asymmetry. The fatigue-damaged specimens are affected by matrix-cracking and fiber-matrix debonding, and the 4-point bending specimens contain broken fibers, which also reduce the modulus. Changes in the specimens with the drilled hole can be explained by the reduced stiffness and mass.

As shown in the literature, a strong correlation can often be found between relative frequency reduction and the area damaged by a particular mechanism, however it is difficult to draw any conclusions about the criticality of the damage since there is no information regarding the form of the damage or its orientation. This limitation is illustrated by a delamination with an area of 5 x 2 cm that has a significantly different effect on a structure depending on whether the longer delamination direction is oriented parallel or perpendicular to the sensor, as seen in **Table 3.3**. Delamination that is more severe along the length of a specimen tends to cause a larger reduction on the bending modes, while delamination along the width appears to affect the torsional modes more adversely. It is also important to note that the 5-10% reduction in natural frequency caused by a 5 cm diameter through-hole yields almost identical transfer function results to that of a 10 x 2 cm center delamination, however there is a noteworthy difference in the significance to the structure for failure strength and mode. The only type of damage that was slightly distinguishable at low frequency ranges was fatigue damage, which produced many high-energy local modes that were not present in any of the other specimens. Based on these results, it is likely that an observer could discern whether a structure has been damaged by

observing its frequency response, however it would be difficult to differentiate reliably between damage types, locations and orientations without capturing several accurate bending and torsional modes and building a large database of damage simulations model and experimental data.

3.5.2 Comparison of analytical and experimental results

In comparing the analytical and experimental results presented in **Table 3.1** and **Table 3.2**, a good correlation was found without tuning or adjusting the models. These results were also similar to the simple beam theory solutions, which did not account for the anisotropy of the material, or the presence of torsional and longitudinal modes with its first order approximations. The models consistently yielded the correct progression of mode shapes, and natural frequencies between 1-8% above those found in experiments, which could be explained by a variety of factors. A small amount of error could be attributed to fiber misalignment and resin flow or bleed-out during curing that created slight differences in the modulus, density and thickness of the laminate, affecting the natural frequencies by a factor of $(Et^2/\rho)^{1/2}$, which is a manipulated version of the previous constant where t is the thickness and ρ the density. The experimentally obtained averages of these variables were identical to those entered into the model, however significant variances are associated with them, which would account for as much as a 4% deviation from the predicted solution. Another small possible difference could have been introduced by the PZT wafers, which add mass to the specimens and may also have shifted the measurement equipment slightly out of phase due to the elasticity in the thin adhesive layer between them and the composite laminate. The largest variable sensitivity in the system was found to be in the simulated clamped boundary condition. It was experimentally found that by

slightly loosening the torque on the clamp, the lowest natural frequencies in the control specimen could drop as much as 10%, which overshadowed most forms of damage that were detected in these specimens. This result was confirmed by a finite element model, which replaced the completely clamped boundary condition with a pin on the 25 mm line and a clamp at the base of the specimen. This model yielded a 9% reduction in the first several resonant frequencies. Consequently, much care was taken to produce a consistent clamping pressure with the torque wrench for each of the experiments performed.

The strong dependence on accurate boundary conditions to retrieve accurate frequency responses for even a simple geometry model is the reason why most work in the literature has avoided model-dependent SHM solutions. Instead, they have tended towards time history change comparisons while using this technique. Without the use of models however, the frequency response method is limited to low frequency ranges where the response peaks are still distinct. A consequence of this limitation is that while the principal global modes can be detected, the local modes of the structure, which hold the most detailed information about the damage present, will not be detected. Even so, as will be discussed in the following section, the frequency response method can still play an important role in a SHM system, and preliminary models are useful in predicting the response of a structure to help design a successful sensor layout.

3.5.3 Role of frequency response methods in SHM

There are many advantages to using frequency response methods in a SHM system; they can be implemented cheaply, they can be light and conformal, and they can provide good insight as to the global condition of the system. The limitations are that they provide little information

about the local damage area unless large quantities of sensors are used along with accurate numerical models; and then it can be argued that damage large enough to be detected globally may already be critical in many structures. Clearly this method does not suffice as the sole sensor set in a SHM system, however that does not exclude them from having any role in the system. The most attractive implementation of the frequency response method is one performed passively for low frequencies using ambient vehicle vibrations, caused by the engines or aerodynamic loads for example. Comparing global transfer functions for prescribed frequency ranges at selected positions could provide a good foundation for a first and last line of defense in a SHM system. A passive method such as this could continuously monitor components of a structure without requiring much processing power in order to direct more accurate and energy-intensive active sensor systems where to query for a more detailed survey of potential damage.

Alternatively, widespread fatigue may be too small or gradual to be detected by fine-tuned active methods, and this may be better detected by an ambient frequency response method by setting a global limit on allowable natural frequency decay of the structure over time. To accomplish this role in a SHM system, first a model would have to be built which would be used to select an appropriate range of frequencies to detect resonant frequencies and to test various placements for sensors. Modal reduction can be accomplished using a variety of sensors such as strain gauges, piezoelectric wafers or accelerometers, which must be placed strategically throughout the structure. Then a damaged model should be used to confirm that realistic damage would be detected from the transfer function for the selected frequency range. Lastly these results should be experimentally verified on a representative structure, perhaps by increasing local stiffness externally instead of damaging the structure. In non-critical and smaller components this method may also prove sufficient to detect most forms of damage.

3.6 Conclusions

The potential role of the frequency response of a composite structure in a structural health monitoring system has been investigated in this chapter. A finite element model was built to explore numerically the effects of various types of damage on the normal modes of test coupons, and analogous experiments were performed using a scanning laser vibrometer and impedance meter to verify these results. Good correlation was found between the model and the experimental results for low frequencies, however coalescing modes at higher frequencies made comparison impractical. In both the numerical model and experimental results there was strong correspondence between the extent of damaged (or local stiffness loss) and the reduction in natural frequency, which again was mostly quantifiable at lower frequencies. This result is substantiated in several papers in the literature for delamination and notched specimens. The limitations and sensitivities of the frequency response method are discussed as well. This method appears to be appropriate for detecting global changes in stiffness, and hence damage, for relatively large structures at a low power and weight cost. Additionally it has the potential to deduce this data using only ambient vibration energy in a passive SHM system. A limitation is that not much information about the specifics of location or type of damage can be inferred by this method without the use of large stored models. Even so, using ambient vibrations as an energy source allows the frequency response method to have a potentially useful role in a SHM system, by guiding other active sensor systems to regions of concern and monitoring the global decay of structural stiffness.

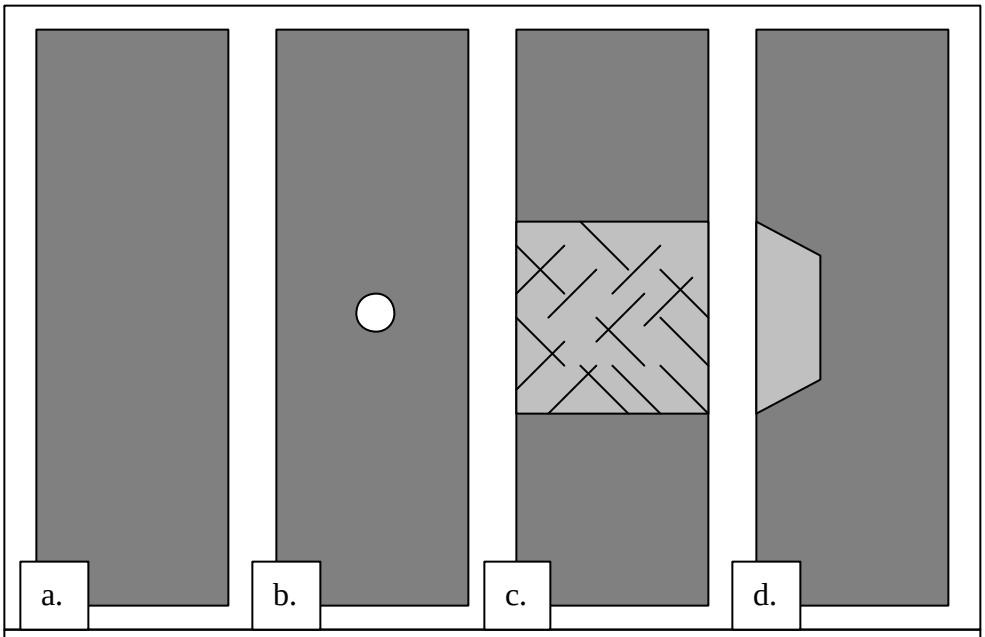

Figure 3.1: Diagrams of damage models:
a. Control specimen with no modeled damage
b. Stress concentration specimen with modeled hole
c. Matrix-crack specimen with modeled area of reduced modulus
d. Delamination specimen with two laminate groups in damaged area

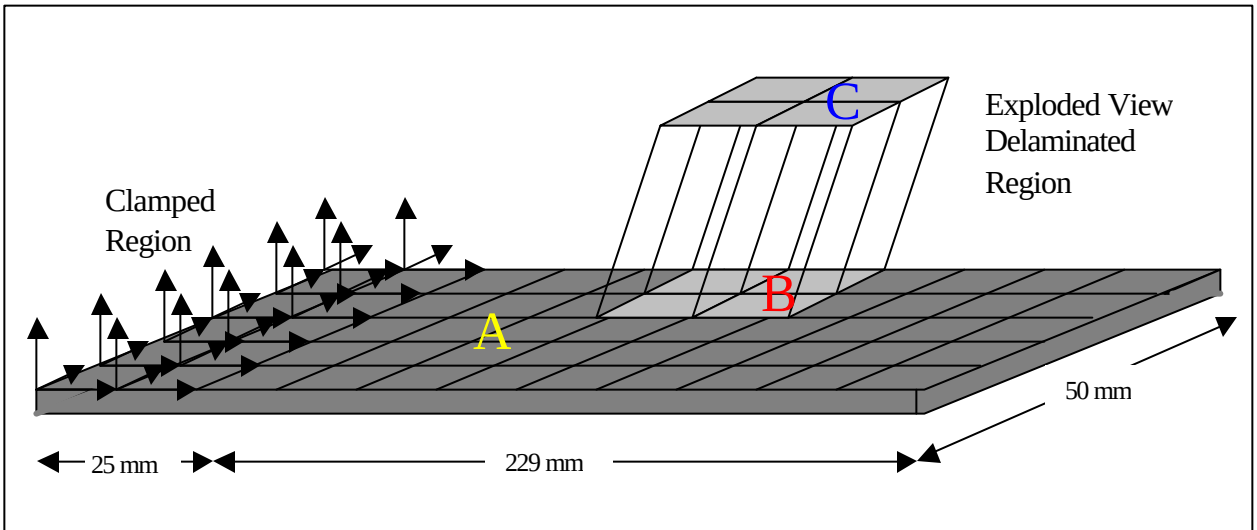

Figure 3.2: Schematic of the delamination modeling procedure. The delaminated area elements were copied, and each half laminate were assigned the appropriate new properties listed below:
- Laminate A: [90/±45/0]s, thickness = 1.0 mm
- Laminate B: [0/±45/90], thickness = 0.5 mm
- Laminate C: [90/±45/0], thickness = 0.5 mm

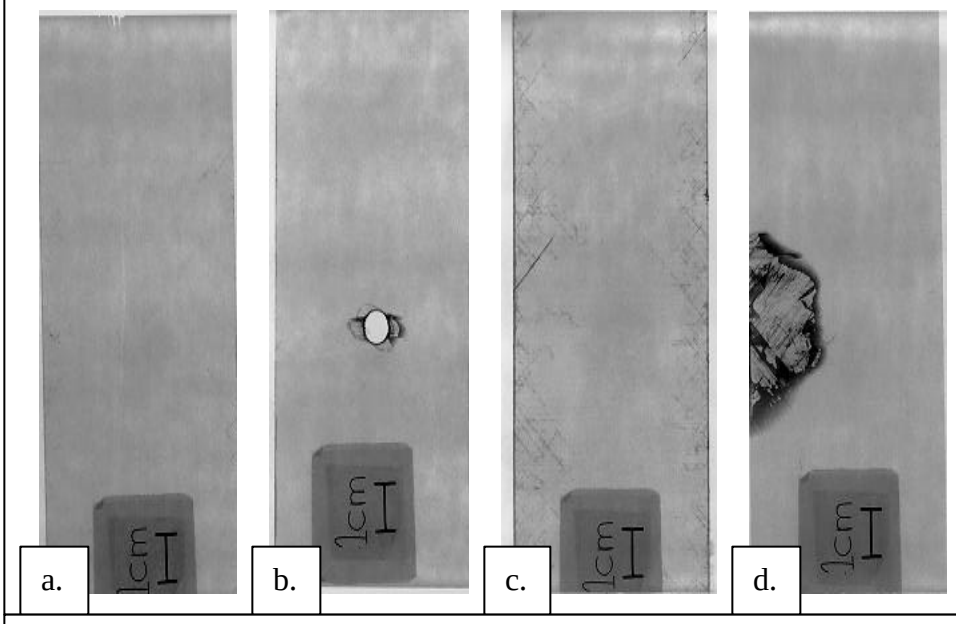

Figure 3.3: X-Radiographs of damaged specimens:
a. Control specimen with no damage present
b. Stress concentration specimen with drilled through-hole
c. Matrix-crack specimen with fatigue induced damage
d. Delamination specimen cut with a thin utility knife at the mid-plane

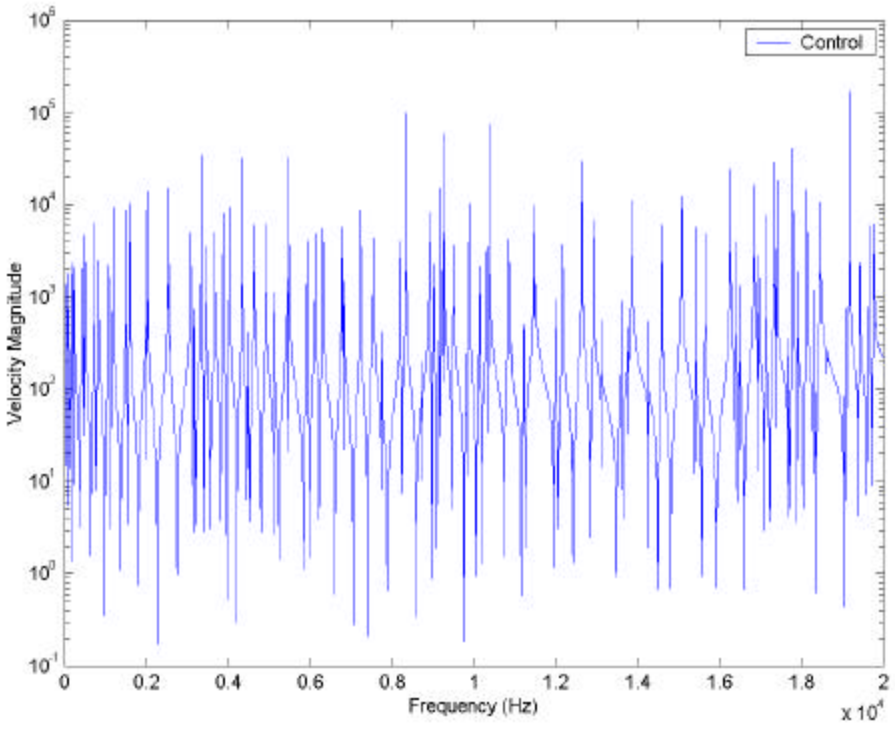

Figure 3.4: Frequency response transfer function plot from FEM in I-DEAS, range 0-20 kHz

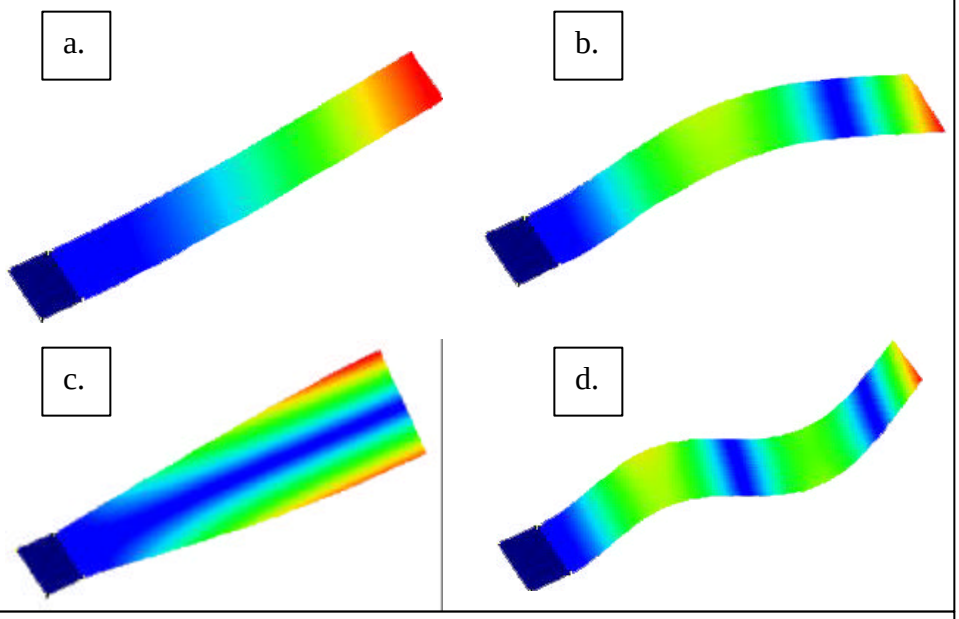

Figure 3.5: First four mode shapes of control specimen plotted in I-DEAS.
a. first bending, b. second bending, c. first torsion, d. third bending

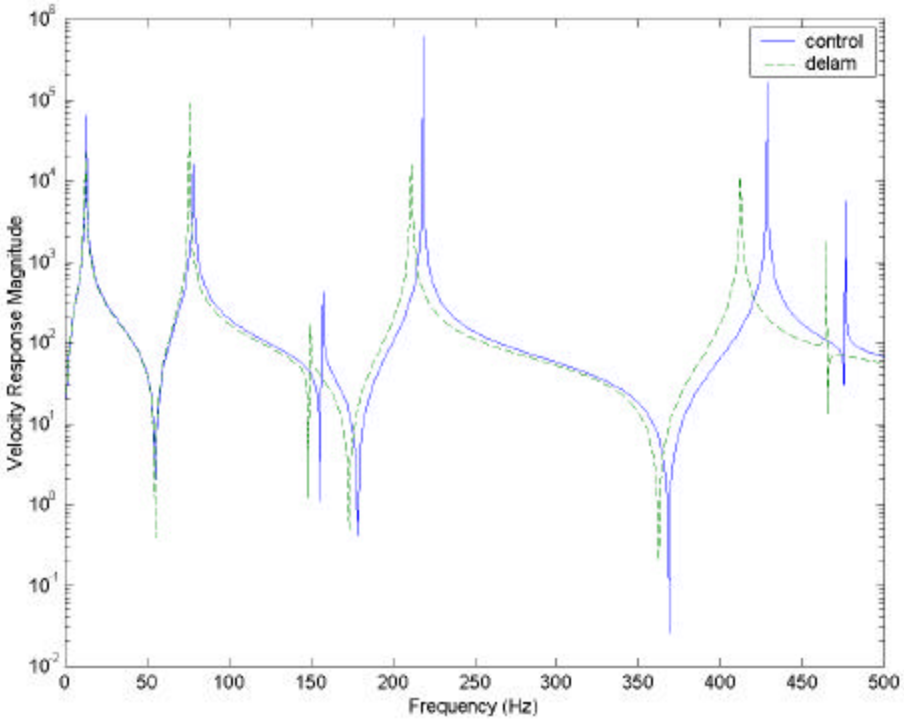

Figure 3.6: Frequency response transfer function plot from I-DEAS, range of 0-500 Hz

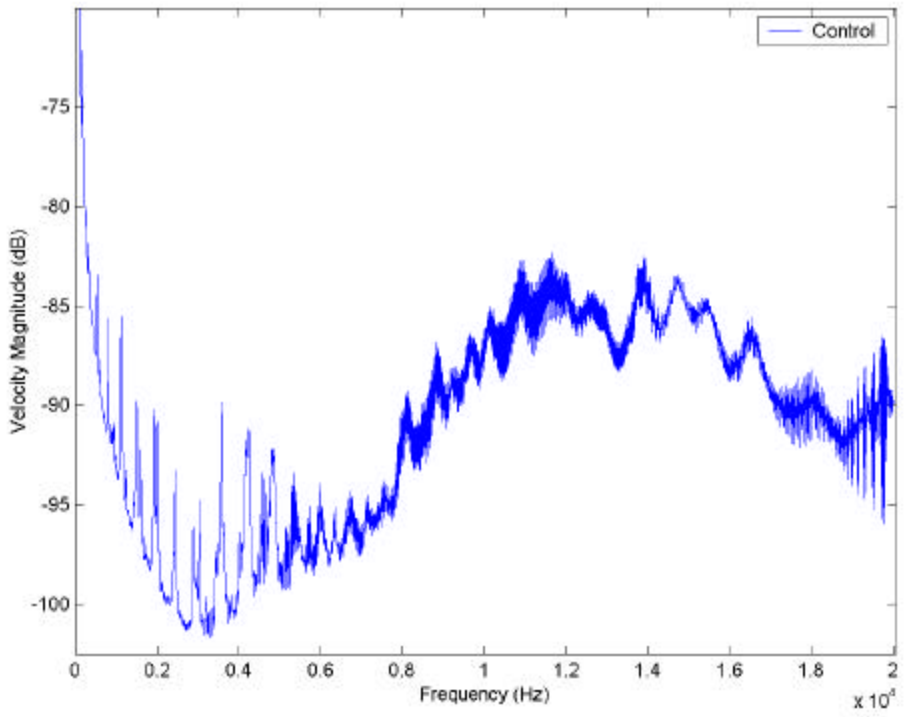

Figure 3.7: Frequency response plot from scanning laser vibrometer for range of 0-20 kHz

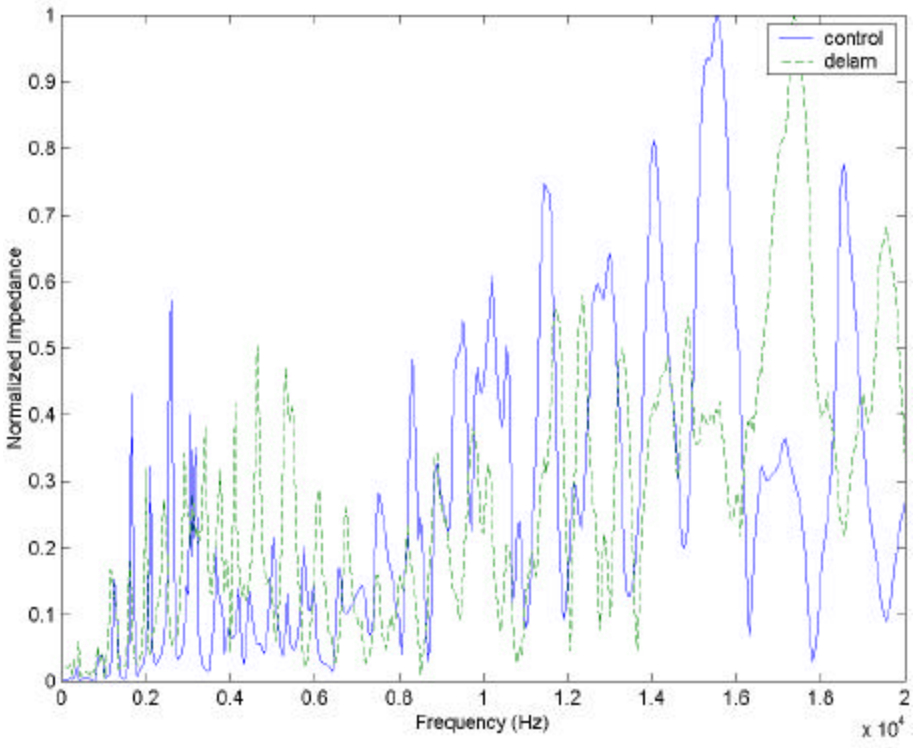

Figure 3.8: Frequency response plot from impedance meter for full tested range of 0-20 kHz

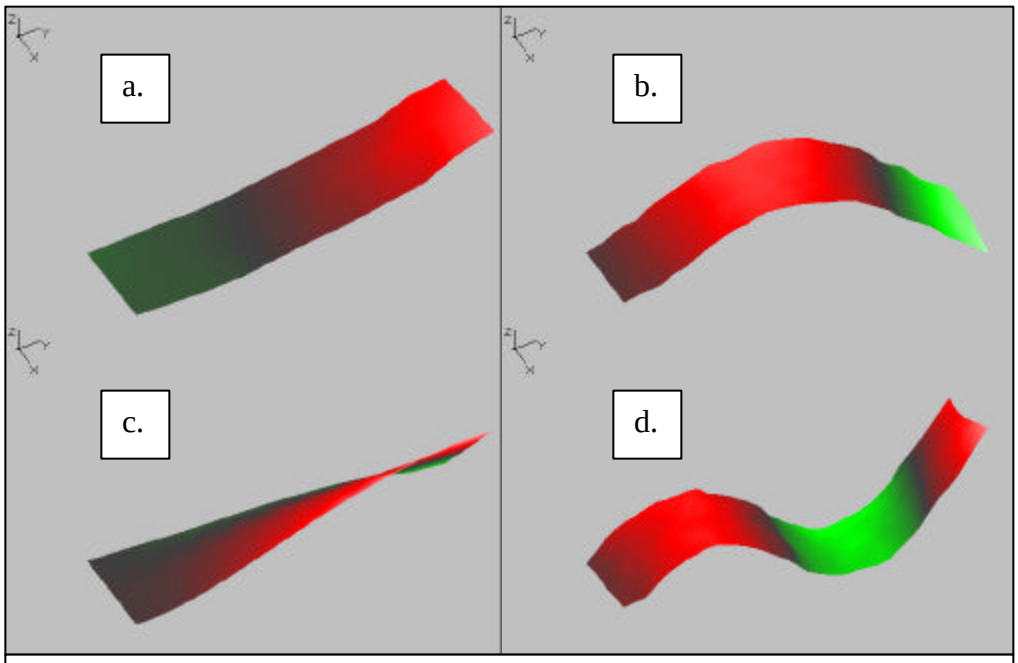

Figure 3.9: First four mode shapes of control specimen using laser vibrometer data.
a. first bending, b. second bending, c. first torsion, d. third bending

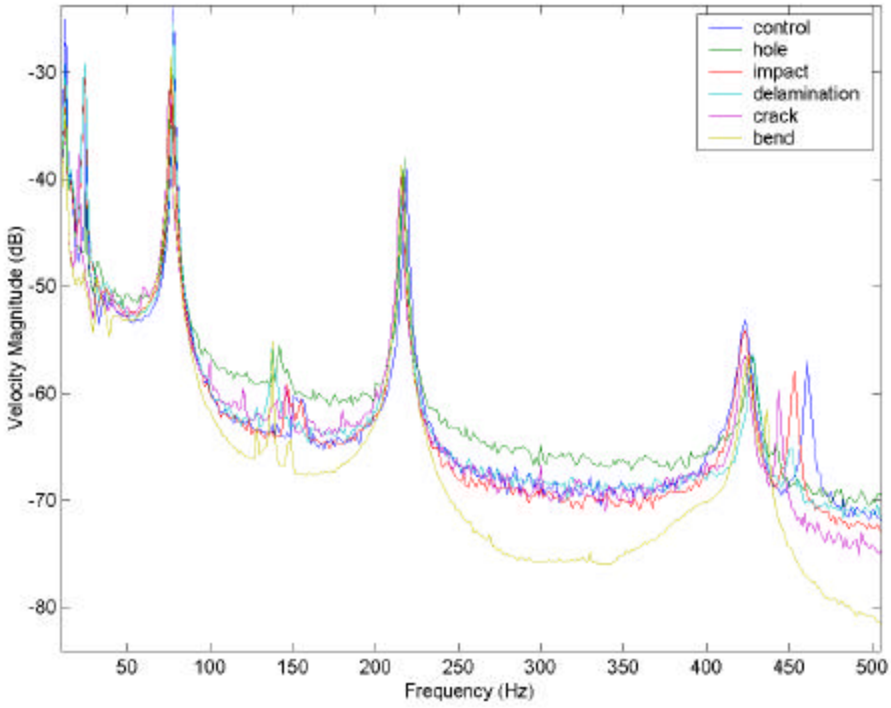

Figure 3.10: Frequency response plot from vibrometer for all specimens, range of 0-500 Hz

Table 3.1: Natural frequencies and mode shapes as determined from FEM in I-DEAS

(All Hz)	Shape	Control	Hole	Impact	Delamination	Fatigue	Bend
Mode 1	1st Bending	12.5	12.4	12.5	12.1	12.1	12.3
Mode 2	2nd Bending	77.8	77.2	77.5	75.5	73.7	76.3
Mode 3	1st Torsion	157	155	156	149	150	154
Mode 4	3rd Bending	218	217	217	211	213	216
Mode 5	4th Bending	428	425	426	412	413	422
Mode 6	2nd Torsion	476	473	474	465	466	472

Table 3.2: Natural frequencies and mode shapes as determined from scanning laser vibrometer data

(All Hz)	Shape	Control	Hole	Impact	Delamination	Fatigue	Bend
Mode 1	1st Bending	12.5	12.5	12.5	12.5	12.5	12.5
Mode 2	2nd Bending	78.1	78.1	76.5	78.1	75.0	76.3
Mode 3	1st Torsion	157	148	147	137	146	137
Mode 4	3rd Bending	218	217	216	215	209	214
Mode 5	4th Bending	423	423	423	428	413	423
Mode 6	2nd Torsion	461	453	453	451	428	432

Table 3.3: Natural frequencies and mode shapes from FEM comparing damage in various orientations

(All Hz)	Shape	5x2cm Delam	10x2cm Delam	5/4cm Delam	Centered Hole	5cm Offset Hole	-5cm Offset Hole
Mode 1	1st Bending	12.3	12.2	12.2	12.3	12.5	12.2
Mode 2	2nd Bending	76.3	75.6	74.8	77.2	76.9	77.7
Mode 3	3rd Bending	216	213	215	217	216	218
Mode 4	4th Bending	422	418	417	425	426	426
Mode 5	5th Bending	701	691	6931	705	705	706
Mode 6	6th Bending	1050	1030	1040	1060	1050	1060

[This page intentionally left blank]

Chapter 4

LAMB WAVE METHODS

This chapter presents analytical and experimental results for the application of Lamb wave techniques to quasi-isotropic graphite/epoxy specimens featuring representative damage modes. Linear wave scans were performed on narrow laminated specimens and sandwich beams with various cores by monitoring the transmitted and reflected waves with piezoelectric sensors. Similar experiments were also performed on laminated plates and built up composite structures. Analytical models were built to select optimal actuator configuration and driving signals for these experiments. Finite element models were also produced for comparison to these experiments, and to help to predict the detection capabilities of these methods on more complex structures. Lamb wave techniques have been proven to provide more information about damage type, severity and location than frequency response methods, and are suitable for structural health monitoring applications since they travel long distances and can be applied with conformable piezoelectric actuators and sensors that require little power.

4.1 Background

Several techniques have been researched for detecting damage in composite materials, however Lamb wave methods have recently re-emerged as a reliable way to locate damage in these materials [4, 7, 33, 83]. These techniques have been implemented in a variety of fashions in the literature, including the use of separate actuators and sensors to monitor transmitted waves

and/or reflected waves, and multipurpose patches which have both actuation and sensing capabilities. Each of these techniques offers their own unique advantages in detecting certain types of damage with various levels of analytical complexity. This section presents the application of Lamb wave methods as published in the literature.

4.1.1 Early Lamb wave theory and applications

Lamb waves are a form of elastic perturbation that can propagate in a solid plate with free boundaries [112, 113]. This type of wave phenomenon was first described in theory by Horace Lamb in 1917, however he never attempted to produce them [114]. Perhaps the earliest recognition of Lamb waves as a means of damage detection came in 1960 by Worlton of the General Electric Company [115]. His report investigated the dispersion curves of aluminum and zirconium to describe analytically the characteristics of the various modes that would pertain to nondestructive testing applications. The motions and velocities of the interior particles are formulated, and the effects of holes and thickness variations are discussed. In the following decade Lamb wave techniques were examined by several investigators, and then the first potential aerospace application was introduced by Demer and Fentnor of the Hughes Aircraft Company [116]. In their work they cited ultrasonic wave testing as one of the most reliable forms of nondestructive testing, and that Lamb waves were emerging as one of the best ways to infer information about the medium's density, elastic properties and thickness. They did however acknowledge the fact that Lamb waves were not readily understood nor easily interpreted. The particular work performed at Hughes focused on Lamb wave propagation in metallic thin sheets and elongated cylindrical forms. Fatigue cracks were located in stainless-steel and aluminum rods by recording the time of flight and attenuated amplitude of the received

ultrasonic signal. Similar experiments were performed on glass, ceramic and plastic specimens with the objective of examining the effects of liquid penetration. In the 1970's and 80's, work on Lamb waves continued and began focusing on various types of actuators. Much of this work was performed under White at Berkeley, who wrote a comprehensive review paper on all available forms of actuators and sensors [117]. In it he described mechanical actuation on a line or using a comb drive, piezoelectric and piezoresistive actuators and sensors operating in d_{11} or d_{13} mode with or without interdigitated electrodes, magnetic or thermal actuators, and optical sensors. The mechanisms and benefits behind each of these methods are discussed at length, and follow-up papers were written on the experimental use of the methods which were found to be the best, which employed silicon-based piezoelectric multisensors [118-120]. Subsequently, several other authors have written papers that focus on the further development of these techniques over the past 20 years [121-129].

Since the mid-1990's, Cawley's group has had some of the most promising research in Lamb wave technologies, working to optimize the generation of directional waves [34, 130]. To allow the implementation of Lamb waves on a real structure, they have been developing flexible, cheap Polyvinylidenedifloride (PVDF) transducers in order to both generate and detect waves. Their work uses interdigital transducer leads to generate highly focused and directional waves without higher mode interference, and they have inspected various metallic specimens with encouraging results. During more recent work, Cawley's group has been experimentally testing the limitations of their methods on large areas and thick structures representing sections of aircraft fuselages [131, 132].

4.1.2 Lamb waves in composite materials

During the late 1980's and early 1990's work began on the application of Lamb waves to composite materials. Research conducted at NASA by Saravanos demonstrated, both analytically and experimentally, the possibility of detecting delamination in composite beams using Lamb waves [133, 134]. Similar conclusions were drawn by Percival and Birt at the Defense & Evaluation Research Agency, UK, who began focusing their work on the two fundamental Lamb wave modes, which will be described further in the following section [135-137]. Detection of other forms of damage in composite materials was also investigated by Seale, who examined fatigue and thermal damage, and Tang who observed the sensitivity of Lamb wave propagation to fiber fracture [138, 139]. This work was extended to composite sandwich plates, including panels subjected to impact damage by Osmont and Rose [80, 140]. There have also been several others recently who have begun to investigate the interaction of Lamb waves with composite materials [64, 141-144].

The most successful work to date using Lamb waves for damage detection in composite materials has been performed by Soutis's group at Imperial College, who have focused on the sensor placement and signal processing issues [81, 82, 144]. They have chosen to use Lead-Zirconate-Titanate (PZT) actuators and sensors over PVDF since they require a factor of ten less voltage to generate Lamb waves, however they are not as conformable. The most complete work from this group can be found in Valdez's PhD thesis [96]. During the course of his work he performed many experiments on quasi-isotropic graphite/epoxy composite specimens, pulsing them with Lamb waves in various configurations to detect controlled artificial delaminations. He also simulated the propagation of Lamb waves in plates of various widths using a finite element code. Much of the Lamb wave research presented in this thesis follows Valdez's work,

extending it to various other types of damage, and furthermore testing sandwich structures and built-up structures as well as addressing self-sensing actuators and analytically optimizing the experimental procedures.

4.2 Analytical Procedures

There are two groups of Lamb waves, symmetric and anti-symmetric, that satisfy the wave equation and boundary conditions for this problem, and each can propagate independently of the other. A graphical representation of these two groups of waves can be seen in **Figure 4.1**. The present work utilizes PZT piezoelectric patches to excite the first anti-symmetric Lamb wave (A_0 mode). This wave was chosen since it can propagate long distances with little dispersion, and no higher modes are present to clutter the resulting response waves [96]. In the following section, analytical models for Lamb wave propagation have been derived, which relate the velocity of the wave-front to the actuating frequency. Using these equations along with other mathematical principles found in the literature, limitations of Lamb wave propagation have also been defined. Lastly, finite element models were built to simulate the travel of these waves in each of the test setups to help specify setup parameters and predict experimental results.

4.2.1 Dispersion curve formulation

The most descriptive way to represent the propagation of a Lamb wave in a particular material is with their dispersion curves, which plot the phase and group velocities versus the excitation frequency [112]. The derivation of these curves begins with the solution to the wave equation for the anti-symmetric Lamb wave as seen in **Equation 4.1**:

$$\frac{\tan(\bar{d}\sqrt{1-z^2})}{\tan(\bar{d}\sqrt{x^2-z^2})}+\frac{(2z^2-1)^2}{4z^2\sqrt{1-z^2}\sqrt{x^2-z^2}}=0 \qquad (4.1)$$

where the non-dimensional parameters are:

$$x^2 = \frac{c_t^2}{c_l^2},\ z^2 = \frac{c_t^2}{c_{phase}^2},\ \bar{d} = \frac{k_t t}{2} \tag{4.2}$$

For an isotropic material, these parameters can be defined in terms of Lamé's constants:

$$m = \frac{E}{2(1+n)},\ l = \frac{En}{(1-2n)(1+n)} \tag{4.3}$$

In which case:

$$c_t^2 = \frac{m}{r},\ c_l^2 = \frac{(l+2m)}{r},\ k_t = \frac{w}{c_t} \tag{4.4}$$

Substituting these equalities into the non-dimensional parameters yields:

$$x^2 = \frac{m}{(l+2m)} = \frac{1-2n}{2-2n},\ z^2 = \frac{m}{rc_{phase}^2} = \frac{E}{2r(1+n)c_{phase}^2}$$
$$\bar{d} = \frac{wt}{2c_t} = \frac{wt}{2}\sqrt{\frac{r}{m}} = \frac{wt}{2}\sqrt{\frac{2r(1+n)}{E}} \tag{4.5}$$

Finally, **Equation 4.5** was substituted into **Equation 4.1** to be solved numerically in Mathematica™, as described in **Appendix A**. For a given material, the Young's Module in the propagation direction E, Poisson Ratio v, and the density r are known, and the phase velocity c_{phase} is the dependent variable being solved for. The independent variable being iteratatively supplied is the frequency-thickness product, where w is the driving frequency in radians. An example of a phase velocity dispersion curve for the first anti-symmetric Lamb wave using the material properties from the specimens used in the present research can be seen in **Figure 4.2**. The other useful plot is the group velocity dispersion curve, which can easily be derived from the phase velocity curve using **Equation 4.6**:

$$K = \frac{2p}{l_w}(\text{wavenumbe r}),\ l_w = \frac{c_{phase}}{f}(\text{wavelength})$$
$$c_{group} = c_{phase} + \frac{\partial c_{phase}}{\partial k}k = \frac{c_{phase}}{1 - \frac{f}{c_{phase}} \cdot \frac{\partial c_{phase}}{\partial f}} \tag{4.6}$$

where f is the frequency in Hz. An example of a group velocity dispersion curve, again using the material properties from the present research can be seen in **Figure 4.3**. At low frequencies, the A_o phase velocity can be approximated in the form of $A\omega^{½}$ and the complementing group velocity as $2A\omega^{½}$, where A is a material property dependant constant. At higher frequencies the phase velocity for this mode tends to the Rayleigh velocity:

$$c_R = \left(\frac{0.87 + 1.12n}{1+n} \right) c_t \tag{4.7}$$

A more thorough derivation of these velocities, starting from Lamb's equalities can be found in **Appendix B**. These dispersion curves are the key to describing and understanding the propagation of Lamb waves in a solid medium, and will be used in the following sections to predict the effects of damage in a given structure.

4.2.2 Propagation and limitations of Lamb waves

The relationship between the material properties of a specimen and the velocity of the propagating Lamb wave is quite complex, however an understanding is necessary to design an appropriate damage detection method. By inspection of **Equation 4.1**, to first order the wave velocity increases with the square root of the modulus, i.e. an increase in modulus slightly speeds the wave velocity. An increase in the density would have the opposite effect slowing wave velocity, as it appears in all the same terms as the modulus but on the reciprocal side of the divisor. The effect of the Poisson's ratio is probably the most complicated, as it appears in most of the terms, and small changes seem to have little to no effect on the wave velocity. The most straightforward parameter is the thickness of the specimen, which has a linear relationship with the Lamb wave velocity—the thicker the specimen the quicker the wavespeed.

Two important concepts to be understood in wave propagation are dispersion and attenuation. Dispersion is the change in wavespeed in a material with respect to frequency, which was demonstrated graphically in the previous section. Since the group velocity is related to the rate of change of the phase velocity at a given frequency, the phase and group velocities are the same for a non-dispersive material. Attenuation is the change in amplitude of a traveling wave over a given distance. While propagating through the solid medium, energy is transferred back and forth between kinetic and elastic potential energy; when this transfer is not perfect, attenuation occurs. This loss in energy can be due to heat being generated, waves leaking into sideband frequencies or spreading into different propagation paths, restraints such as a bonded core, or in the case of composite materials, the fibers can provide reflecting surfaces, which would deteriorate the transmitted wave strength. These two concepts influence each other as well, as increased dispersion causes higher attenuation, and vice-versa. A mathematical approximation to this correlation from the literature that relates the attenuation as a function of propagation distance is:

$$A = \frac{1}{KL} \rightarrow \frac{1}{\sqrt{K_r L}} \tag{4.8}$$

where A is the attenuation factor and L is the propagation distance. A tends to the slower value, using K_r the Rayleigh wave number, as the specimen becomes thicker [112]. An example of this relationship can be seen in the symmetric Lamb wave modes that tend to not travel as far as the anti-symmetric ones, which can be attributed to their dispersive nature (it is difficult to keep the two surfaces of the medium in phase with each other, which causes a high rate of phase velocity change). It has also been experimentally determined that fluids on the surface of a solid can affect the attenuation of the wave, however this effect is limited mostly to the symmetric modes so will not be discussed in detail in this thesis [113]. Analytical studies have also been

performed to formulate the change in dispersion (and hence attenuation) in curved panels [112]. It was found that the phase velocity is changed by the relationship:

$$\overline{c}_p = \left(1 + \frac{c_p^2}{w^2 R^2}\right) c_p \tag{4.9}$$

where c_p is the original phase velocity and R is the radius of curvature. When the phase velocity dispersion curve is adjusted by this formula, the slight increase in dispersion is readily apparent.

The group velocity of a Lamb wave produced by a piezoelectric patch driven at a particular frequency can easily be verified in a control (undamaged) specimen by measuring the time of flight (TOF) in an oscilloscope between two sensors of known separation. The presence of damage in a specimen can then be found without using any analytical models, by measuring the disturbed wave's velocity between the sensor and actuator. An estimation of the extent and size of damage can then be calculated using the Lamb wave equations to determine the loss of stiffness in the specimen. The Lamb wave's group velocity essentially varies in a similar way to that of a structure's resonant frequency, i.e. as $(E/\rho)^{1/2}$, where E is modulus and ρ is density, so as a wave travels across an area of reduced stiffness it will slow down. The other phenomenon associated with damage is analogous to traveling acoustical waves; upon reaching a region of dissimilar wave speed, a portion of the wave is reflected in proportion to the difference in the stiffness and density of the regions. From these two pieces of information, predictions of damage location, size and extent can be deduced.

4.2.3 Finite element modeling

A finite element representation of Lamb wave propagation in narrow coupons and plate structures has been previously presented by Valdez at Imperial College [96]. This analysis was

reproduced in the present research by ABAQUS™ models to observe the small changes in time of flight caused by discontinuities in geometry or material properties. Models were built to represent each of the experiments that were performed, including narrow coupons, sandwich beams, 2-D plates with and without stiffening ribs, and finally a tube structure with sandwich construction. Each of these models were constructed identically to those described in the previous frequency response methods chapter, using 1 cm^2 square shell elements, where the actuators were simulated by a coupled nodal moment. Again regions of cracked matrix were modeled as a local loss in stiffness, and delaminations were modeled by two half laminates with coincident unconnected nodes. Representative input files for these models can be found in **Appendix C** Once processed, the time-steps were visualized as a movie file to measure the time of flight of the Lamb waves across the specimens, and to record visual evidence of dispersion and attenuation. By comparing the times of flight in these models, it was possible to determine the required distance between the piezoceramic actuator and sensors necessary to resolve the difference between waves traveling in a control versus a damaged specimen.

A different approach was taken by Prosper at MIT, who produced a thin layered laminated medium finite element code to solve for the propagation of elastic waves in a two-dimensional through-thickness cross-section [145]. This code was modified by Prosper for the present research to incorporate the graphite/epoxy material properties, thickness and driving signal used in the experimental procedure to observe the progression of Lamb waves. Models were created for both control and delaminated specimen, by leaving a section of layered nodes unconnected. The results of the finite element simulations were animations to observe the motion of the deflected surface material with respect to time to be compared with the more traditional two-dimensional surface finite element models from ABAQUS™.

4.3 Optimization Procedures

There is currently no standard or even a best-practice precedent for damage detection via Lamb wave testing. Several procedures have been developed in the literature, each with valuable characteristics, and each with some degree of arbitrariness. A major goal of the present research was to optimize, analytically and experimentally, the Lamb wave testing procedure, and to determine what effects various parameters have on the sensitivity of damage detection. These parameters can be divided into three categories: actuating frequency, pulse shape, and sensor geometry. The following sections provide selection guidelines for each of these categories, which were used to define the testing parameters for the experimental procedures that followed. This set of tools could be used in parallel by an engineer developing a SHM system for a vehicle to decide if the Lamb wave method would provide satisfying results for their application, and to determine the appropriate driving parameters to obtain the best damage detection resolution.

4.3.1 Frequency selection

The first step in defining an appropriate Lamb wave damage detection solution is to select an appropriate driving frequency, as demonstrated in the flowchart in **Figure 4.4**. This procedure commences by finding the Lamb solution for the wave equation, and plotting the dispersion curves for each section to be monitored. The equations presented previously in this chapter are intended for isotropic materials, however it has been shown in the literature that the A_o mode is fairly invariant to the layup of a composite material, and can be closely approximated by using the bulk laminate properties [136]. Finite element techniques have been used by other researchers in the literature to more accurately determine the wave velocities in composite materials [135, 138]. By entering the material properties (E, ν, and ρ) for a particular material,

the resulting dispersion curves provide a range of potential wave velocities for the A_0 mode driven at different frequency-thickness products. For a given thickness, ideally one would like to choose the least dispersive driving frequency for the Lamb wave being generated, which generally exists where the slope of the phase velocity curve is equal to zero. This is because at low frequencies, the dispersion curves have steep slopes and thus are very sensitive to small variations in frequency making it difficult to maintain a constant velocity to predict the time of flight. The A_0 mode, however, follows a square root relationship until higher frequencies, thus the frequency needs to be chosen by a different criteria. The higher the frequency the smaller the slope of the A_0 dispersion curve, although at a certain point other higher order Lamb waves begin to exist simultaneously and the signal becomes cluttered. The wave velocities are also much quicker at higher frequencies, increasing the requirements for data acquisition.

To balance these issues, the following procedure should be followed. First plot the dispersion curves for the material, and locate the frequencies at which the Rayleigh velocity is obtained and where the A_1 mode begins to be excited. If the Rayleigh velocity is below the point where the next anti-symmetric mode is generated (which normally is not true) then this is the critical frequency; otherwise it would be wise to choose a point about 10% below the A_1 origin point as the critical frequency. Next, it must be determined if the data acquisition capabilities are able to capture a wave traveling at this velocity. Typically, the data acquisition rate should be 10 times the frequency of the signal it is sampling, so the selected driving frequency may have to be lowered if the sampling rate is unobtainable. Also, with knowledge of the effects of various damage types on the stiffness of a particular material, the resolution of change for the resultant signal, or "observeability," can be predicted in order to determine the detection limitations with respect to flaw size for a given data acquisition capability. It would also be prudent to check on

the actuator capabilities to generate that range of frequencies. A final consideration to fine tune the driving frequency is to calculate the natural frequencies of the structure to be monitored, either analytically or by finite element models, and to select a driving frequency that coincides with a normal mode in the desired frequency range. The natural frequencies of the structure play a small role in the amplification or attenuation of the transmitted wave, whereas the wave can travel with less disturbance at a resonant frequency.

Using this approach, an effective experimental test procedure was determined for the present research. The material constants in the propagation direction for the composite laminates to be analyzed were calculated by classical laminated plate theory, and then entered into the Lamb wave model. For the narrow coupon tests, 15 kHz was selected as an optimal frequency, 50 kHz for the sandwich beam tests, and 40 kHz for the micro-satellite bus structure (all to be described further in the experimental procedures section). These frequencies were obtained from their slope and location on the dispersion curves, evidence from previous research suggesting these frequencies for specimen of similar geometries, and brief experimentation using a function generator to verify the maximum response amplitude for the range of driving frequencies. Following this procedure it was determined that graphite/epoxy composite materials were a good candidate for Lamb wave methods, and that with the detection capabilities of the data acquisition system that a reasonable change in stiffness (5-10%) could be resolved.

4.3.2 Pulse shape selection

The second set of variables explored was the actuation pulse parameters. These included the pulse shape, amplitude and number of cycles to be sent during each pulse period. These parameters were varied analytically and verified experimentally on a control specimen to observe

their effect on the Lamb waves generated. First, several candidate signal shapes were compared in Matlab™ by using their power-spectral-density (PSD) plots. Similarly the effect of the number of cycles per period for the different shaped signals was observed in the PSD plots by comparing the energy dedicated to the principal driving frequency. The more energy dedicated to the desired driving frequency, the stronger the Lamb wave and the more accurate the wavespeed calculation, and hence the more sensitive and reliable the damage detection capability. Of the signal shapes that were analyzed and experimented, pure sinusoidal shapes appear to excite Lamb wave harmonics the most efficiently, since they are periodic, smooth and have comparatively quick rise times to their peak amplitude as compared to a parabolic shape. A Hanning window (approximated by a half-sine wave multiplied over the pulse width) helps to narrow the bandwidth further to focus the maximum amount of energy into the desired actuating frequency with the least "spill-over" from neighboring frequencies.

Once the driving frequency and signal shape have been selected, there is then a trade between the number of waves that can be sent in an actuating pulse and the distance from abrupt features in the structure. The number of cycles of a periodic function desired to actuate the piezoelectric actuator is one of the more complicated decisions to be made for Lamb wave techniques. The fast Fourier transform (FFT) of a continuous sine wave would yield a single peak at the driving frequency, however for a few finite cycles, the FFT appears as a Gaussian curve with a peak at the driving frequency. Thus, the more waves sent into a driving pulse, the narrower the bandwidth and the less dispersion. The problem in a short specimens though, or in applications where the actuator and sensors are spaced close together, is the more waves in the pulse the less time between the last signal sent and the first returning reflected signal, so the response is more difficult to interpret. An appropriate number of cycles can be determined by

the maximum number of waves that can be sent in the time it takes for the lead wave to travel to the sensing PZT patch. It is also convenient to use intervals of half cycles so that the sent sinusoidal pulse becomes symmetric. Research from the literature has used signals varying from 3.5 to 13.5 cycles per actuating pulse [34, 80-82, 96, 144]. Since the specimens in the current research are relatively short, few cycles could be actuated without disturbing the received signal thus 3.5 cycles were used to drive the piezoceramic actuators.

Lastly, by increasing the driving voltage the magnitude of the strain produced by the propagating Lamb wave proportionately increases. In these experiments, driving the piezopatches at an amplitude of 5-10V produced a 10-25 mV response due to the wave sensed by the PZT patch. Increasing the amplitude also increases the signal-to-noise ratio to yield a clearer signal, since the static noise received by the PZT patch is usually in the 1-5 mV range. Higher voltage however also tended to increase the drift in the signal, which deteriorated the resolution capabilities of the data acquisition system. Also, a SHM system should be as low power as possible, thus the voltage should be chosen to be the minimum required to resolve the desired damage size. The driving voltage was chosen to be 10V peak-to-peak for these experiments.

4.3.3 Actuator selection

PZT 5H piezoceramic actuators were chosen for the present research due to their high force output at relatively low voltages, and their good response qualities at both low and high frequencies. The shape of the actuator should be chosen based upon desired propagation or reception directions. Researchers in various fields have examined the effects of piezoelectric wafer dimensions on the efficiency of their actuation [146, 147]. Waves propagated parallel to each edge of the actuator, i.e. longitudinally and transversely for a rectangular patch and

circumferentially from a circular actuator. The width of the actuator in the propagation direction is not critical, however the wider it is, the more uniform the waveform created. As cited in the literature though, there is an important sinusoidal relationship between actuating frequency and actuator length [112]. In the direction of propagation the desired actuator length $2a$ is:

$$2a = l\left(n+\frac{1}{2}\right) = \frac{c_p}{f}\left(n+\frac{1}{2}\right) \quad \text{for n} = 0, 1, 2, 3... \tag{4.10}$$

This value of $2a$ could either be a rectangular side length or the diameter of a circular actuator. This equation could also be used to determine actuator minimum dimensions, in order to inhibit waves from propagating in undesired directions. For the experimental procedures in the present research, PZT actuators of 1.5 cm x 0.75 cm were selected based upon this equation.

The other critical issue with actuator selection is the determination of spacing between the actuators and sensors. A design objective of a SHM system is to achieve the most structural coverage with the least number of sensors, thus the optimal sensor spacing must be calculated. The governing equation to estimate this spacing is the attenuation equation presented in a previous section (**Equation 4.8**), which specified an inversely proportional relationship between propagation distance and signal amplitude that was also dependant on the wave number. An acceptable signal loss can be specified for the voltage sensitivity of a data acquisition system, which was determined to be 25% for the present experiments, and from this percentage an estimated actuator-sensor spacing can be calculated.

4.3.4 Signal interpretation

The key to reliable and high-resolution damage detection is good signal interpretation. The raw signals taken from the sensors are in the form of a time history of small voltages caused

by strains induced by the impinging Lamb waves. The first problem with this recorded signal is noise. The largest source of error in the present research was parasitic capacitance in the data acquisition system. In order to acquire data at high frequencies through several channels most data acquisition systems use multiplexers, or MUX. These devices scan through each channel one at a time, making an electrical connection to charge a capacitor from which the voltage measurement is taken, and then moving on to the next channel. The principal limitation on this approach is the occurrence of parasitic capacitance when the data acquisition rate is higher than the settling time of the system, so that residual charge is left on the capacitor in the MUX as it moves from one channel to the next. This effect was further enhanced in the present research since the triggering channel was measuring the driving signal voltage at a range of ±5 V and the other channels were using a range of ±50 mV to measure the sensor voltages. This resulted in a large "ghosting" effect across all the channels, where the driving signal could be seen at a slightly reduced voltage in each of the other measurements. Since the high rate of data sampling was necessary to record the impinging waves, the solution adopted was to use an attenuator to reduce the amplitude of the driving signal being measured in the data acquisition system, while not affecting the driving voltage being split off to the actuator. All of the other systematic sources of noise, which included strains caused from external sources such as air currents and vibrations in the building, were accounted for by connecting an unattached sensor to a blank channel, and using it to normalize the signals from the other channels.

Perhaps the most important factor that has allowed Lamb wave techniques to flourish recently is the development of wavelet analysis. Wavelet decomposition is similar to the Fourier decomposition, however instead of just using sines and cosines, complex "mother wavelets" are used to break down the signal [148]. The idea for the wavelet decomposition was first presented

by Haar in 1910, however the square wave he used was not very practical for most applications. It was not until 1988 when Daubechies introduced a fractal-like mother wavelet, that the full potential of wavelet analysis for signal decomposition and compression realized. The mother wavelet is essentially used as an orthogonal basis vector to filter the signal, and is scaled and shifted to approximate the frequency components of the signal. Typically this decomposition is not done continuously since most of the mother wavelets have no closed form solutions. As result a discrete transform on buffered portions of a signal is typically used. This can be performed in commercial software packages such as MATLAB™ using codes such as that presented in **Appendix D**.

The present research used the Morlet wavelet to decompose the signals, since its shape was closest to the driving pulse shape, which makes the processing more accurate and efficient [34]. To analyze the measurements, the Morlet wavelet was scaled between 0 Hz and twice the driving frequency and it was subsequently shifted through the entire time axis. The results of this analysis could be visualized in two forms. The first was a waterfall plot, which plots all the frequency scales versus time, representing the energy present at a point by color-coded intensity. Secondly, each of these scale bands could be plotted independently to allow observation of the numerical amplitude of signal energy versus time. Using the second method, by looking at the central scale band one could filter out all frequencies other than the central driving frequency from the received signals. This provides a clear, filtered view of the transmitted energy from the actuator to the sensors over time for an accurate time of flight measurement. Then, by looking at the waterfall plot, one could potentially gain insight into the damage in the specimen from the intensities of energy that have been shed into sideband frequencies. The experimental results presented later in this chapter were created using this procedure.

4.4 Experimental Procedures

This section describes the experimental procedures that were followed during the course of the present research to validate the effectiveness of Lamb wave methods as a means of damage detection in composite materials. These experiments followed a building block approach [149], commencing with the reinvestigation of the narrow coupon specimens used during the frequency response tests, then investigating laminated plates and finally built-up structures. Core-filled sandwich panel structures were also tested. All of these tests used PZT piezoceramics as both actuators and sensor in pulse-transmission mode. Separate experiments were performed to evaluate a method that used "self-sensing" PZT actuators.

4.4.1 Narrow coupon tests

The first set of experiments was conducted on narrow composite coupons. The laminates used for this present research, both for control specimens and those with simulated damage, were manufactured during previous tests that explored frequency response methods as a means of damage detection, and were re-used to compare directly the effectiveness of the two methods [150]. The specimens were 25 x 5 cm rectangular $[90/\pm45/0]_s$ quasi-isotropic laminates of the AS4/3501-6 graphite/epoxy system, which were clamped on one end to match the boundary conditions from the previous research (however experimentation proved that the boundary conditions around the frame of the specimen had no effect on the Lamb wave traveling between two piezoceramic patches). Three PZT piezoceramic patches were affixed to each specimen, as shown in **Figure 4.5**, using 3M ThermoBond™ thermoplastic tape so that they were firmly attached during testing, but could be removed afterwards to recover the specimens for future tests. The PZT was cut into 2 x 0.5 cm patches so that the longitudinal wave would be favored

over the transverse one, and three patches were used on each specimen to actuate and to measure the transmitted and reflected waves. Both the actuation and the data acquisition were performed using a portable NI-Daqpad™ 6070E data acquisition board, and a laptop running Labview™ as a virtual controller. A Labview™ VI-file, seen in **Appendix E**, was created which would load an arbitrary waveform from Matlab™ and output it at the desired frequency and amplitude, while simultaneously acquiring data on four channels at 600,000 samples per second. The output channel was connected directly to the actuating PZT, generating the desired waveform with an amplitude of 10V. The first input channel, which served as the trigger for all of the channels, was connected to the output channel through an attenuator to scale the amplitude down by two orders of magnitude, two others were connected to the sensing piezoceramic patches, and the final channel was connected to a PZT sensor not attached to the specimen to serve as a control channel in order to zero out drift. A single pulse of the optimal signal found in the previous section, shown in **Figure 4.6**, was sent to the driving PZT patch to stimulate an A_0 mode Lamb wave, and concurrently the strain-induced voltage outputs of the other two patches were recorded for 1 ms to monitor the wave propagation.

The data was then passed to Matlab™ where the drift was filtered out and the waveforms could be compared and analyzed within two specialized toolboxes. In the signal processing toolbox the waves could be superimposed, and a peak detector was used to determine accurately the time of flight for each signal, and the delay in time of arrival between two specimens. Subsequently, in the wavelet toolbox a Morlet wavelet was used to perform a time-frequency decomposition of the data. By plotting the magnitude of the wavelet coefficient at the peak driving frequency, the energy remaining from the input signal could be compared [151]. This procedure was carried out for three of each specimen types at a driving frequency of 15 kHz.

4.4.2 Sandwich beam tests

Analogous experiments were performed on sandwich coupons to that of the narrow laminates in order to test the effect of various types of core materials on the propagation of Lamb waves. Four different cores were used: low and high density (referred to as LD and HD) aluminum honeycomb, Nomex™, and Rohacell™, all seen in **Figure 4.7**. Each specimen contained two facesheets identical to the undamaged laminates in the previous section surrounding a 2 cm thick core, which were adhered using FM-123 film adhesive in a secondary curing process [110]. Two controls and two damaged specimens of each type were manufactured for testing. In the damaged specimens, a 5 x 2.5 cm piece of Teflon was placed between the adhesive and the core in a central 2.5 cm region during the cure so that the facesheet would not bond to the honeycomb to simulate a delamination. An additional specimen was also manufactured with the high density aluminum core that had a 2 cm diameter circular piece of Teflon placed between the layers on either side so that it was indistinguishable from the controls by sight. This specimen was used for a "blind test" of the proposed Lamb wave damage detection method, where it was tested alongside the two control specimens to determine which had the artificial flaw. The test setup and data analysis procedure for the sandwich beam experiments were identical to that of the thin specimens with the exception of the driving frequency, which was determined to be more effective at 50 kHz for these tests.

4.4.3 Stiffened plate tests

The next set of experiments examined damage detection in more complex stiffened specimens using Lamb waves. Laminated plates were manufactured similarly to the ones from the previous sections, however these specimens included a secondary cure in which ribs were

bonded across the center of the plate using Cytec™ FM-123 film adhesive. Three different configurations of ribs were tested during this section of research, as seen in **Figure 4.8**. The first had a thin 2.5 cm wide aluminum C-channel rib with 1.2 cm tall webs, which was adhered to the laminate with the flat side facing down and the channel parallel to the sensors. The second configuration used two scrap pieces of the same composite laminate, one 2.5 cm wide and the other 1.2 cm wide, which were bonded with FM-123 in a pyramid-like stack in the center of the laminate, again parallel to the sensors [110]. The final configuration was identical to the second one, except it had a 2.5 cm square Teflon strip inserted between the stiffening rib and the composite to create an artificial delamination in the center of the rib. For each of the configurations, actuating and sensing PZT sensors were affixed to opposite sides of the rib on the edges of the laminate in three locations—one pair that was centered on the laminate and one pair on either side of the centerline spaced 7.5 cm away. The purpose of these experiments was first to examine how the rib would effect the propagation of the Lamb waves, then to compare the propagation through ribs of various stiffness, and lastly to ascertain the feasibility of locating a delaminated region under a rib by comparing the received signal with undamaged regions. The test setup and data analysis procedure for the stiffened panel experiments were identical to that of the thin specimens with a driving frequency of 15 kHz.

4.4.4 Composite sandwich cylinder tests

The next level of complexity involved examining a relatively large built-up structure, a cylinder with a 40 cm diameter and length of 120 cm, seen in **Figure 4.9**, which was constructed during previous research as a composite micro-satellite structure [152]. The two facesheets of the sandwich structure were manufactured from the same composite material as the other tested

specimens and were of similar layup, and a 2.5 cm thick low-density aluminum honeycomb was bonded between them. An identical setup to that used on the other specimens was used on this cylinder to determine the feasibility of detecting known damaged regions in a large curved built-up structure. First, in a control region with no visual damage, an actuating PZT wafer was placed on one end of the cylinder, and then sensing piezoceramic patches were placed down the length of the cylinder every 10 cm for 60 cm. These tests would not only provide a controlled time of flight for the structure, but would also provide data for the attenuation of the wave in a representative structure. Next sensors were placed every 10 cm circumferentially over a 30 cm span to examine the attenuation of the Lamb wave signal in a curved section. Lastly, piezoelectric sensors were adhered in positions 10 cm away longitudinally and at 5 cm increments circumferentially to attempt to quantify how far away from the main propagation channel the sensors could be placed to still sense a reliable measurement. Once again, the data analysis procedure for these experiments were identical to that of all the others, with a driving frequency of 40 kHz in this case because of the honeycomb core and slightly different layup.

4.4.5 2-D plate tests

The final test performed in pulse-transmission mode was to scan 2-D laminated plates for damage. Graphite/epoxy panels measuring 30 x 30 cm were manufactured similarly to those of the previous experiments, but were not milled into smaller specimen for these experiments. Square PZT sensors measuring 1.5 cm on each side were affixed along the perimeter of the laminate, in the center of each side as seen in **Figure 4.10**. The driving pulse was sent to actuate each PZT piece one at a time at 15 kHz, and simultaneously readings of resulting strains were

measured from each of the other three patches; this would occur four times, each time actuating a different piezoelectric sensor. These results were also decomposed using the Morlet wavelet.

4.4.6 Self-sensing tests

As an alternative to pulse-transmission, some preliminary testing was also performed for the pulse-reflection of Lamb waves. Theoretically, this method should provide more information about damage location, since the time of flight of damage from reflection sites would be recorded so a triangulation could be performed. The setup for these tests was identical to the configuration from the 2-D plate tests, with PZT sensors placed in the center of each side. The only difference for these tests was that each PZT piece would serve as both a sensor and receiver simultaneously, collecting the reflected as well as the transmitted strain data for each pulse actuation. This "self-sensing" capability was achieved by using a full bridge circuit, represented in **Figure 4.11**, which was developed in the literature and adapted for use in these experiments. This circuit design would allow the data acquisition equipment to monitor the 10 mV strain measurements from the PZT without being overwhelmed by the 5 V driving signal [153].

4.5 Results

This section presents the results for analytical and experimental procedures previously described in this chapter. The analytical results are in the form of time of flight measurements taken from the movie files created by the finite element solution in ABAQUS™. Several snapshots of the propagating waves are also displayed. The experimental results summarize the comparison of the wavelet-decomposed signal between the control specimen and the specimens with various forms of damage. The presence of damage in the specimens caused the amplitude

of the wave coefficients to decrease significantly, as well as slowing the wave velocity for many of the specimens. These results are presented for narrow coupons, sandwich beams, stiffened panels, a composite sandwich cylinder and a 2-D laminated plate. A discussion of these results is presented in the following section.

4.5.1 Analytical results

The first set of analytical results were obtained from the thin layered laminated medium finite element code written by Prosper at MIT as described previously, which accurately characterized the cross-sectional variation due to the Lamb wave, however was incapable of analyzing changes in the width direction. A representative plot showing the vertical displacement over time at a point 25 cm away from the 60 kHz actuation point can be seen in **Figure 4.12**. The solid line in this figure represents the undamaged graphite/epoxy specimen that appears to have a wave velocity of around 1.95 km/s, while the broken line is a simulation of the Lamb wave traveling at 1.85 km/s in a specimen with a 2.5 cm center delamination. There also appears to be a slight change in wave frequency content for the Lamb wave in the delaminated specimen.

The next set of results were obtained from the finite element models created in ABAQUS™, which simulated the behavior of the Lamb waves as they traveled across the thin-shelled laminate. The products of these analyses were movie files that animated the vertical displacement of the nodes over time as the Lamb waves propagated from the loaded nodes. A series of still shots of a Lamb wave propagating in a control model can be seen in **Figure 4.13** and for a delaminated model in **Figure 4.14**. A summary comparing the recorded times of flight for each of the models that were analyzed can be found in **Table 4.1**. The FE results did not

show much of a change between the control and cracked models for time of flight, however there was a noticeable reflected wave traveling from the cracked region after the Lamb wave had passed over it. The model with the through-hole exhibited a slight change in time of flight, and a small reflected wave was observed as well. For both delamination models there was a significant increase in the time of flight due to the damage, and in addition, reflected waves were generated which had almost half the amplitude of the traveling wave. Additionally, the model with the asymmetric delamination created two wave fronts traveling at different speeds, which began to interfere with each other as they continued down the laminate. These FE results appear to be consistent with the experimental results, as will be further discussed in the following section.

Comparable results were found for each of the sandwich beam models, control and stiffened plate models and curved sandwich panel models. The time of flight measured for each of these models is documented in **Table 4.2**. Perhaps the most interesting results were discovered for the stiffened plate models. First, **Figure 4.15** displays the Lamb wave as it propagated across a plate with no stiffener attached as a controlled reference. Next, as seen in the series of stills for the plate with bonded composite stiffeners in **Figure 4.16**, as the wave traveled radially from the actuation region and reached the stiffened region, a uniform reflected wave began to propagate back towards the actuator, while the forward moving wave continued towards the opposite side, briefly speeding up in the stiffened region and shrinking in amplitude. For the stiffener with a delaminated region, seen in **Figure 4.17**, when the Lamb wave reached the stiffener it continued at the same speed and amplitude through the delaminated region while changing speed and displacement amplitude in the non-delaminated region. The fascinating result was that the delaminated "slot" caused a fringe pattern to appear in both the continuing and reflecting waves, which there were regions of maximum and minimum displacement amplitudes

radiating in constant angle intervals from the front of the delaminated area. The effect of a delaminated region in a curved sandwich panel can be seen by comparing the stills in **Figure 4.18** and **Figure 4.19**, where a very small amplitude wave propagates across the thick panel and is significantly reflected by the damage.

4.5.2 Experimental results

There were two sets of results obtained for both the thin coupons and the narrow sandwich beams. The first set of results included the raw time traces of voltage from the PZT sensor at the far end of the specimen. For the thin coupons, 1 ms of data was taken and the average peak voltage was approximately 20 mV. The time traces for one of each type of specimen along with a superimposed control specimen are shown in **Figure 4.20**, and **Table 4.3** summarizes the estimated time of flight for each of the specimens based upon the plots. Similarly, 500 μs of data was taken for the sandwich beams with an average peak voltage of approximately 10 mV. For these specimens, time traces of each control beam are plotted against their delaminated counterpart in **Figure 4.21**. In each of these plots, a parasitic portion of the sent signal leaking across the data acquisition board can be seen at the beginning of the time trace. Since the channels were all triggered at the 5V peak voltage, exactly half of the sent signal is visible so this became a convenient way to measure the time of flight. The second set of results for each specimen group was the outcome of the wavelet decomposition. For each specimen, the "bleed–through" portion of the signal was filtered out, and the wavelet coefficient magnitude of the dominant frequency (15 kHz for the thin coupons and 50 kHz for the beams) was plotted over time. For the thin coupons, **Figure 4.22** compares these coefficients, and thus the transmitted energy, for one of each type of specimen. Finally, **Figure 4.23** displays the

wavelet coefficient results for the "blind test," comparing the two high density aluminum core control specimens with one known and one unknown damaged specimen.

Similar results were found for the built-up composite structures. The voltage time traces for each of the stiffened plate tests can be seen in **Figure 4.24** and the complementary wavelet plots in **Figure 4.25**. As described in the experimental procedure section, several sensors were placed along the composite sandwich cylinder at regular intervals. The time traces and wavelet plots for the axial propagation of the Lamb waves can be seen in **Figure 4.26** and **Figure 4.27** respectively, and **Figure 4.28** for the circumferentially traveling waves. Similar plots for the sensors along the path of the delaminated region are seen in **Figure 4.29** and **Figure 4.30**. The last sets of results are for the 2-D plate specimen. The series of time traces for each of the four independent tests actuating with different piezoceramics can be seen in **Figure 4.31** and the wavelet plots in **Figure 4.32**. The time trace for the single "self-sensing" test performed at 45 kHz can be found in **Figure 4.33**. This test proved the feasibility of an actuator being used as a sensor as well, however the reflected signal was quite small, and as elaborated in the discussion section, more work would need to be performed to use this kind of sensor in future tests.

4.6 Discussion

The following sections provide a discussion to evaluate the significance of the Lamb wave method tests. The effect of various types of damage on the propagation of Lamb waves is quantified for both the analytical models and the experimental procedures. The results of the FE models and physical tests are then compared, and conclusions are drawn about their accuracy. Finally, suggestions are provided for the potential role of Lamb wave methods within a structural health monitoring system architecture.

4.6.1 Effect of damage on Lamb waves

There are generally five goals for damage detection, each of which is gained with increasing difficulty and complexity. The first is the determination of the presence of damage in a specimen. The second is an estimation of the extent of severity of the damage. The third goal is to be able to differentiate between different types of damage. The fourth is to be able to calculate where the damage is located. The final one is to estimate the dimensions of the damage. It appears that Lamb wave methods carry enough information potentially to meet all of these goals with a strategically placed array of sensors and suitable processing codes, however the current scope of this research focuses on the first two goals only.

The results from the narrow coupon tests clearly show the presence of damage in all of the specimens. First of all, when the time traces of all of the control specimens were overlaid, there was a high degree of visible correlation, especially for the first half of the voltage time trace. The slight variation in the second half of the data can be attributed to the reflected signals returning from the far end of the specimen and passing under the PZT sensor again, which may encounter a slight cutting bias in the composite to cause a change in phase. Of the artificially damaged specimens, the Teflon-induced delamination was most easily quantified. When compared to the control specimens, these time traces appear at the same phase and frequency, only having been delayed about 55 μs due to the damage. For the other types of damage the frequency often remained the same, however there was a large reduction in amplitude, and a large and varying change in phase. Time traces were reproducible within a single specimen, although the results were not consistent across multiple specimens with identical forms of damage. This was due to the scatter and reflecting of the waves on the various damage features, which may not be identical specimen to specimen. This makes a "damage signature" difficult to

define. The most distinctly altered signal was that of the through-hole, having the same diameter as the actuator and sensor widths, which had the smallest sensed voltage amplitude of all the specimens. The most obvious method to distinguish between damaged and undamaged specimens however is by regarding the wavelet decomposition plots. The control specimens retained over twice as much energy at the peak frequency as compared to all of the damaged specimens, and especially contained much more energy in the reflected waves. The loss of energy in the damaged specimens again is due to the dispersion caused by the micro-cracks within the laminate in the excitation of high-frequency local modes.

The sandwich beam results were more difficult to interpret, due to the damping nature of the cores, which significantly reduced the signal captured by the PZT sensors. The high density aluminum core, which was the stiffest of the four tested, provided the clearest results; the other specimens yielded decreasing magnitude voltages as the stiffness decreased thus increasing the damping factor. There were two basic trends across all the specimens. The first was that the responses of the control specimens were larger than those that were delaminated for each core type. This is most likely due to the loss of energy of the wave in a local mode over the delaminated region. The second trend was the appearance of more reflected waves after the initial pulse in the time trace in the delaminated specimens, which again was probably due to other higher frequency modes being excited in the region of reduced thickness and dampening. The most significant result with regard to the viability of the Lamb wave method came from the "blind test." Four high density aluminum-core beam specimen were tested, one of which had a known delamination in its center, while of the remaining three specimens it was unknown which contained the circular disbond and which two were the undamaged controls. By comparing the four wavelet coefficient plots in **Figure 4.23**, one can easily deduce that the two control

specimens are the ones with much more energy in the transmitted signals, while the third specimen (Control C) obviously has the flaw that reduces energy to a similar level to that of the known delaminated specimen. This test serves as a testament to the viability of the Lamb Wave method being able to detect damage in at least simple structures.

Similar effects of damage were observed in each of the built-up composite structure cases. In the stiffened plates, the Lamb waves were able to propagate across the stiffened region without much dispersion since they were well bonded and uniform across the specimen. By comparing the stiffened plates with and without a delamination, a reproducible signal was transmitted across each of the intact portions of the composite stiffeners while it was obvious that the signal traveling through the delaminated region was propagating at a different speed. Finally, in the composite sandwich cylinder, the impacted region caused severe dispersion of the traveling Lamb wave, which in turn attenuated the received signal at each sensor further down the tube. For all of the tested specimen, all forms of damage were easily perceived by comparing the time of flight and wavelet coefficient magnitudes for the control versus damaged signal. This result contributes to the argument that Lamb wave techniques could provide valuable information for the in-situ inspection of composite materials.

4.6.2 Comparison of analytical and experimental results

Good correlation was found between the FE and experimental results. By comparing **Table 4.1** with **Table 4.3** a margin of error below 6% is found between the predicted and measured results for each of the narrow coupon specimens besides the delaminated ones, which were below 25% error. The best agreement was found between the control model and the analog experiment since the representative damage in the test specimens did not correspond exactly to

how they had been modeled, and often there were multiple forms of damage present in each specimen. It was difficult to compare the built-up composite structure experiments with the FE results for two reasons: firstly because the received signal was highly attenuated; and secondly because at the higher driving frequencies in the stiffer structures, the Lamb waves traveled much quicker so that the response wave was received within the noise of the actuating signal (as described in the above section on parasitic capacitance). While the time of flight was difficult to compare for these structures, the trends observed in each of the models was verified by experimental results. Lamb waves propagating in sandwich structures of any core material demonstrated much lower displacement amplitudes than those traveling in thin laminates. More attenuation due to higher dispersion was observed in Lamb waves propagating in the circumferential direction of curved models and specimens. Lastly, good correlation was found between the experimental results and the FE results for the times of flight in the stiffened plate with and without delamination, with margins of error of 10% and 2% respectively. The results for Lamb wave propagation within laminates appeared to have matched well enough to be able to use a simple structural FEM to simulate the waves' interaction with damage with confidence for design purposes. For sandwich structures some of the effects were captured by the 2-D shell model, however a 3-D or plain-strain model was necessary to capture all of the effects of Lamb waves traveling at different velocities in various layers. Neither of these types of models for composite material are practical to be incorporated into a structural model for a vehicle, so more investigation should be performed in this area in the future to design a Lamb wave system for a composite sandwich structure based on FEA.

4.6.3 Role of Lamb wave methods in SHM

Lamb wave techniques have good potential for implementation in a SHM system. These methods provide useful information about the presence and extent of damage in composite materials, hold the potential of determining location and type of damage, and can be applied to a structure with conformable piezoelectric devices. The major disadvantage of this method is that it is active; it requires a voltage supply and function generating signal to be supplied. This can be complicated in a large structure, especially if the SHM system is to be implemented wirelessly; it has been suggested in the literature however that PZT can be actuated remotely using radio frequency waves [96]. Another difficult requirement is the high data acquisition rate needed to gain useful signal resolution. If a system is sampling at 0.5 MHz from several sensors, a large volume of data will accumulate quickly; this implies the need for local processing. The data acquisition capabilities dictate the limitations of flaw size able to be resolved by a system using this method. In order to conserve power and data storage space, the Lamb wave method should most likely be placed into a SHM system in conjunction with another passive detection method, such as a frequency response method. The piezoelectric patches used to actuate the Lamb waves could passively record frequency response data until a certain threshold of change is surpassed, and then trigger the generation of Lamb waves to gain more specific data about the damaged region. Three to four piezoelectric multi-functioning actuator/sensor patches would be placed in the same vicinity in order to be able to triangulate damage location based upon reciprocal times of flight and reflected waves. Another possible scheme could rely on long strips of piezoelectric material, which would be able to send and receive wide uniform Lamb waves, and integrate the received and reflected energy in order to determine the state of the material between them. The separation between sensing patches in either of these configurations would

depend on several parameters such as the material properties, damping characteristics and curvature of the structure, which for flat areas could be as large as 2 meters apart [96]. The detailed specifications of the Lamb wave driving parameters to be used for a particular application would be designed by the procedure described in the optimization section.

In the previous discussion sections, it has been shown that there is a good correlation between FE models and experimental results for Lamb wave propagation, so the effectiveness of this method in a particular application can be simulated using existing structural models with slight modifications. Lamb wave methods have demonstrated their effectiveness in detecting the presence of several forms of damage in a variety of shapes and constructions of composite components. From these experiments there are indications that these methods should be capable of measuring the severity, size and location of damage as well. For the delaminated stiffener for example, by integrating the energy present in a series of time steps the presence of delamination should be obvious due to the non-uniform wave front, while the fringe pattern in the transmitted and reflected wave should contain enough information to determine the width of the delamination. Similarly, for the impacted cylinder case, a time integration of the energy transmitted would clearly reveal the damage presence. The application of Lamb wave techniques to a SHM architecture will be discussed further in Chapter 6.

4.7 Conclusions

This chapter has explored the optimization and application of Lamb wave methods to damage detection in composite materials. A collection of equations is offered in order to optimize the driving parameters and actuator dimensions for testing. With these tools, an optimal configuration was selected for the experimental section of this research. Using this

procedure, several narrow graphite/epoxy specimens were tested with various forms of pre-existing damage, such as delamination, matrix-cracks and through–thickness holes. Similar tests were also performed on narrow sandwich beams using cores of various densities and stiffness. These tests demonstrated the feasibility of detecting several types of flaws in representative composite structures, and this method was validated successfully by a "blind test" of several beam specimens. Tests were also performed on built-up composite structures such as stiffened plates and curved sandwich structures. Analytical modeling of these specimens yielded similar results. Lamb wave techniques have the potential to provide more information than previously tested methods, such as frequency response methods, since they are more sensitive to the local effects of damage to a material than the global response of a structure. Similar to frequency response methods, their results are limited at higher frequencies, however their low frequency results should provide sufficient data to predict damage. The disadvantage of Lamb wave methods is that they require an active driving mechanism to propagate the waves, and the resulting data can be more complicated to interpret than for many other techniques. Overall however, Lamb wave methods have been found to be the most effective for the in-situ determination of the presence and severity of damage in composite materials of the methods examined in this thesis.

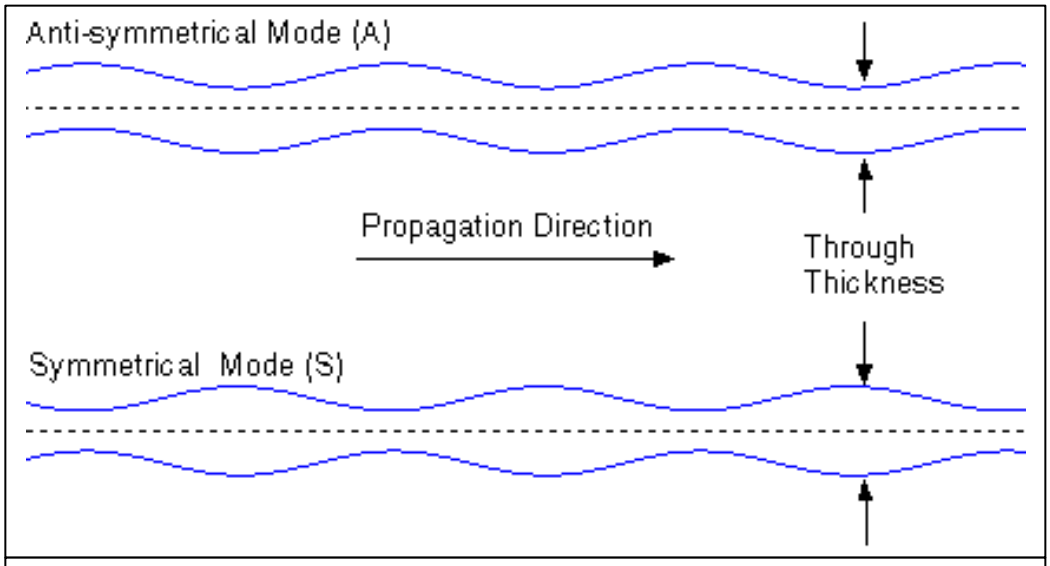

Figure 4.1: Graphical representation of *A* and *S* Lamb wave shapes

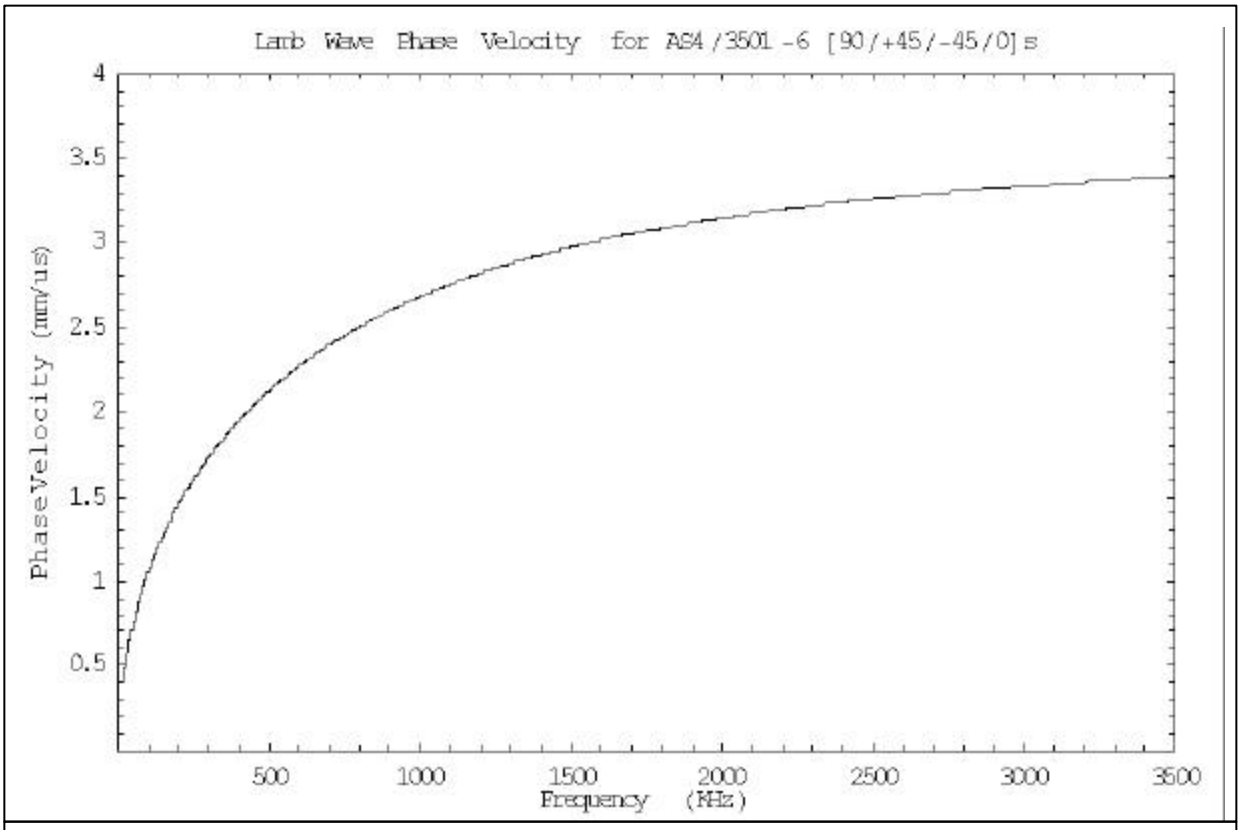

Figure 4.2: Phase velocity dispersion curve for the Ao mode of an 8-ply composite laminate

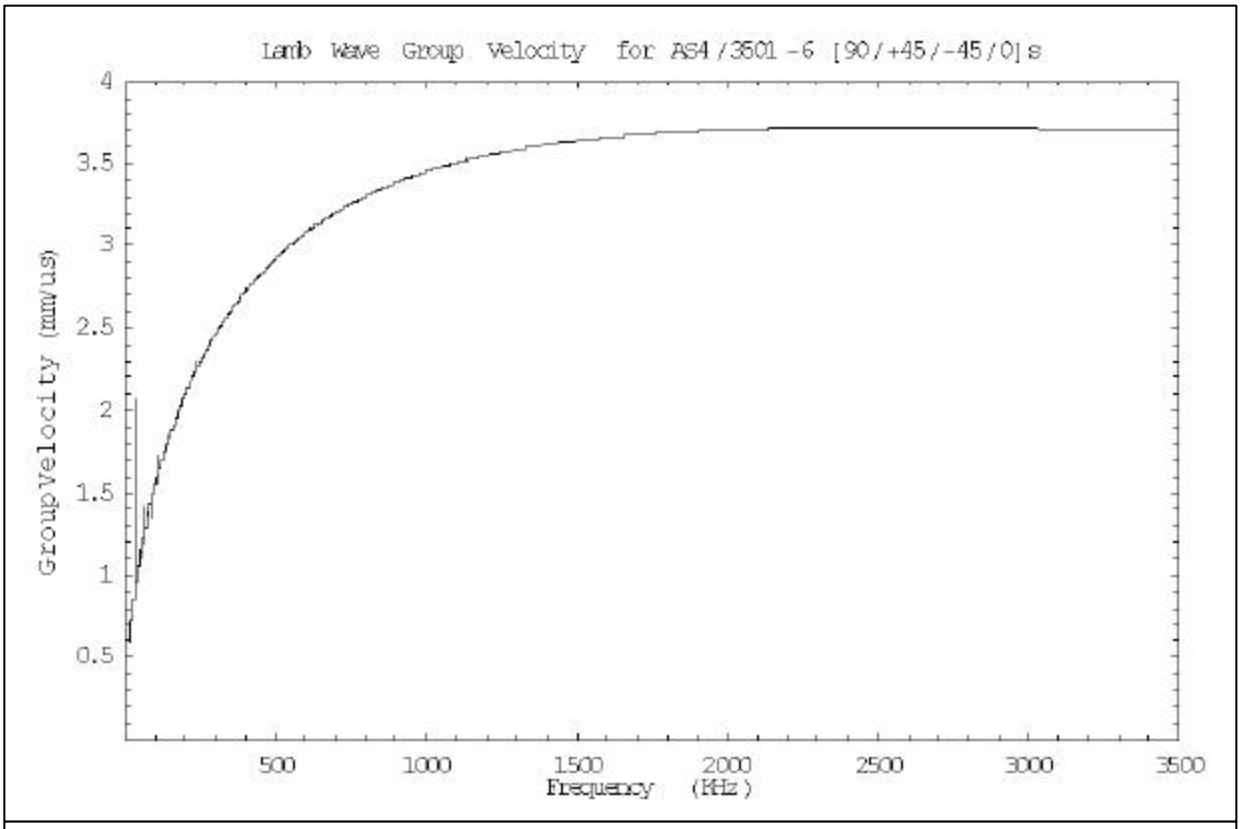

Figure 4.3: Group velocity dispersion curve for the Ao mode of an 8-ply composite laminate

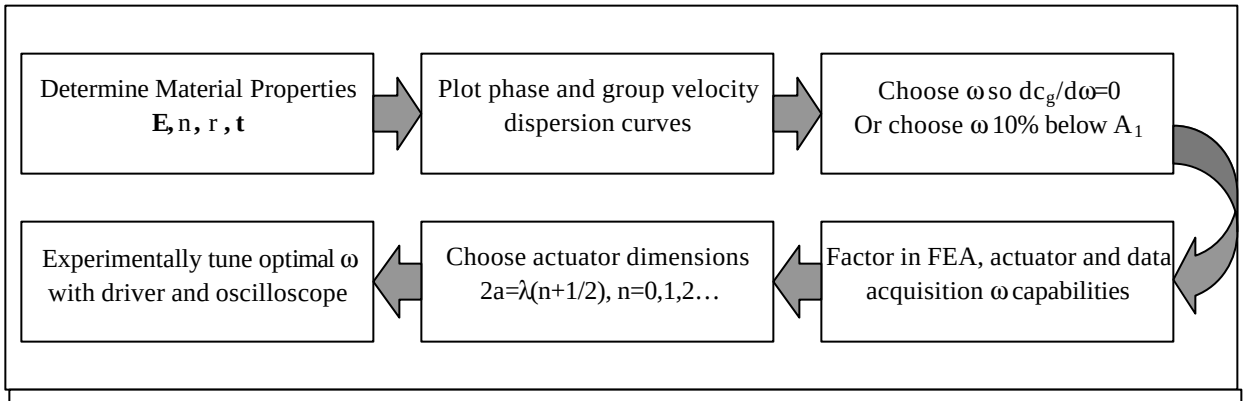

Figure 4.4: Lamb wave actuation frequency selection flow chart

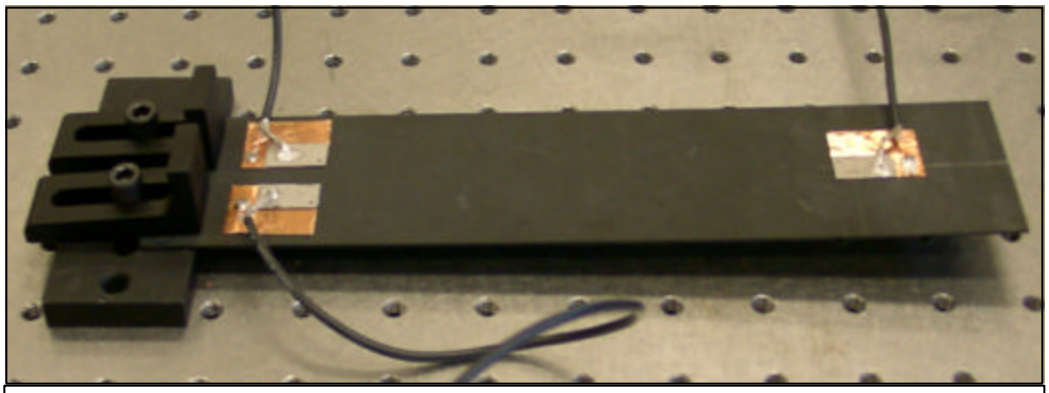

Figure 4.5: CFRP specimen (250mm x 50mm) with piezoceramic actuator and sensors

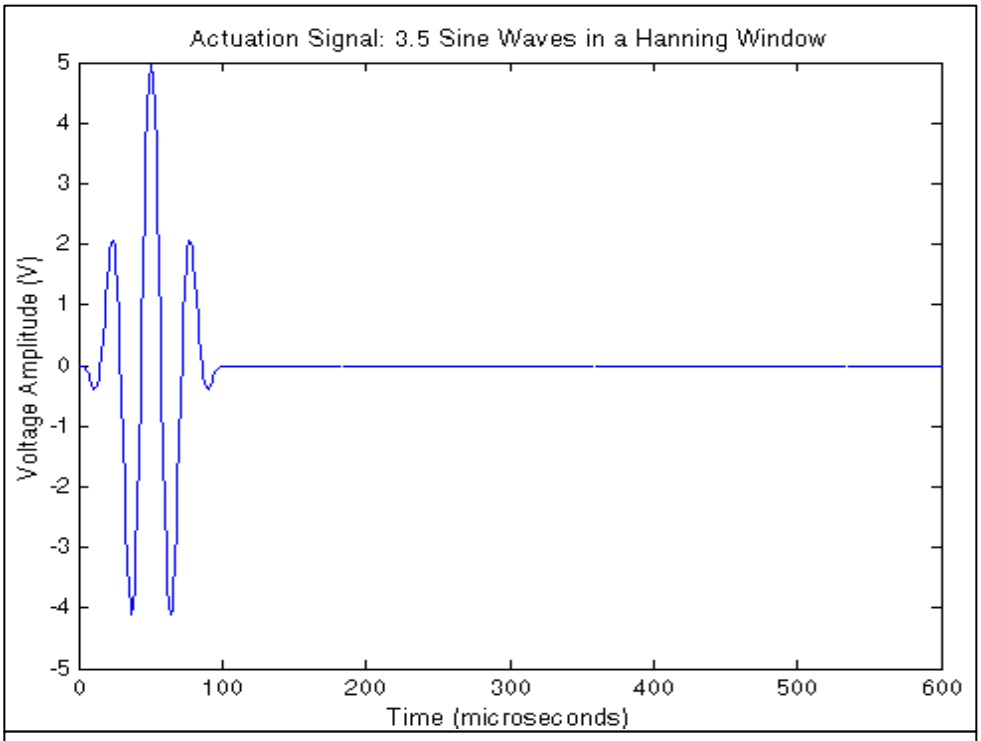

Figure 4.6: Actuation signal used to generate Lamb waves, 3.5 sine waves at 15 kHz

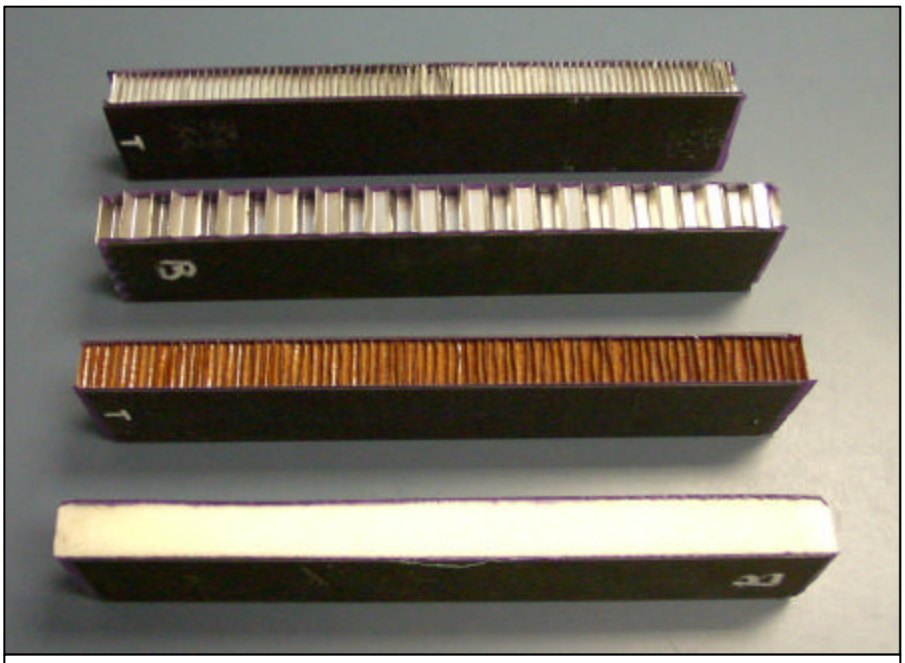

Figure 4.7: Sandwich beam specimens (250mm x 50mm) with various cores
Listed from top to bottom: high-density aluminum honeycomb, low-density aluminum honeycomb, Nomex and Rohacell

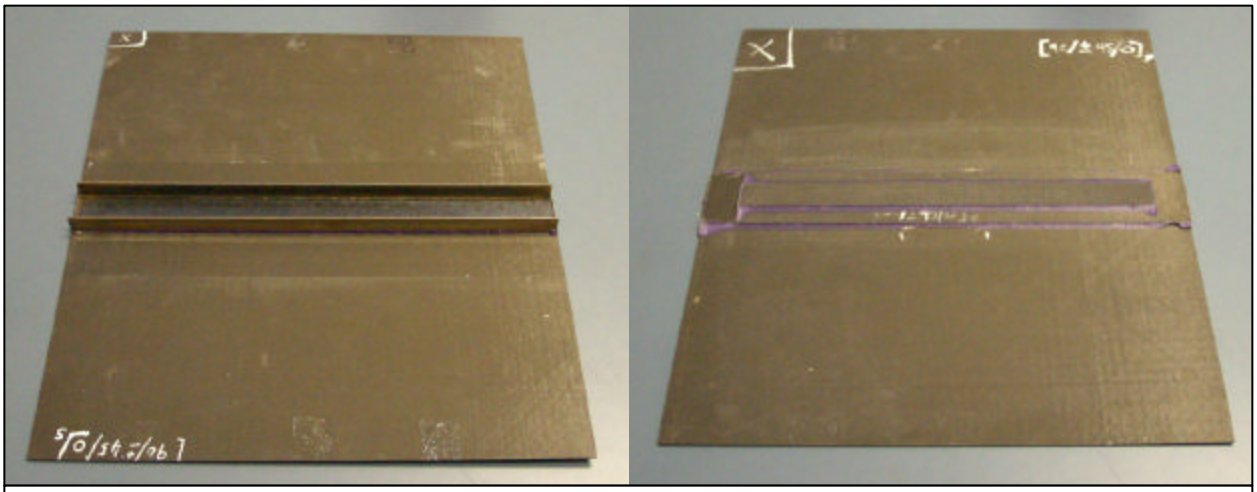

Figure 4.8: Composite plates (250mm x 250mm) with bonded stiffeners. On left, steel C-channel measuring 40mm x 250mm x 20mm. On right, CFRP doublers, 40mm x 250mm x 2mm (16 plies).

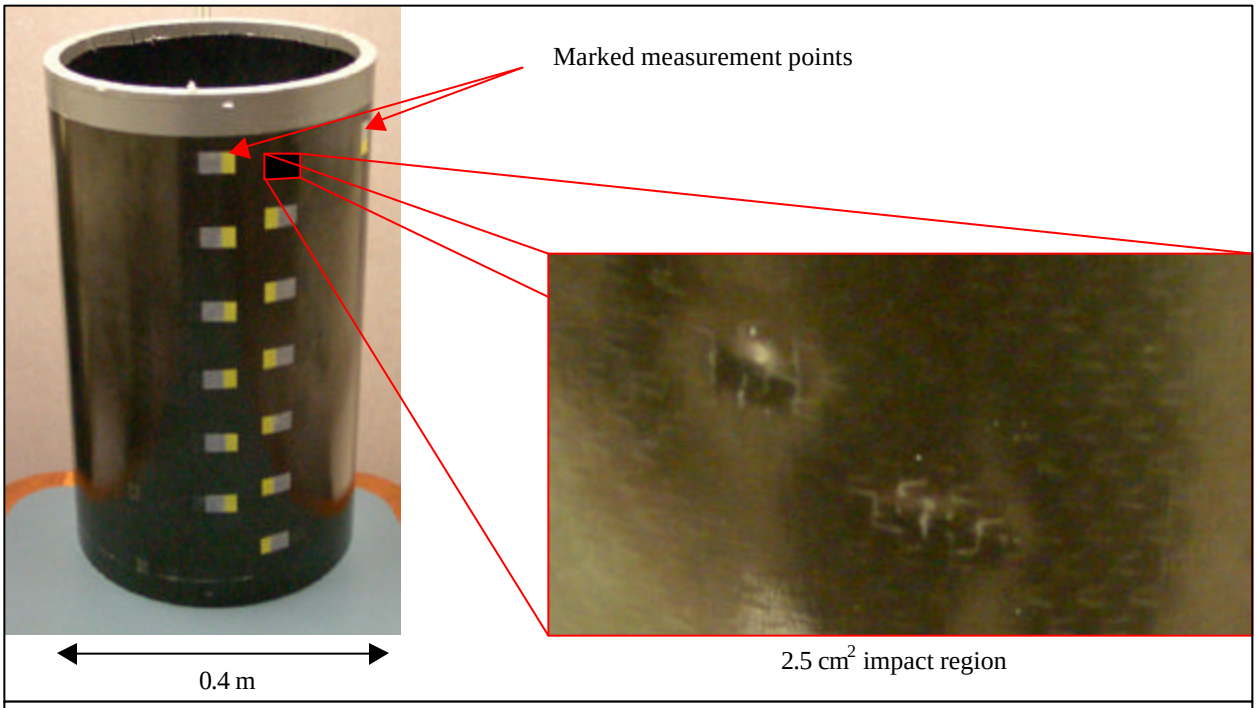

Figure 4.9: Composite sandwich cylinder with small impacted region

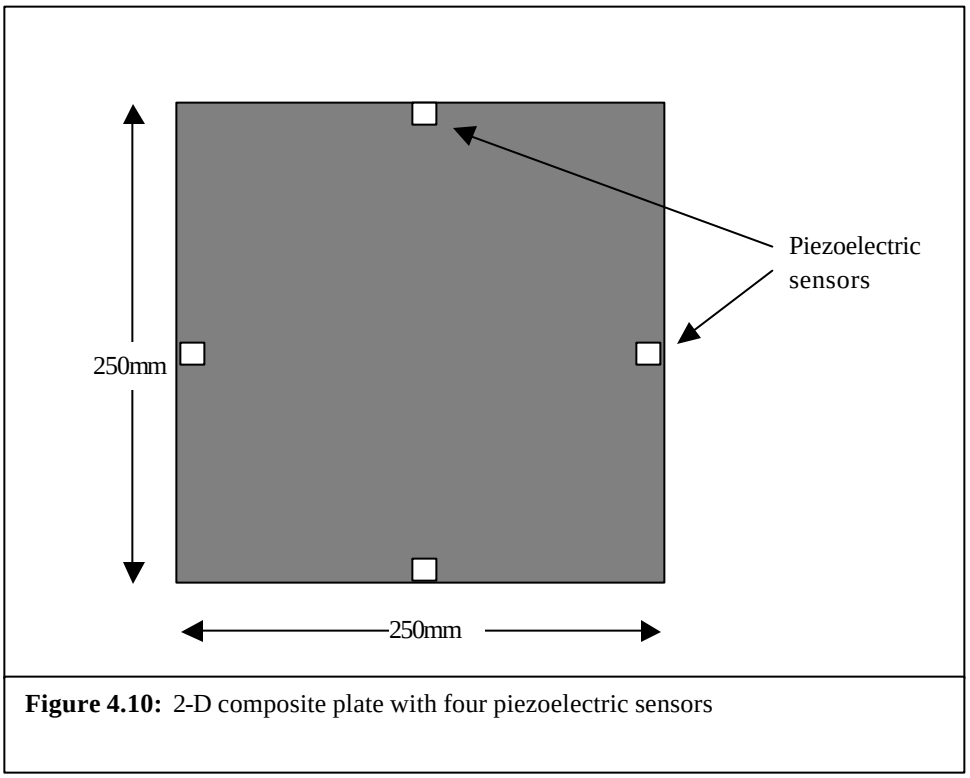

Figure 4.10: 2-D composite plate with four piezoelectric sensors

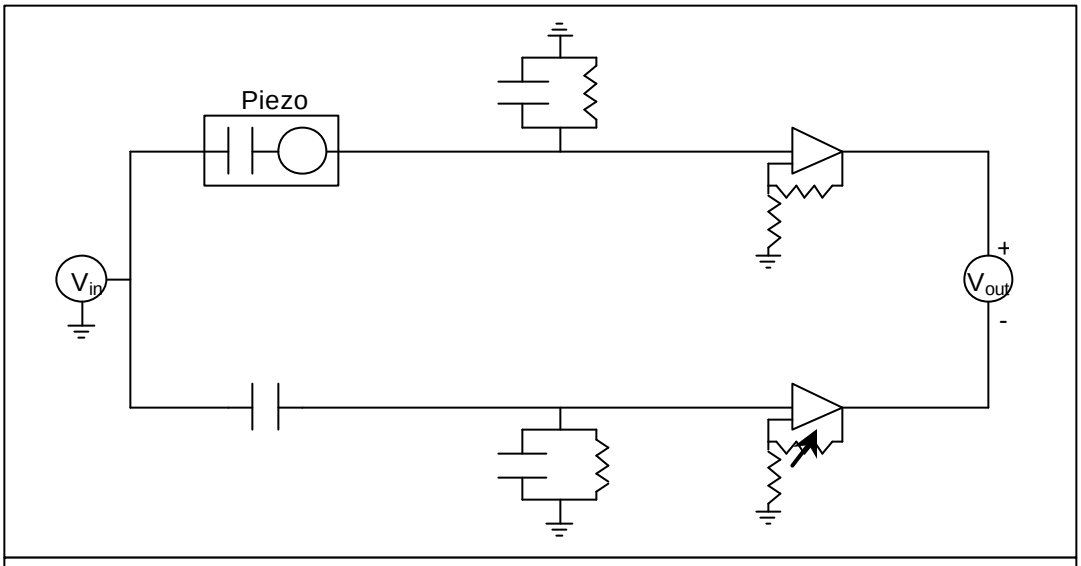

Figure 4.11: Self-sensing circuit allows piezoelectric actuator to sense reflected Lamb waves

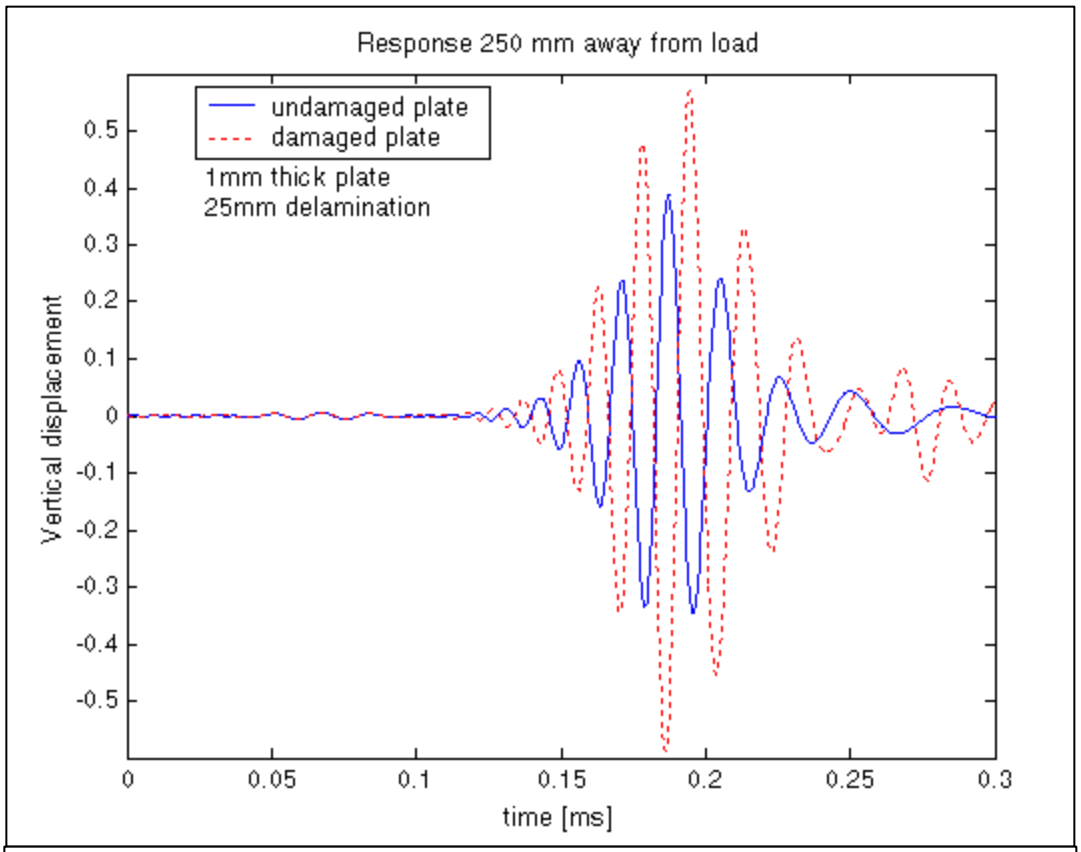

Figure 4.12: Preliminary analytical results for 60 kHz signal using Prosper code from MIT

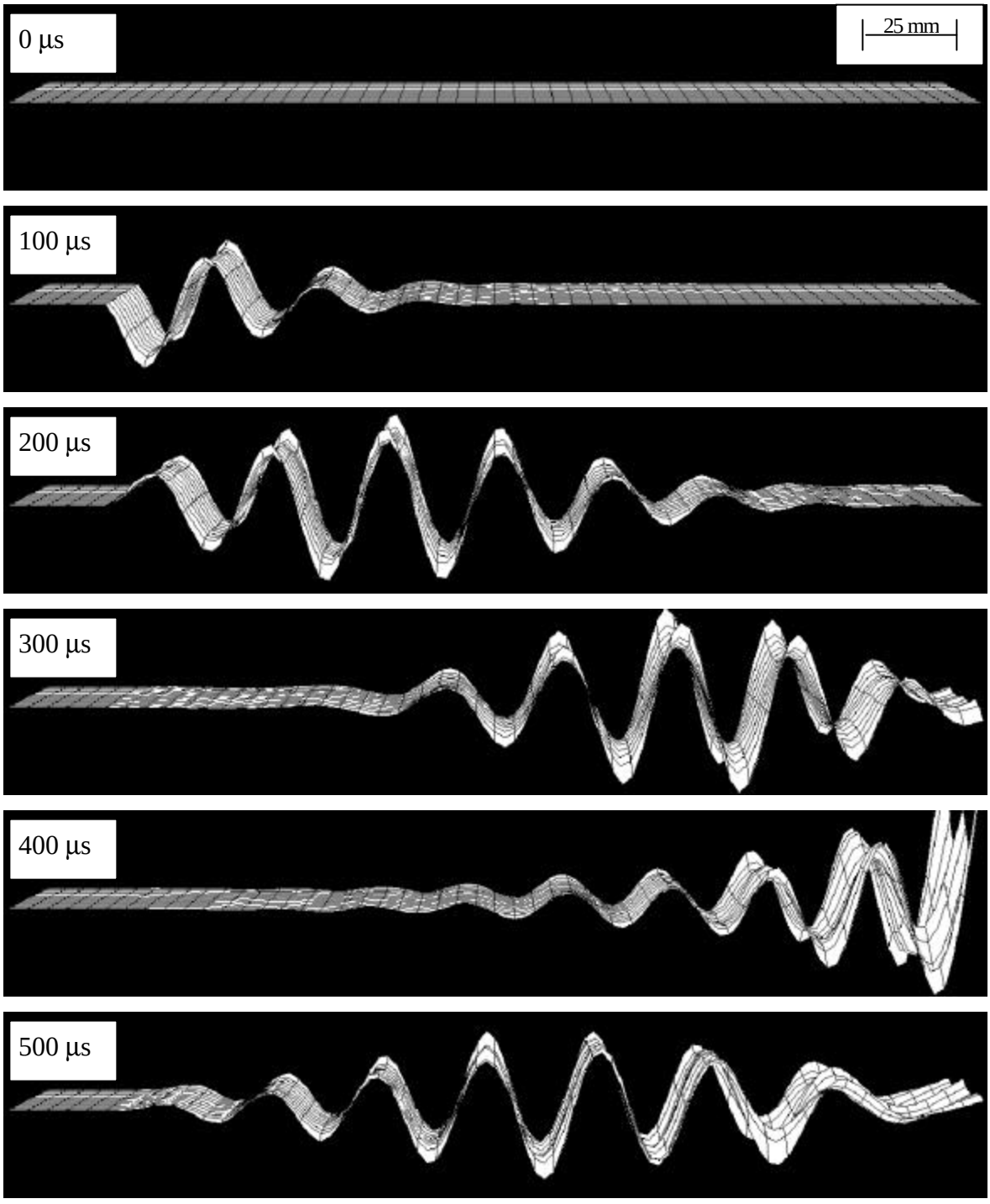

Figure 4.13: FEA results for narrow coupon with no damage at 100 microsecond intervals

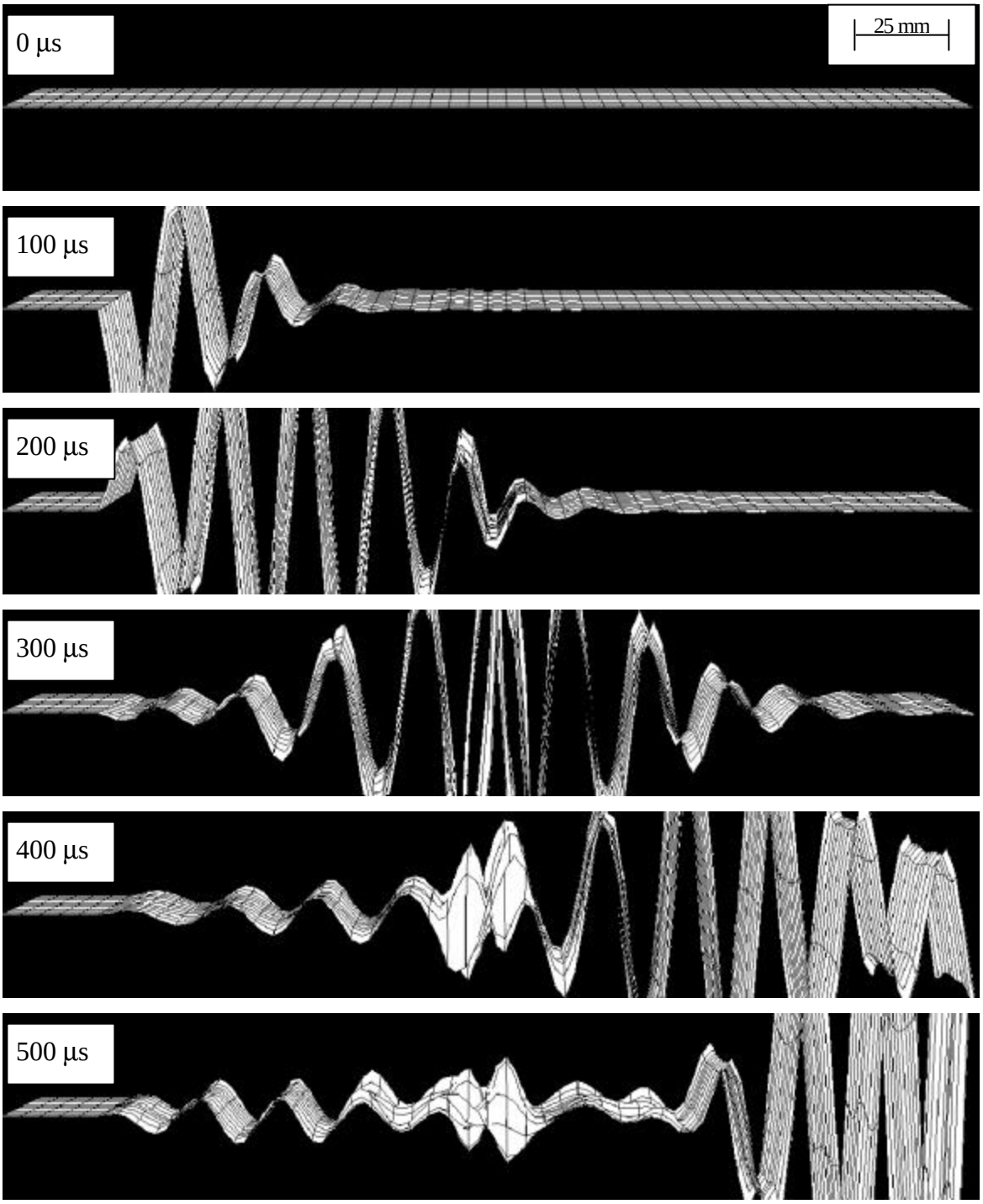

Figure 4.14: FEA results for narrow coupon with 25mm center delamination at 100 microsecond intervals

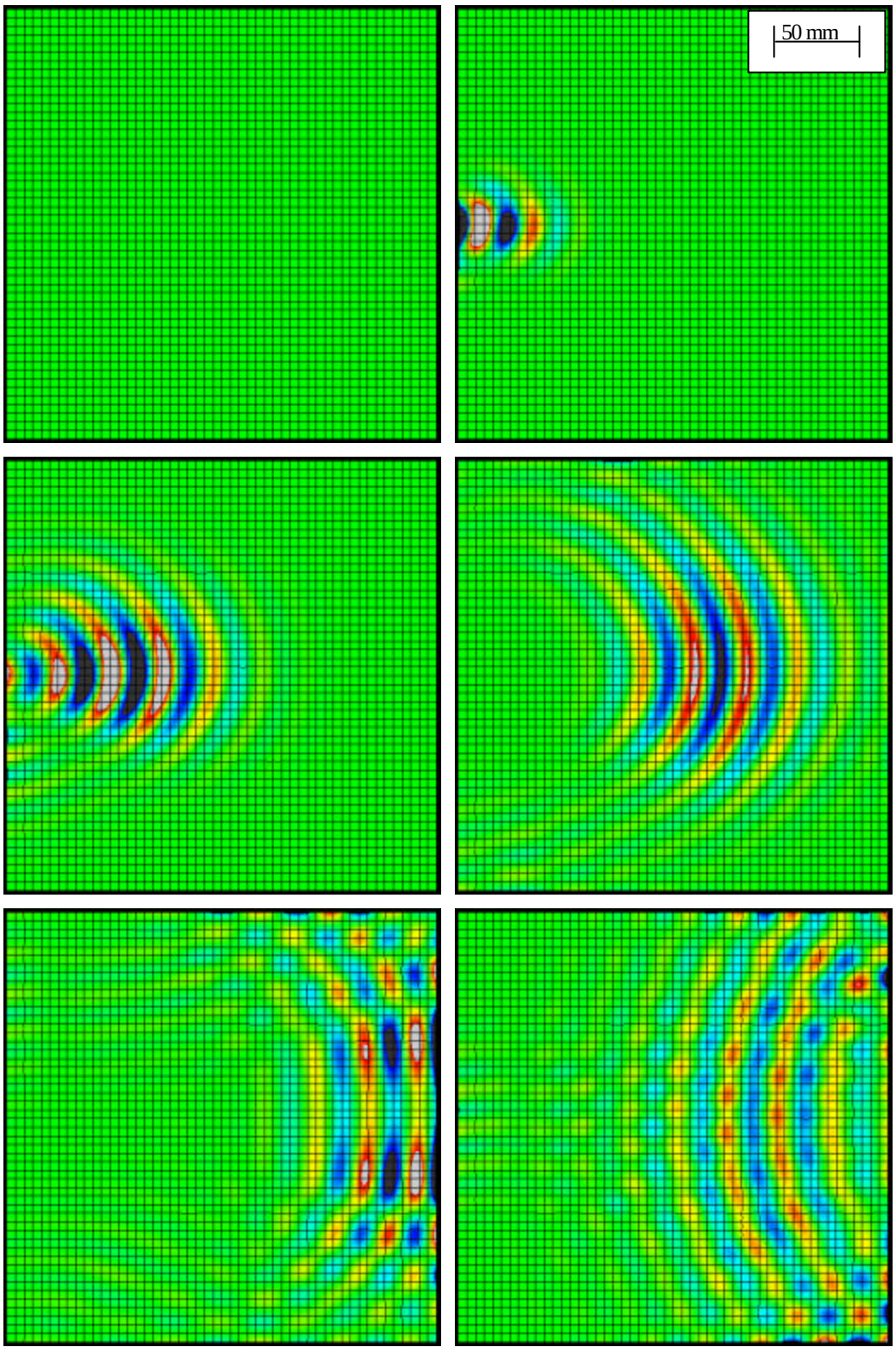

Figure 4.15: FEA results for 2-D plate with no stiffener at 100 microsecond intervals

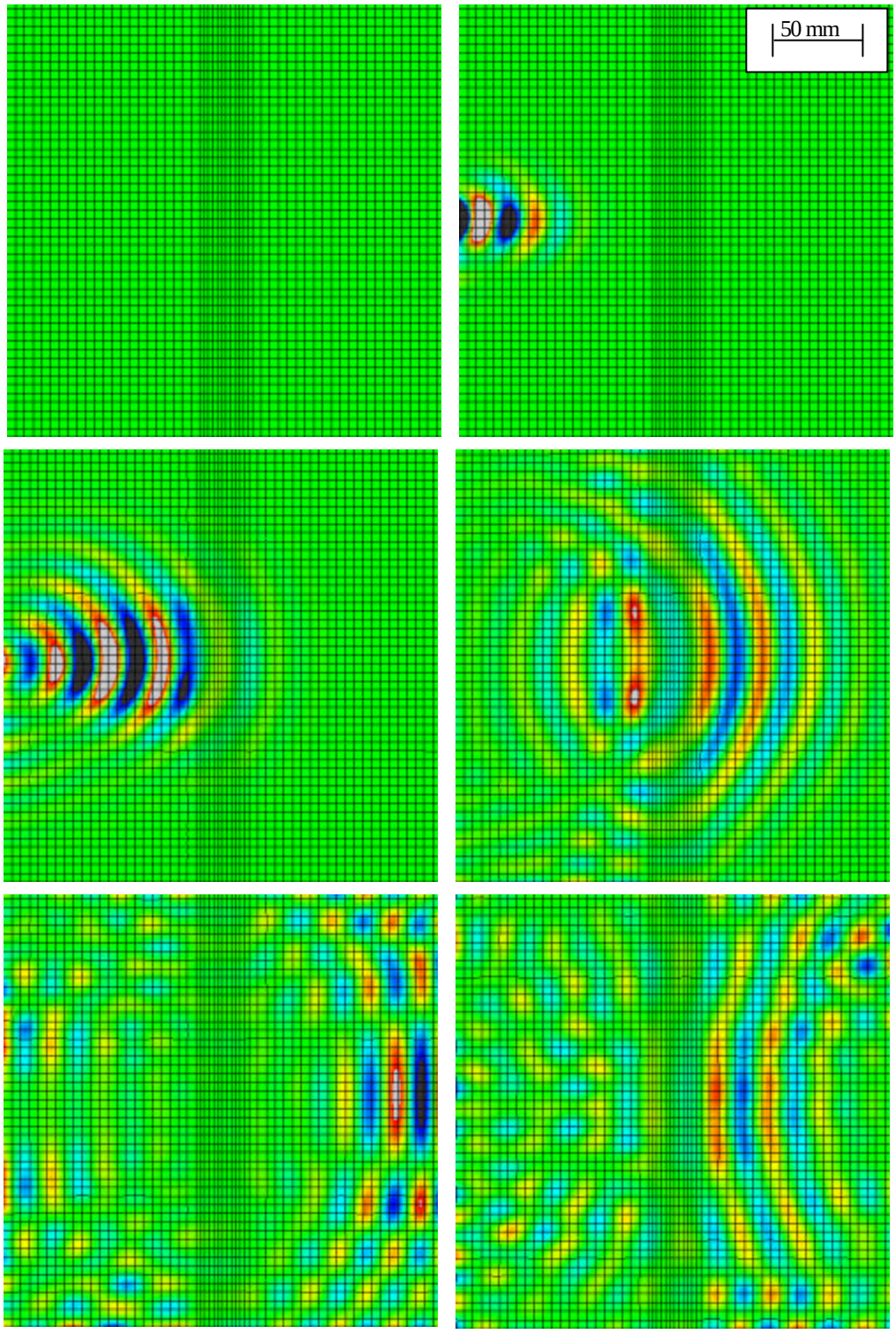

Figure 4.16: FEA results for 2-D plate with composite stiffener (no damage) at 100 microsecond intervals

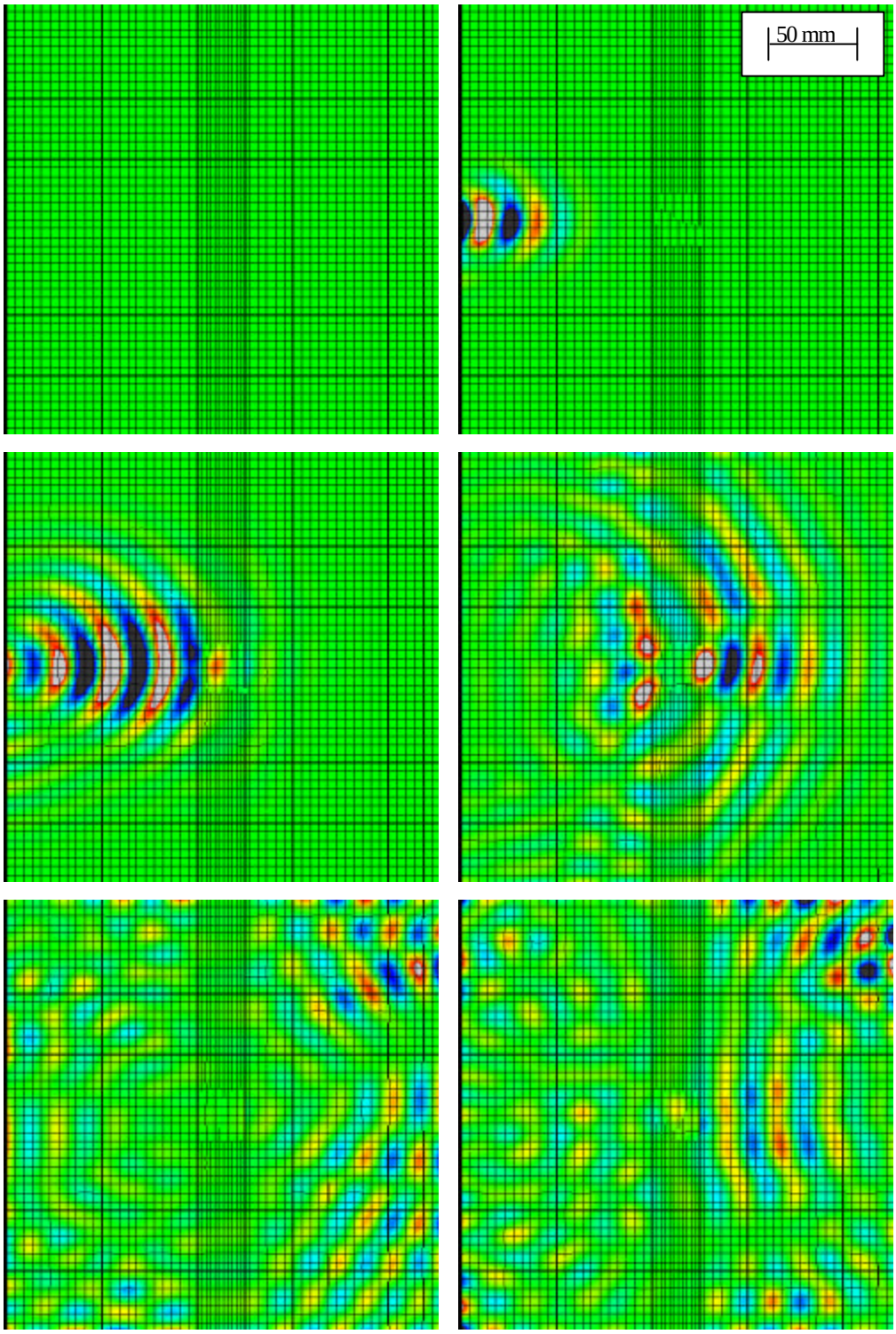

Figure 4.17: FEA results for 2-D plate with delaminated composite stiffener at 100 microsecond intervals

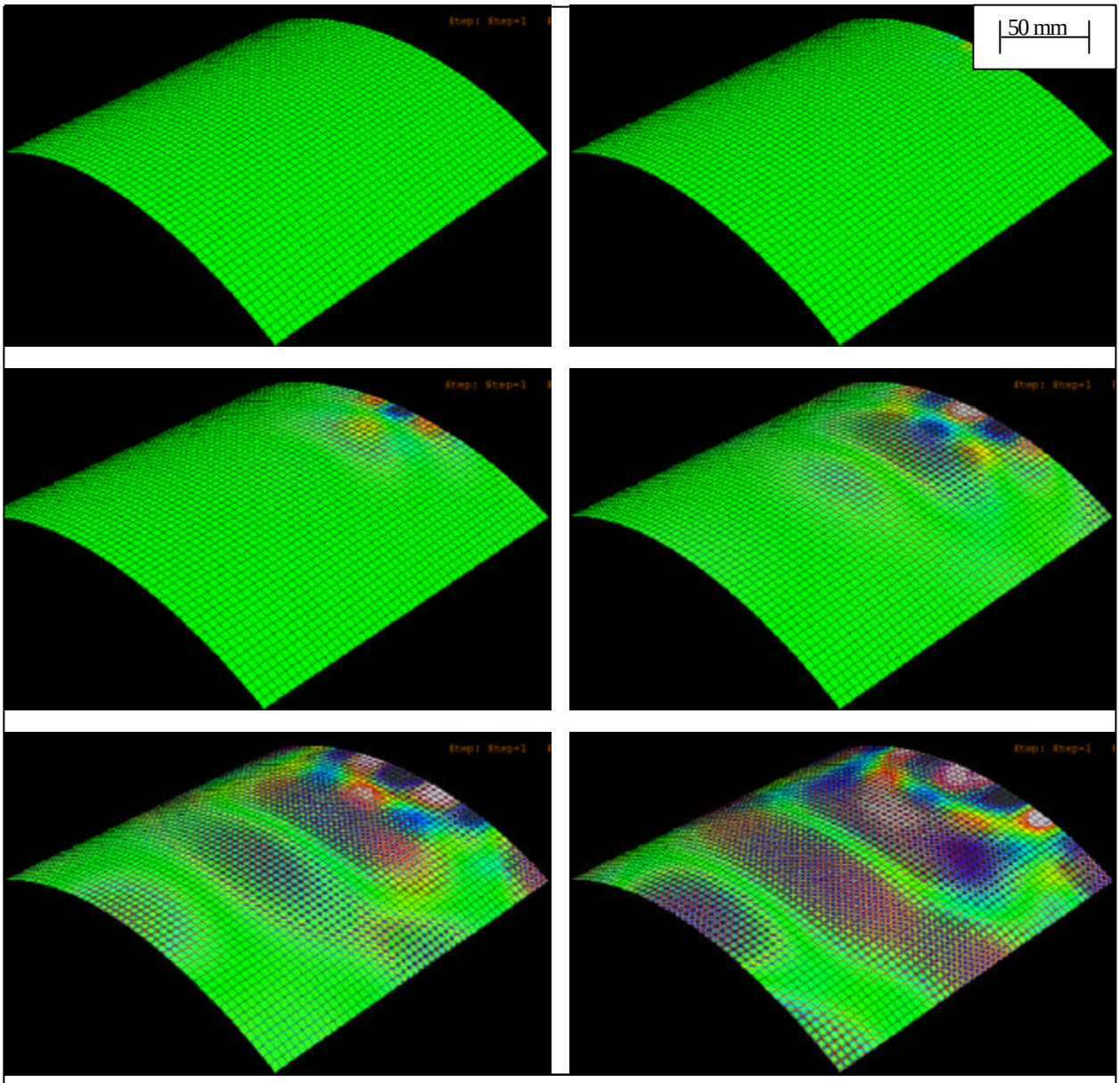

Figure 4.18: FEA results for curved sandwich panel with no damage at 10 microsecond intervals

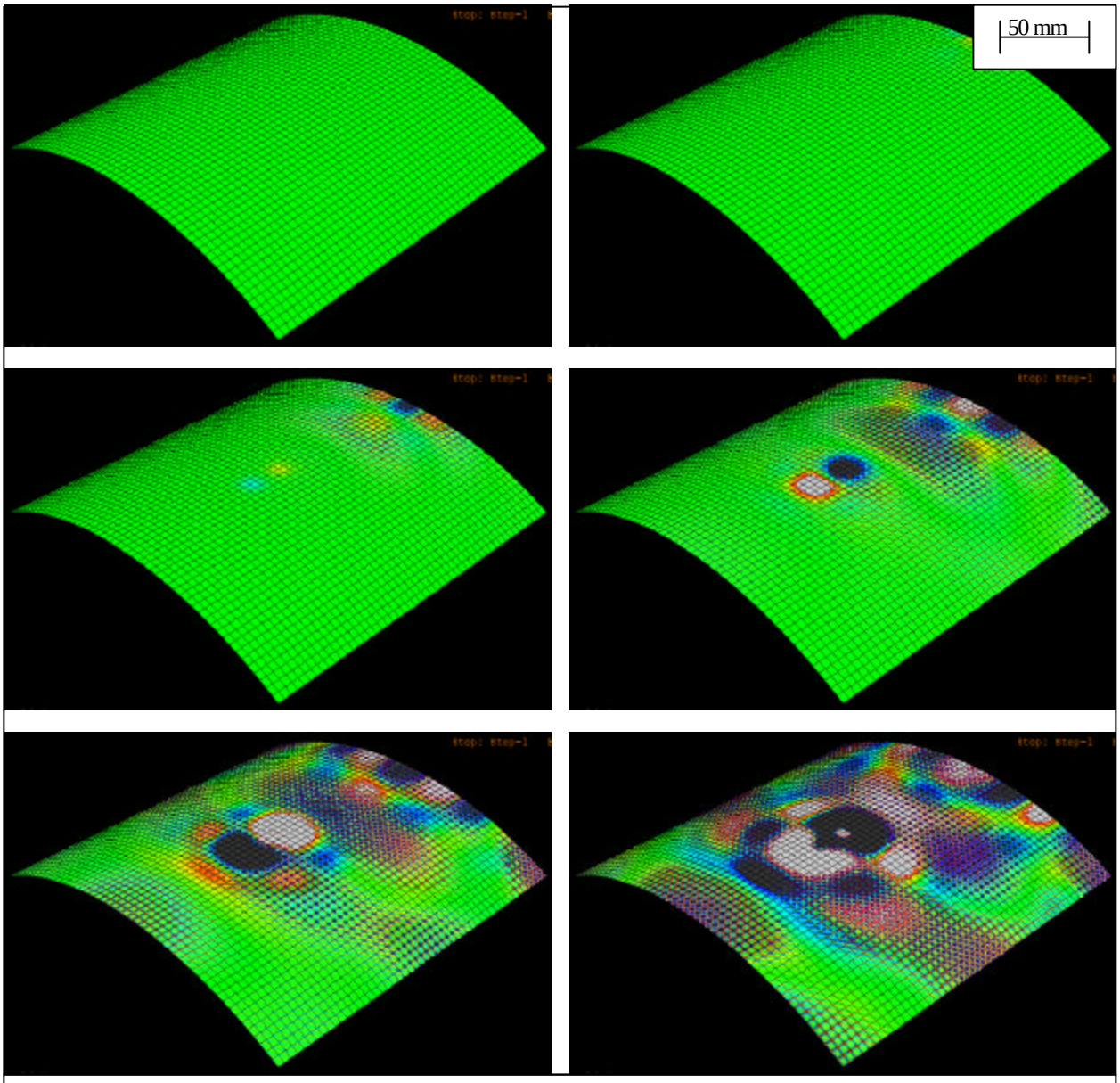

Figure 4.19: FEA results for curved sandwich panel with impact damage at 10 microsecond intervals

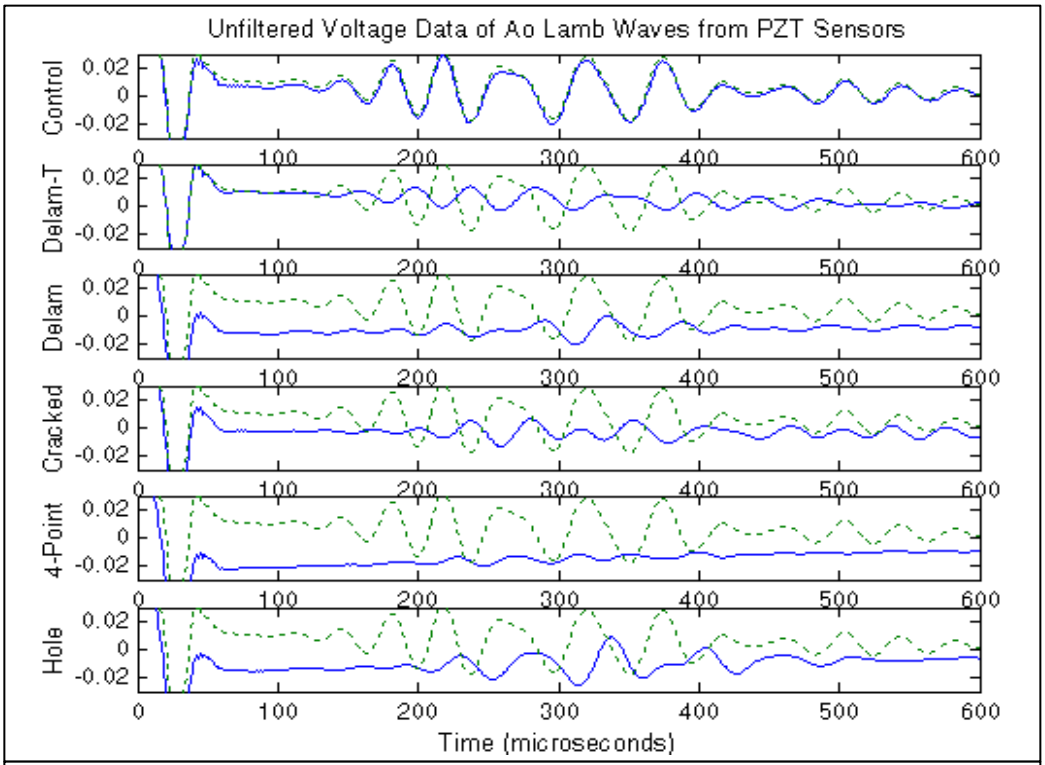

Figure 4.20: Time-trace of voltage signal from sensor 20 cm from actuator, 15 kHz signal
Solid lines are damaged specimens; control is superimposed as a dashed line

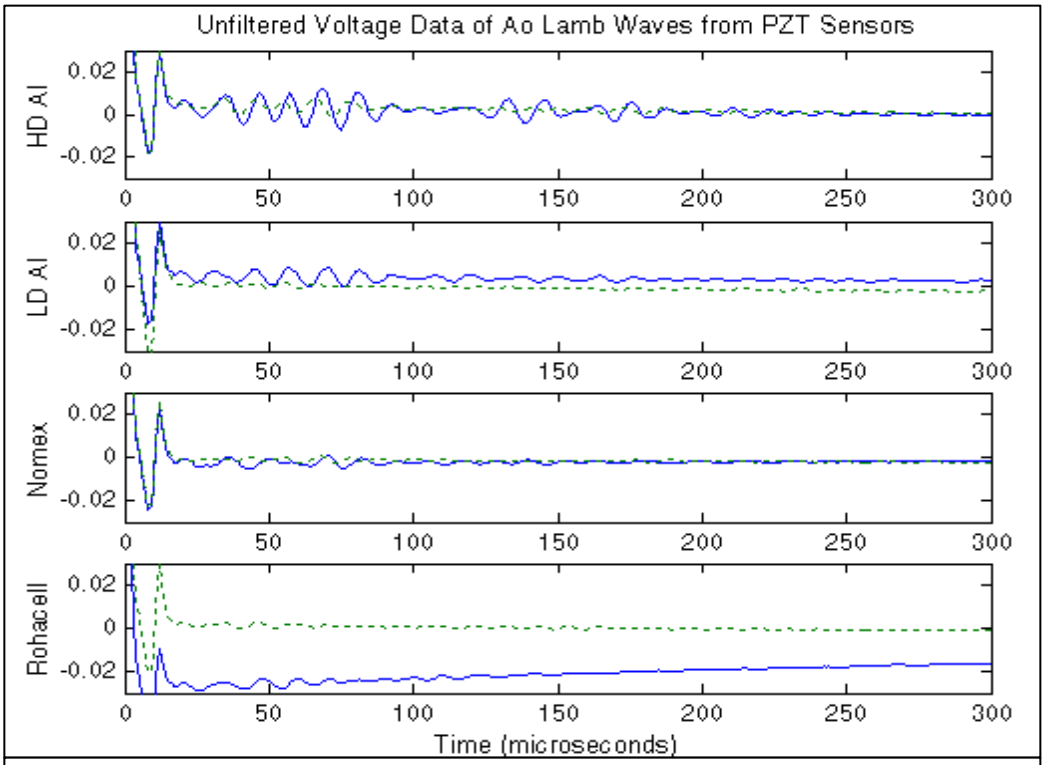

Figure 4.21: Time-trace of voltage signal from sensor 20 cm from actuator, 50 kHz signal
Solid lines are undamaged beams, debonded specimens have dashed lines

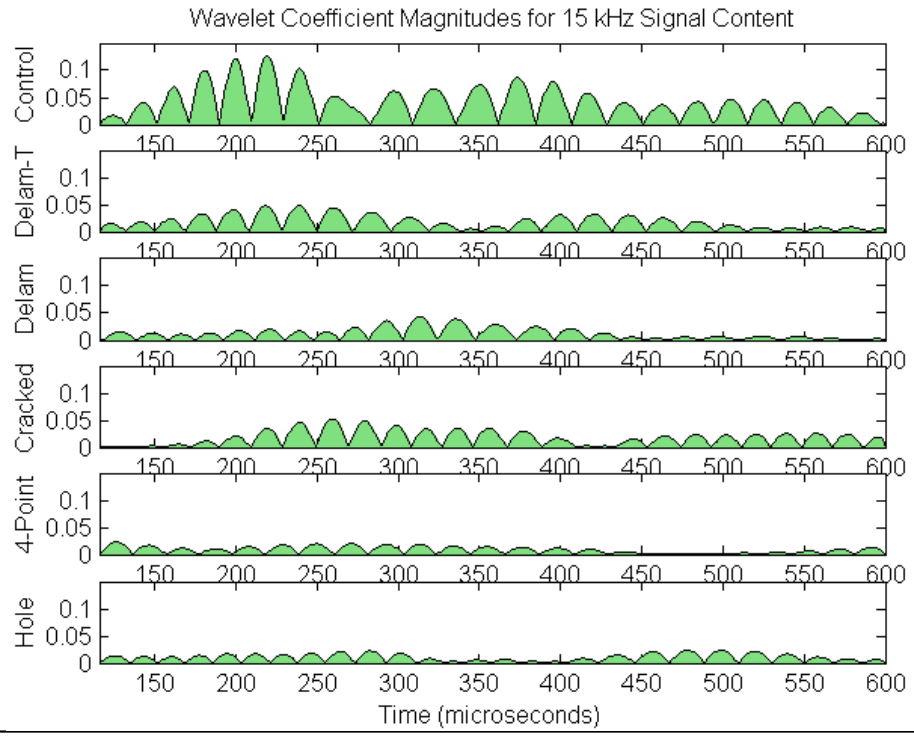

Figure 4.22: Wavelet coefficients for thin coupons; compares 15 kHz energy content

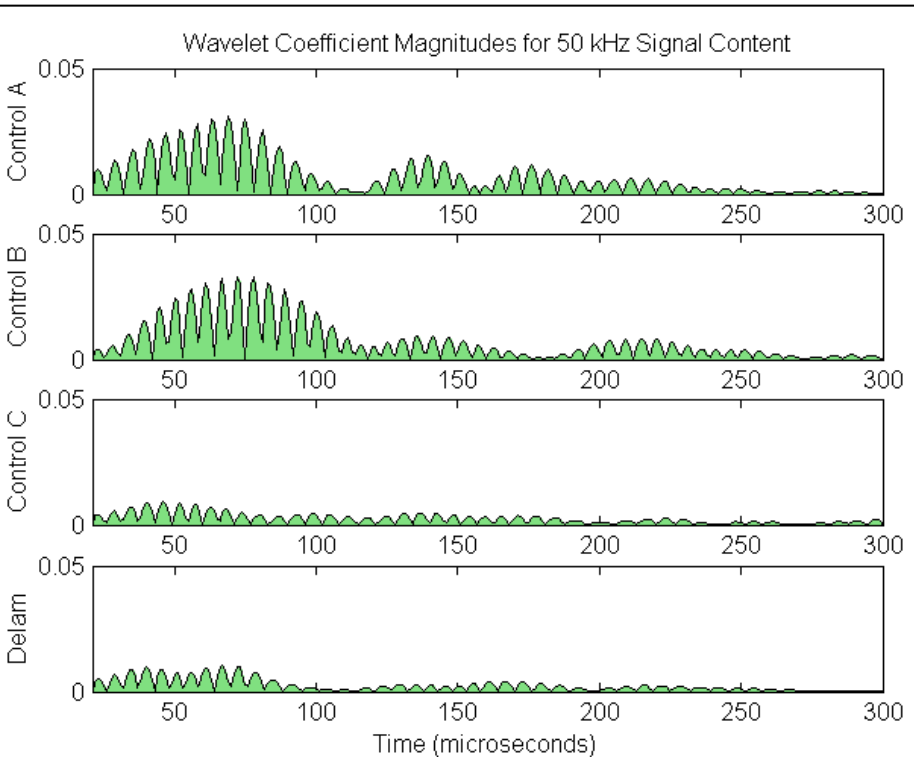

Figure 4.23: Wavelet coefficients for beam "blind test"; compares 50 kHz energy content

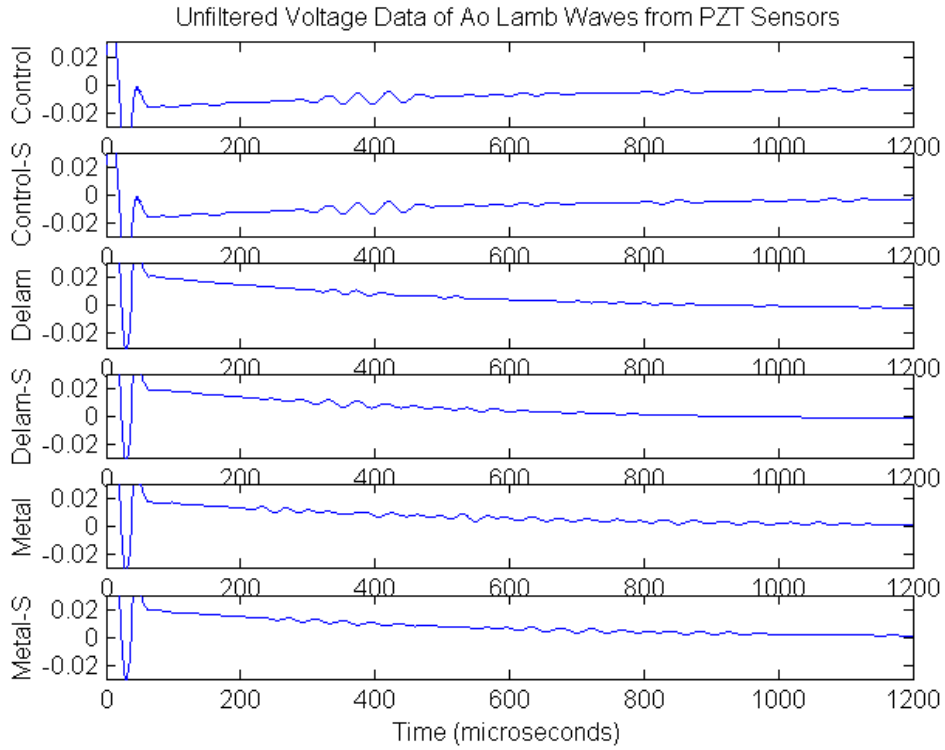

Figure 4.24: Time-trace of voltage signal for stiffened plates, 15 kHz signal

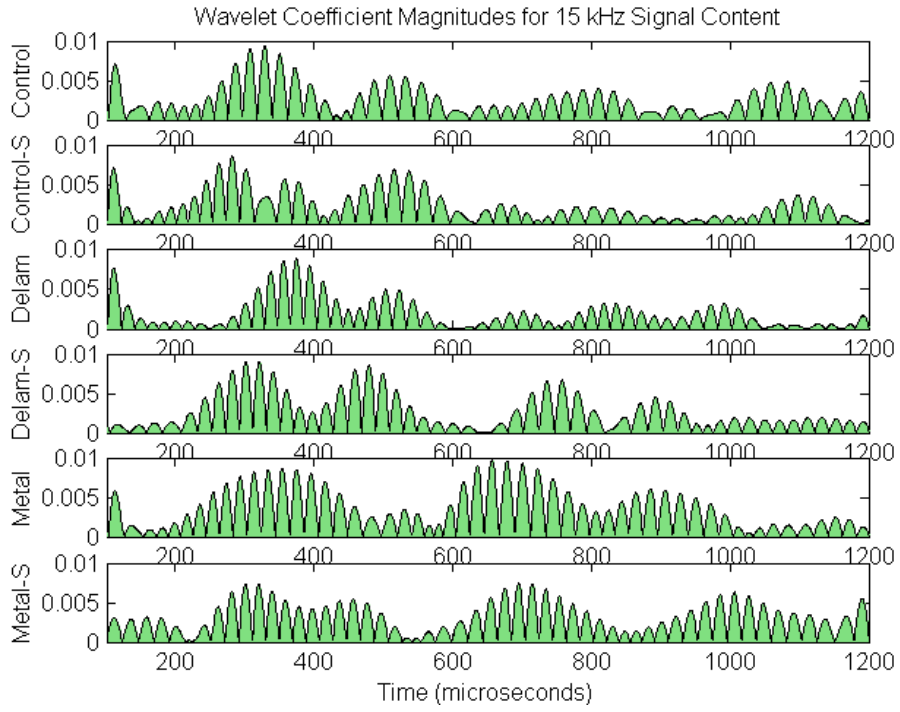

Figure 4.25: Wavelet coefficients for stiffened plates; compares 15 kHz energy content

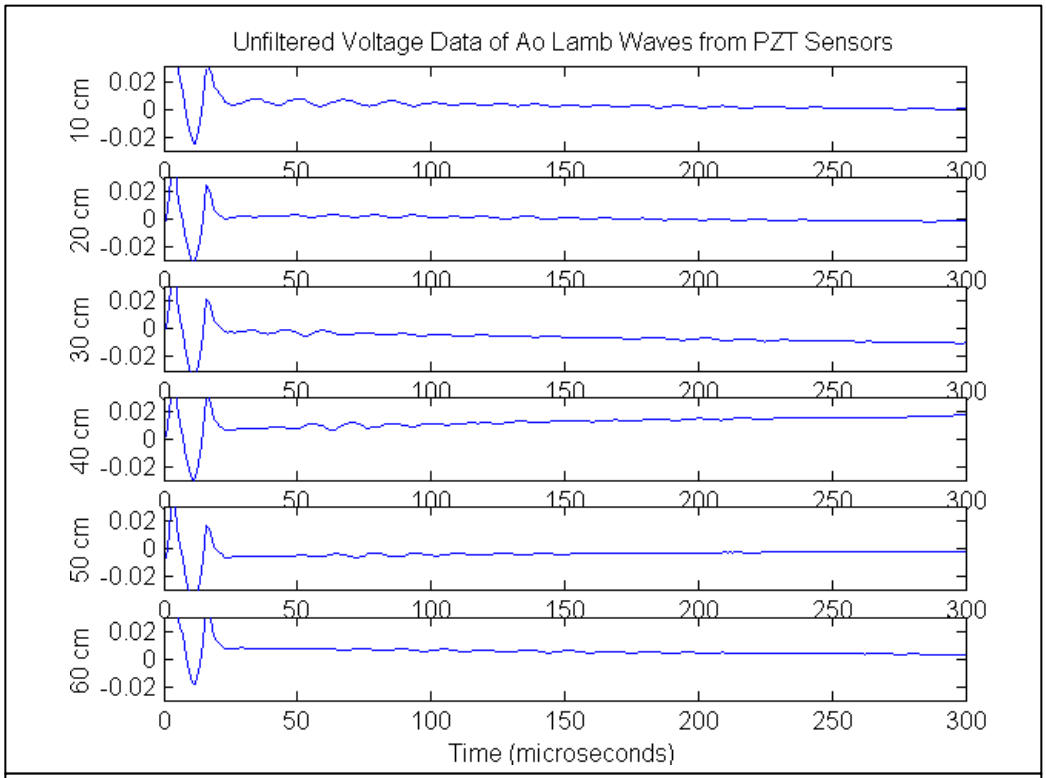

Figure 4.26: Time-trace of voltage signal for composite sandwich cylinder, 40 kHz signal

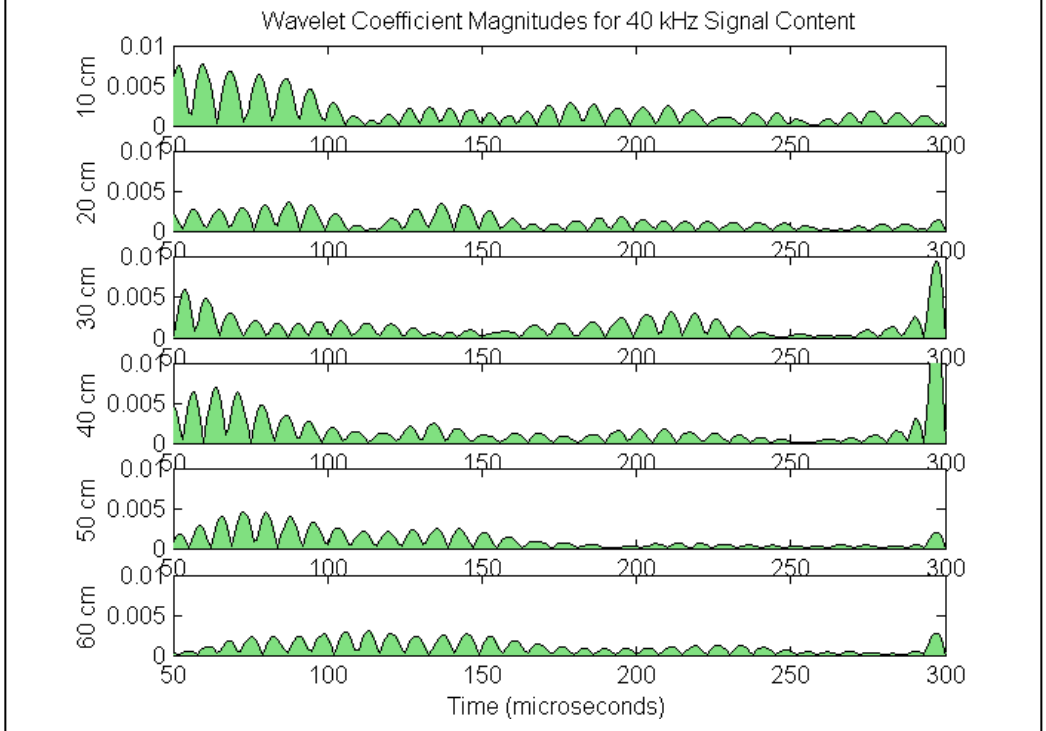

Figure 4.27: Wavelet coefficients for composite cylinder; compares 40 kHz energy content

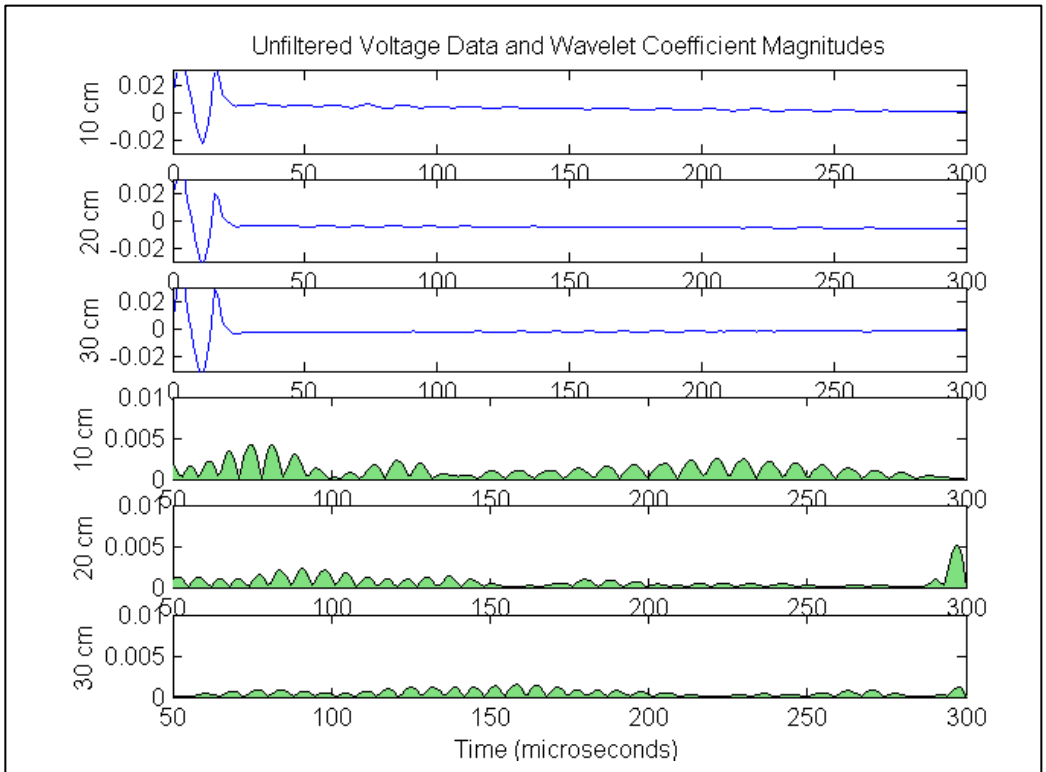

Figure 4.28: Time-trace and wavelet coefficients for circumferential scan, 40 kHz signal

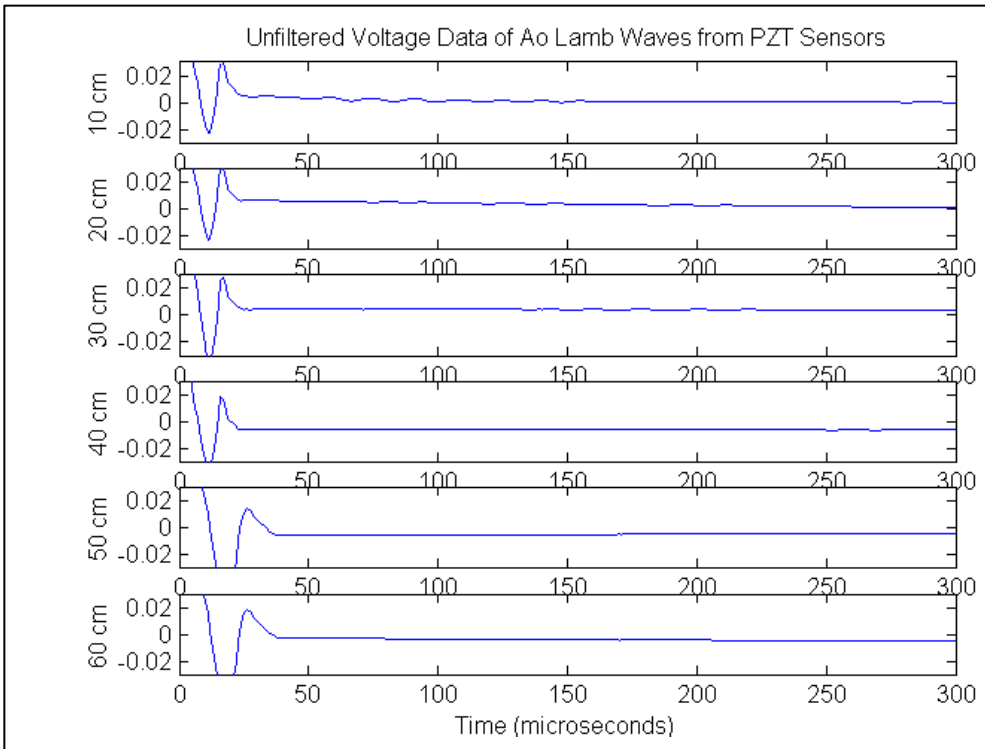

Figure 4.29: Time-trace of voltage signal for impacted cylinder, 40 kHz signal

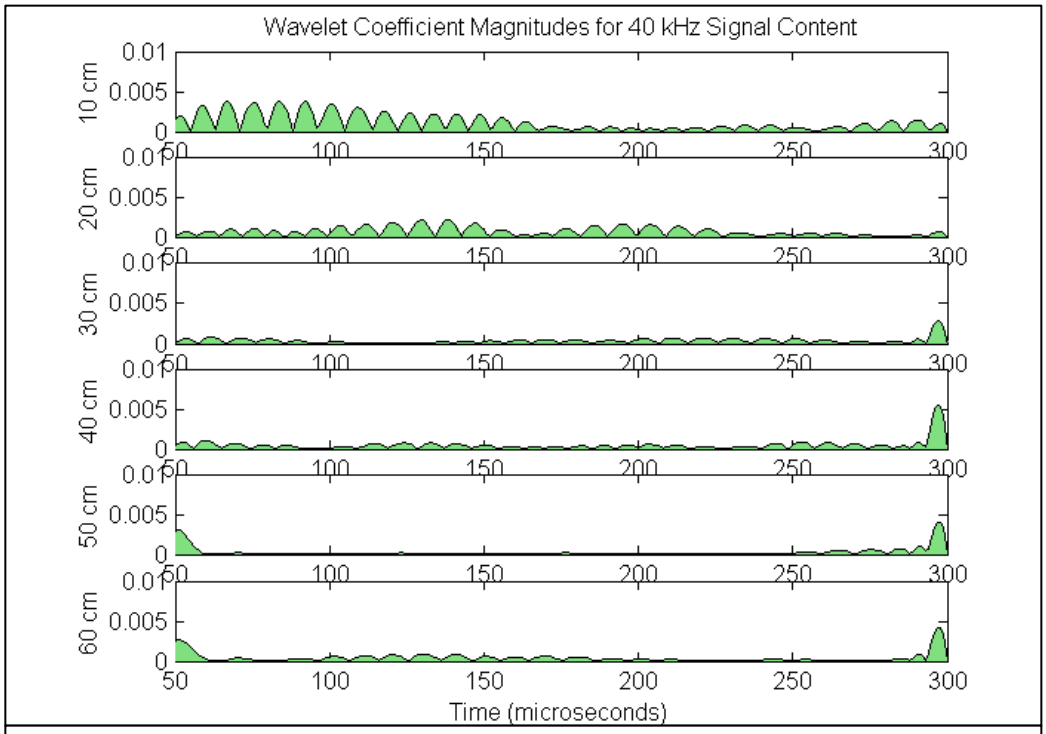

Figure 4.30: Wavelet coefficients for impacted cylinder; compares 40 kHz energy content

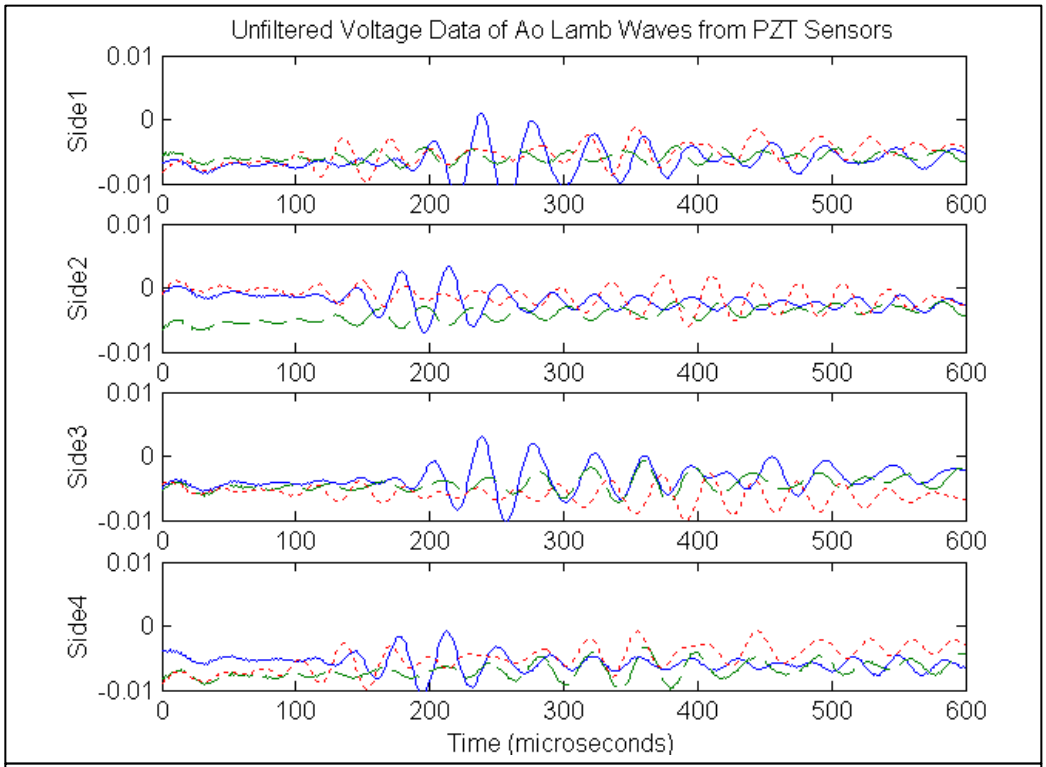

Figure 4.31: Time-trace of voltage signal for 2-D plate, 15 kHz signal. Each plot represents actuation from a different side. Blue curve is sensed wave directly across from actuator. Red and green curves are sensed waves on sides adjacent to actuator.

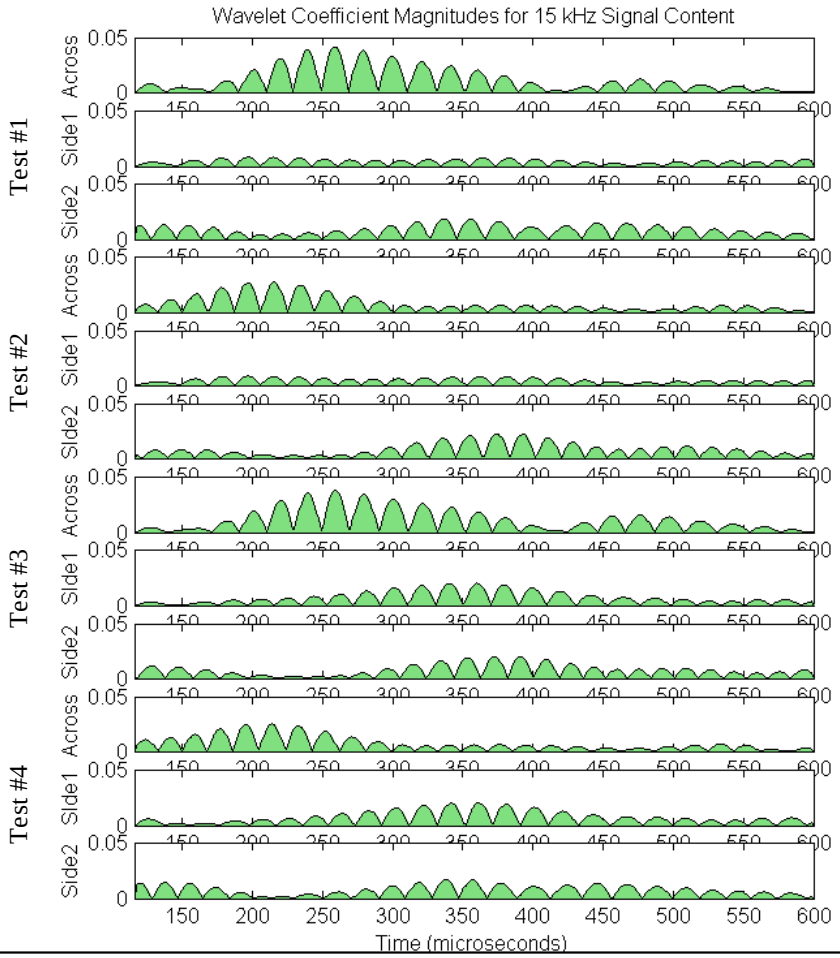

Figure 4.32: Wavelet coefficients for 2-D plate; compares 15 kHz energy content

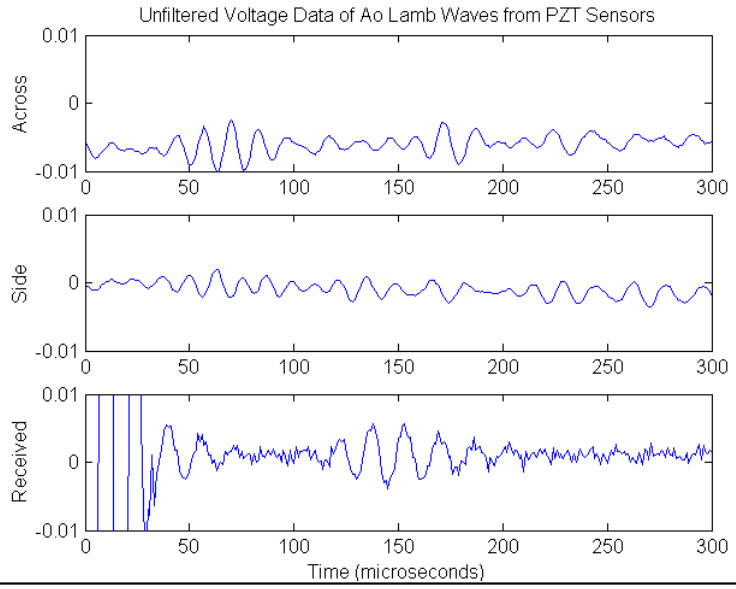

Figure 4.33: Time-trace of voltage signal for self-sensing actuator, 45 kHz signal

Table 4.1: Lamb wave times of flight and group velocities for narrow coupons as observed from FEM solutions

(times in microseconds, velocities in m/s)	TOF based on initial arrival	TOF based on peak arrival	Cg based on initial arrival	Cg based on peak arrival	Δt from undamaged
Undamaged	230	230	894	894	-
Center cracked region	231	231	891	891	1
Center 5mm hole	237	231	868	891	7
Center 50x50mm delam	306	280	672	735	76
Side 50x25mm delam	292	354	704	581	62

Table 4.2: Lamb wave times of flight and group velocities for all geometries as observed from FEM solutions

(times in microseconds, velocities in m/s)	TOF based on initial arrival	TOF based on peak arrival	Cg based on initial arrival	Cg based on peak arrival	Δt from undamaged
High density Al	26	26	7910	7910	-
High density Al w/delam	32	36	6430	5720	6
Low density Al	45	43	4572	4780	-
2-D plate	318	290	647	709	-
2-D plate w/CFRP rib	308	310	668	664	-10
2-D plate w/CFRP rib delam	314	300	655	686	-4
2-D plate w/steel c-channel	308	290	668	709	-10

Table 4.3: Lamb wave times of flight and group velocities for narrow coupons as observed experimentally

(times in microseconds, velocities in m/s)	TOF based on initial arrival	TOF based on peak arrival	Cg based on initial arrival	Cg based on peak arrival	Δt from undamaged
Undamaged	216	218	952	944	-
Center cracked region	238	233	864	883	22
Center 5mm hole	226	230	910	894	10
Center 50x50mm delam	261	258	788	797	45
Side 50x25mm delam	231	220	890	935	15

Table 4.4: Lamb wave times of flight and group velocities for sandwich beams as observed experimentally

(times in microseconds, velocities in m/s)	TOF based on initial arrival	TOF based on peak arrival	Cg based on initial arrival	Cg based on peak arrival	Δt from undamaged
High density Al	24	27	8570	7620	-
High density Al w/delam	30	31	6860	6640	6
Low density Al	30	37	6860	5560	-
Low density Al w/delam	37	41	5560	5020	7
Nomex	36	35	5720	5880	-
Rohacell	27	28	7620	7350	-

Chapter 5

OTHER PIEZOELECTRIC-BASED SENSING METHODS

There are many advantages to using piezoelectric sensors in SHM applications; they are light, can be conformable, use little power and are sensitive to small strains and accelerations. The two previous chapters of this thesis have given a detailed account of the frequency response and Lamb wave methods using piezoelectric sensors and actuators. Both of these methods have demonstrated useful sensitivity to damage, however they are most effectively implemented actively by using powered actuators in a pulse-transmission or pulse-echo mode. Perhaps the greatest advantage of using piezoelectric material for sensors, is that they can be used for a wide variety of detection techniques by simply altering the time scale of analysis or actuating signal. This chapter gives an overview of two further techniques, acoustic emission and strain monitoring, which could be implemented via the piezoelectric sensors and system infrastructure used for the previous two methods presented, to detect damage passively without the use of actuators. These methods can offer supplemental information about the state of the structure, while only requiring some additional software. Background for these methods are presented from the literature, as well as results from simple proof of concept experiments that were performed.

5.1 Background

As mentioned previously in Chapter 2, one of the earliest forms of damage monitoring in vehicles involved observing strains using resistive foil gauges. These sensors are applied easily to the surface of a structure, and output data that is simple to analyze with little processing. Operators have used records from strain gauges to check for over-strains in components, as well as to calculate stresses based on stiffness estimations [7]. Optical fibers have been embedded in composite structures to serve the same purposes over a distributed area with slightly more complexity [154]. More recently, piezoelectric sensors have been considered for the in-situ monitoring of operational strains. There have been a few articles in the literature that have suggested piezoelectric sensors for this role. Rees *et al* suggested the use of piezoelectric patch sensors placed around a boron/epoxy repair site to monitor cracks growing in the epoxy [155]. A finite element approach was used to show the strain increase from the stress concentration developing under the sensor as the crack grew. A sensitivity study showed that cracks larger than 11 mm would be able to be detected by this scheme. The majority of this work was analytical, however experimental validation was provided in a second paper that showed the detection of a 10x10 mm disbond in a boron/epoxy repair patch adhered to an aluminum structure [156]. This study also concluded that the impedance properties of the piezoelectric sensor would start to degrade above 2000 microstrain. Moreover, in another experimental paper, Hautamaki *et al* have fabricated and demonstrated a series of MEMS piezoelectric sensors, which exhibited linear results through 1000 microstrain [157]. Strain based damage monitoring methods have shown potential to detect cracks on the order of a centimeter in length, however their results are localized to the area beneath the sensors which would require many more sensors for vehicle coverage as compared to frequency response or Lamb wave methods.

Another commonly implemented use of piezoelectric sensors for damage detection in composite structures has been acoustic emission. This method has become well accepted since it does not require actuation, and its results can provide better information regarding damage location than most other techniques. In its simplest form, this method involves measuring the time of flight of a circular pattern of stress waves emanating from a point source; depending on the sensitivity of the system, this point source could be an impact event or a fiber breaking. Often resonant sensors are designed so that they are tuned to the expected frequency of particular forms of damage to amplify their presence while other ambient vibrations are damped out [32]. Several researchers have investigated this and other techniques in the literature [29, 158-160]. The reason why acoustic emission has not become standard practice is because of the complexities that arise from wave propagation in composite materials. Analytically the triangulation of a damage detection site can be easily calculated in an elastic isotropic material based on time of flight measurements, however in anisotropic and inhomogeneous composite materials these waves do not behave perfectly, and there can be much dispersion and attenuation due to the fiber structure that distorts the signals and makes a damage location prediction difficult. Chang's group at Stanford has had the most success in this field [161]. In their smart-structures program, they have successfully been able to determine the location of an impact even in stiffened composite panels to within 10% accuracy with sensors spaced about 25 cm apart, by using a model-based approach. The metric for the type and size of damage detectable by acoustic emission differs significantly from most techniques however, since this method is based on the amount of energy being released by an impact event or crack propagation, and it can only be detected while that energy is being released. This is compared to the three previous methods described in this thesis, which can be queried to search for the presence of damage at any instant

during or after the initiation of the damage. Acoustic emission methods have the possibility to cover a large area with few sensors, alert an operator to an impact event, and possibly even the location of the damage with some additional data processing. In the following sections, experiments are described to demonstrate the use of strain monitoring and acoustic emission techniques with piezoelectric sensors using the infrastructure created for the other two approaches developed in Chapters 3 and 4.

5.2 Narrow Coupon Tensile Tests

At the conclusion of the present research studying frequency response and Lamb wave methods, a few proof of concept experiments were performed to verify that the sensors and infrastructure designed for the previous tests could be used simultaneously for other types of passive testing. In the first of these tests, narrow coupon specimens were tested in tension. These specimens, shown in **Figure 5.1**, were manufactured identically to all the other graphite/epoxy laminates in this research, and were machined into narrow strips to fit into the grips of the servo-hydraulic tensile testing machine. Two specimens were tested—first a control coupon with no visible damage, and the second with a 6 mm through hole drilled at its center to form a stress concentration. On both of these specimens, a 1 cm^2 square piezoelectric patch was affixed above the center point of the coupon, and a strain gauge rosette was attached in the corresponding position on the reverse side of the specimen. These specimens were then loaded in tension at 2.5 mm per min until failure while the data acquisition system collected the load, stroke, strain and piezoelectric data at 50 samples per second. The data collected from each test was then analyzed in two ways: as acoustic emission results, and as strain monitoring results.

5.2.1 Acoustic emission results

The purpose of this exercise was to match acoustic events with changes in slope on the stress-strain curve, and to predict ultimate failure based upon the observation of increased acoustic activity. **Figure 5.2** and **Figure 5.3** show the stress-stain curve for each of the specimens, using the applied stress data as the independent variable, with the normalized piezoelectric voltage data superimposed over the plot. The data taken from the piezoelectric sensors did not demonstrate many obvious acoustic events, seen as spikes in the averaged data, and the stress-strain curves (plotted with the strain gauge data) were quite linear with no drops in stiffness. There was also no indication from the voltage data that either specimen was near failure. In both plots, an apparent event is evident near the 330 MPa far field stress mark, which was the point where audible events could be heard. While conclusive results were not obtained during this test, methods in the literature have had success when using sensors that had been tuned for their application [161]. By using the procedures found in the literature along with the ones presented in Chapter 4, a piezoelectric sensor could be designed to suite both detection methods. The functionality of a passive acoustic emission sensor has already been implemented in another program at MIT, where a similar setup was used to monitor the rupture of a silicon diaphragm in a MEMS micro-reactor device [162]. A PZT patch was bonded to a steel component in contact with the silicon part, then the pressure was ramped and as soon as the pressure dropped off, a large spike could be seen in the PZT output signifying an acoustic wave had traveled from the ruptured diaphragm. This proved to be a reliable and reproducible indicator for arresting the fluid flow to the device. This attests to the possibility of using acoustic emission to monitor the release of energy from a damage site with a multi-purpose sensor that is suitable for the desired frequency range for both this and other detection methods.

5.2.2 Strain monitoring results

The second way the data was analyzed was to assess the accuracy of the piezoelectric sensors for the measurement of strain by contrasting them to the foil-gauge results, again as shown in **Figure 5.2** and **Figure 5.3**. The stress-strain curves using the strain gauge data were very linear, however the curves using the PZT data was significantly nonlinear. These curves could be divided into three regions which are roughly linear in themselves, however the significance of these regions in not readily obvious. As described in the previous background section, many piezoelectric materials only respond linearly to strain below certain limits, such as 1000 microstrain, and while the test presented in this section was preformed at a much lower strain level, the PZT used as the sensor in the test had not been previously characterized for its linear strain limit since the strains due to Lamb waves were extremely low. A more reasonable explanation attributes this non-linearity to the thermoplastic tape that attached the sensor to the specimens. The first linear region most likely corresponded to the data up until the linear-elastic limit of the thermoplastic, followed by the second in its plastic region and then the final region where the tape was beginning to detach from the specimen. Upon failure of the specimen, the sensor completely detached itself from the composite leaving all of the thermoplastic attached to the copper on the back of the sensor, indicating that at the time of failure there was not a good bond between the sensor and the specimen. Again, this test did not provide conclusive results, however as demonstrated in the literature, piezoelectric materials have been used to monitor strain, and with some more experimentation with attachment method to be employed and the determination of the proper linear region for the sensor selected, it should be possible to use piezoelectric sensors for direct strain measurement within the infrastructure of other testing methods that have been presented in this thesis.

5.3 2-D Plate Tests

A second set of tests was performed on a laminated plate in order to further explore the feasibility of using the PZT sensors from the present research to monitor damage events passively, and attempt to perform a triangulation to locate the damaged area. The graphite/epoxy laminate used for the 2-D plate Lamb wave tests in Chapter 4 was re-used for these tests, with the four sensors patches affixed in the same locations in the center of each of the sides along the perimeter. Data was collected at 50 Hz (so as not to generate a large volume of data points) as a graphite pencil tip was broken in several locations on the laminate in a clockwise fashion, shown in **Figure 5.4**, as is common practice for acoustic emission verifications tests. The data was sampled simultaneously from each of the 4 sensors in order to attempt to triangulate the location of the pencil break using the previously calculated characteristic speed in this laminate from Chapter 4. The voltage results from these tests are plotted in **Figure 5.5**, and **Figure 5.6** shows the wavelet decomposition of these signals. From the voltage plots, one can see the acoustic event within the signal by the voltage spike present following each pencil break. At this data sampling rate however, it was not possible to resolve the arrival times of the voltage spikes accurately enough to perform a triangulation calculation. A reasonable prediction of the pencil break site could be made from wavelet plots though, by comparing the magnitude of the energy present for each sensor at the time of the breakage. In **Figure 5.5** for example, it can be seen that for the first test where the pencil was broken once near each sensor, that event excited the largest response from the adjacent sensor since the traveling acoustic wave would have attenuated before reaching the other sensors. The same can be seen for the second test shown in **Figure 5.6** where the pencil was broken between a pair of sensors, and these pairs consistently exhibited the largest response. From these comparisons, an estimate could be made as to the proximity of the

damage to each sensor. Using the present infrastructure and sensors suggested in Chapters 3 and 4 for the frequency response and Lamb wave methods, once a threshold value is surmounted to trigger the system, a comparison could be made between the magnitude of received energy at each sensor to predict the location of an impact event. If a higher data acquisition rate was available to the system, much more information regarding the damage location would be evident using the time of arrival data.

5.4 Discussion

The purpose of this chapter was to introduce other damage detection methods that could be performed within the infrastructure of piezoelectric sensors and the data acquisition system used for the frequency response and Lamb wave methods presented in Chapters 3 and 4 of this thesis. The first method considered in this chapter was the strain monitoring of specimens. By measuring the peak strain witnessed at the surface of a laminate, a prediction of failure can be made based upon the strain limitations of the material. The specific results in the current experiments did not provide sufficiently consistent information to make these predictions, however several researchers in the literature have successfully fabricated piezoelectric based strain gauges that are valid for certain strain rates and ranges. Additional research would have to be performed to find a more appropriate attachment mechanism for this method to be successful. Similarly, the second method, which focused on acoustic emission, did not provide as much information as previous researchers have reported with similar techniques, which is due to the slow data acquisition rate and non-optimal sensor configuration. As presented in the background section, prior successful acoustic emission work has been performed using sampling rates between 300 kHz and 3 MHz, however for the current setup these sampling rates were not

practical for continuous monitoring because of the amount of data that would have been produced. Previous researchers have bypassed this problem by using an instrumented striking device to trigger the system to capture a small buffer worth of data points at very short time steps. To monitor continuously without a trigger, custom software would have to be used along with complex hardware, in order to collect small buffered series of data at high acquisition rates, and then scan that data for voltage spikes while collecting the next buffer full of data. This process would have to take place very quickly and efficiently so that the non-essential buffered data could be purged from the system before a large volume of useless data began to fill the storage device. Regardless, acoustic emission methods have shown the potential to provide valuable information concerning the occurrence of an impact event and proximity to the sensor.

Although the experimental results presented in this chapter were not conclusive, coupled with the results presented in the literature this preliminary data demonstrated the possibility that the piezoelectric sensors could passively collect useful data with some additional software and data processing capabilities. The most encouraging result came from the wavelet decomposition of the pencil break test, which clearly indicated the occurrence of each breakage event, and by comparing the wavelet energy magnitudes provided information to help deduce the impact location. One proposed system architecture could perform these methods passively, by using sensors that are present for other detection methods, to obtain early warning signs of damage such as an impact event or a higher than ordinary strain level. Subsequently, the system could then respond by using more robust methods, such as transfer-function frequency response or Lamb waves, to more aggressively pinpoint the type and location of damage. These ideas will be further elaborated upon within Chapter 6, which describes the other components of an SHM system and provides suggestions for a successful system architecture.

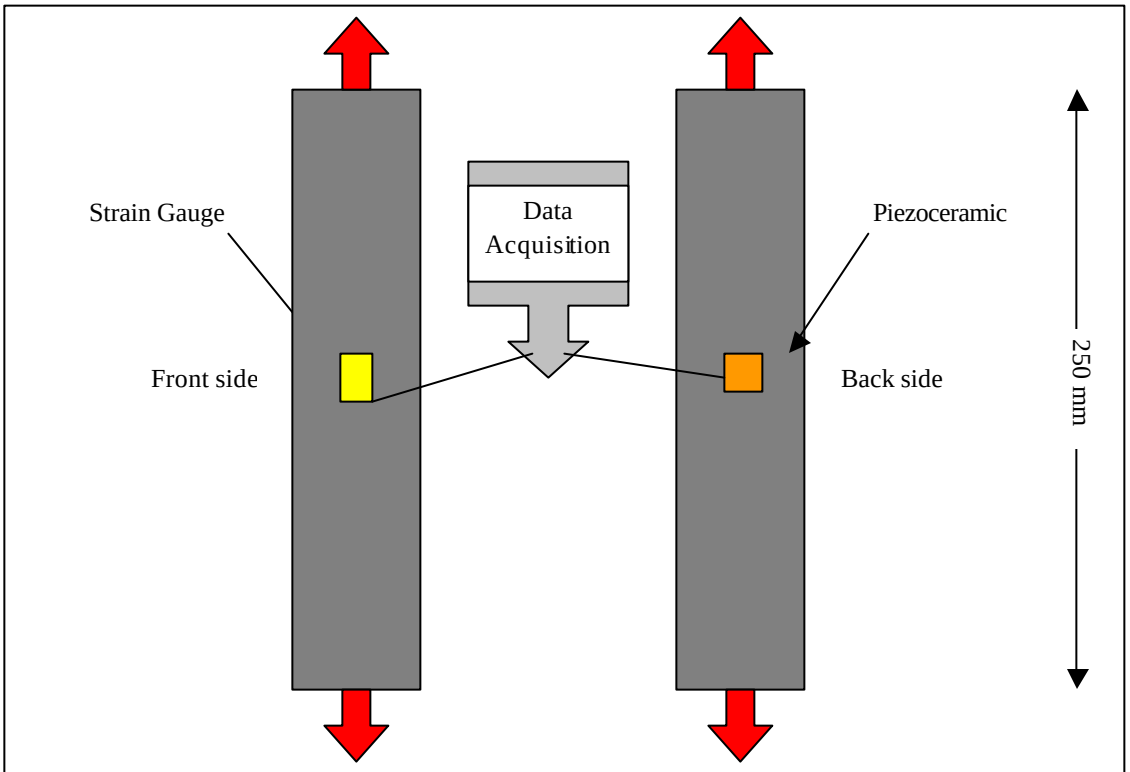

Figure 5.1: Narrow coupon tensile specimen with strain gauge rosette and piezo sensor attached

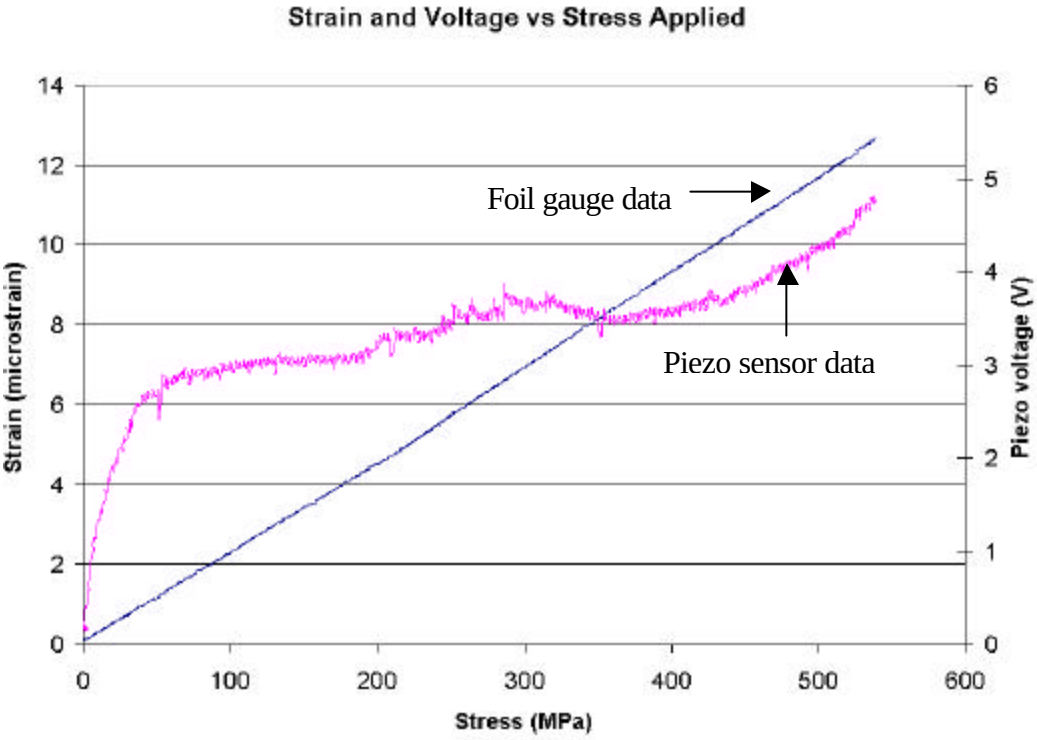

Figure 5.2: Rotated stress-strain plot for control coupon, piezo voltage data superimposed

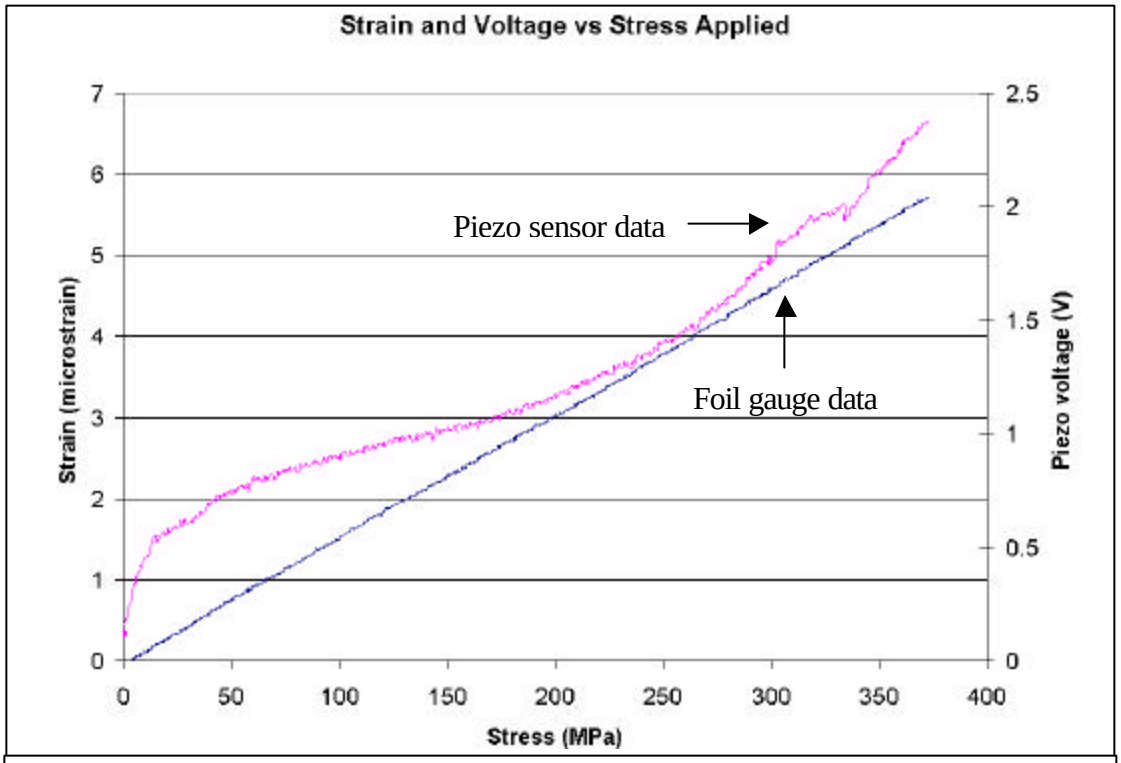

Figure 5.3: Rotated stress-strain plot for coupon with hole, piezo voltage data superimposed

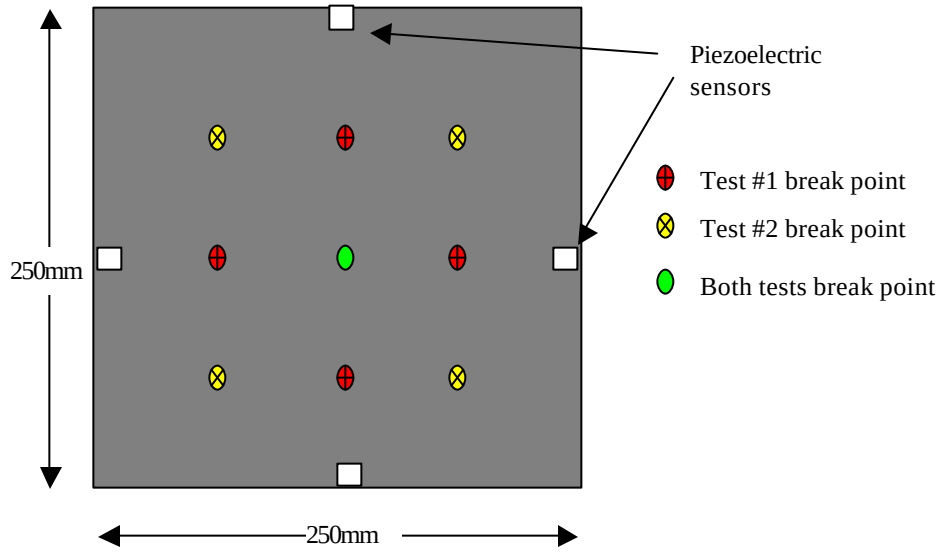

Figure 5.4: Acoustic emission setup. Pencil break points for tests #1 and #2 are labeled

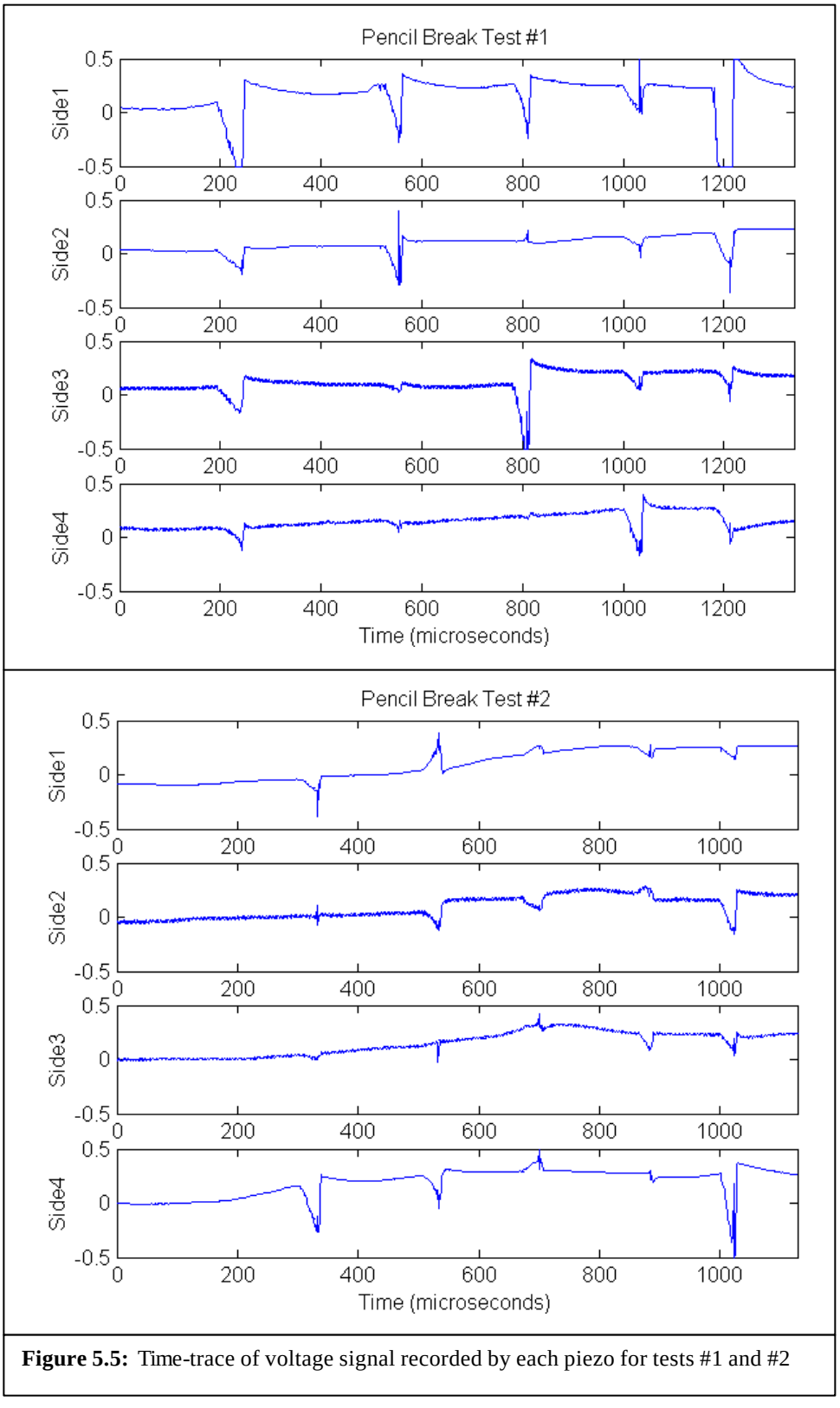

Figure 5.5: Time-trace of voltage signal recorded by each piezo for tests #1 and #2

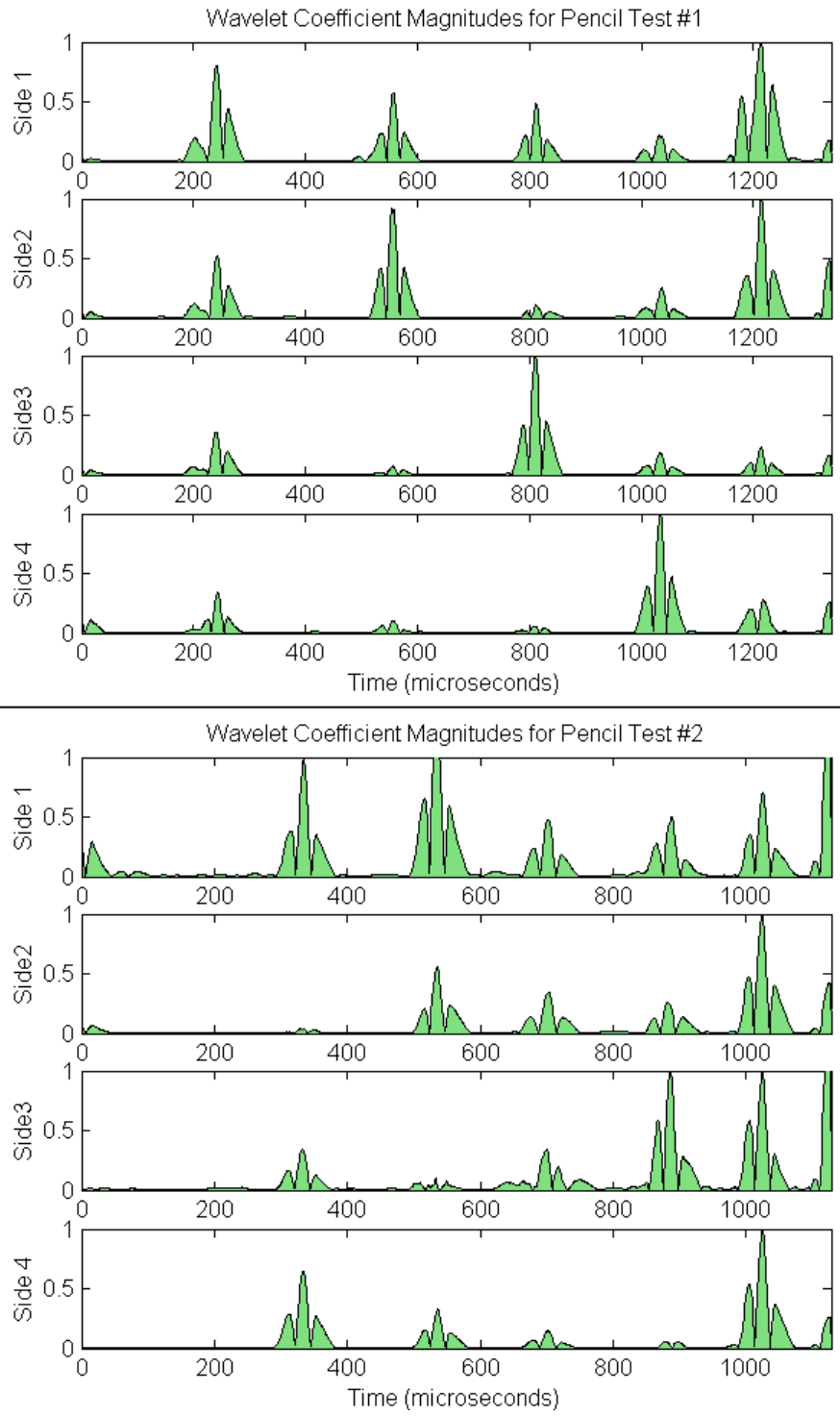

Figure 5.6: Wavelet coefficients for acoustic emission tests #1 and #2

[This page intentionally left blank]

Chapter 6

STRUCTURAL HEALTH MONITORING SYSTEMS

In the previous chapters of this thesis, the concept of a Structural Health Monitoring system was introduced, and the motivation for implementing one was presented. The focus until this point has been on sensors and sensing methods, concentrating mostly on piezoelectric based methods such as frequency response and Lamb waves. This chapter delineates the relevant considerations and components necessary for a complete SHM system. It continues with recommendations for implementation of SHM within composite structures based on the present research, and concludes with a discussion of possible directions for the future of SHM systems.

6.1 Components of SHMS

This section introduces the necessary components of a SHM system. The focus of the previous chapters of this thesis has been on the sensors used for the actual damage detection in the structure, however perhaps of equal importance and challenge are the other components used to convert, process and transmit the data from these sensors. An overall SHM system architecture is necessary to integrate strategically all of the other components for the most efficient operation. Characteristic damage signatures must be known for the particular material and structure to select appropriate sensors and sensing methods. The data from the sensors must be communicated between the sensors and to a processing unit, and algorithms are needed to

interpret this data. Some systems may require an intervention component as well. All of these components must work together to gather the information about damage in the structure, and flawlessly relay this information to an operator for the system to work reliably.

6.1.1 Architecture

The architecture of a SHM system is not a particular physical component, nevertheless it is an important preliminary consideration for the design process. The requirements of the end users are incorporated into the architecture in order to define the types of damage to be monitored, the critical flaw size, the weight and power budget for the system, and the level of importance of the various structural members that need to be monitored. It includes the layout of where the physical components of the SHM system lie and how they interact. One decision is the choice between a real-time (continuous) and discontinuous SHM system. A real-time SHM system is one that continually monitors a structure during operation, and produces data that can be directly utilized at any point by either an operator or ground control station. A discontinuous SHM system is one that data can only be accessed post-operation and could contain either a stored record of operational health data or might involve performing an integral inspection upon demand. Discontinuous systems are much less complex than real-time ones since much of the infrastructure needed to power, transfer and analyze the damage detection data can be contained in an external unit that is used to access key in-situ components. Additionally the level redundancy for each component needs to be assigned to achieve a desired level of reliability in catching false-positives as well as true-positives.

There are several other questions a SHM system designer encounters when specifying the architecture. Is the system to be designed for an aging or new vehicle? What material is being

used for the structure? Should the system be embedded or surface mounted? The designer must also determine the sensor placement density and pattern; the more sensors the better the damage resolution, with increased power and weight as penalties. One architectural concept introduced in this chapter is that of the SHM patch. This scheme clusters several sensors and other components together to be incorporated on the structure to operate independently of other patches. A few suggested systems architectures can be found in the literature, with one thorough description given by Ikegami from Boeing [163]. In this paper, he provides flow charts for the transfer of data between the various components and provides suggestions for implementation.

6.1.2 Damage characterization

Damage characterization might be considered a subsystem of the architecture, however it is sufficiently important to be discussed in depth. This is probably the most fundamental aspect of detecting damage; the familiarity of what kinds of damage are common in a type of material, and the knowledge of what "changes" correspond to these forms of damage. These damage characteristics are dependent on the type of material the structure is manufactured with, as well as the structural configuration. With metallic structures, designers are mostly concerned with fatigue cracks and corrosion, while for composite materials, delamination and impact damage are more of a concern. Structural configuration includes secondary structures that may introduce new areas for damage to exist, or influence the effect of damage on the primary structure. Examples of this include core materials or stiffeners in a composite structure that can delaminate, and ribs or fasteners in metallic structures that can introduce stress concentrations or crack initiation sites. Once an understanding of the damage signature in the material of concern is reached, then the sensing method and sensors can be selected.

6.1.3 Sensors

Sensors are used to record variables such as strain, acceleration, sound waves, electrical or magnetic impedance, pressure or temperature. Previous chapters have gone into depth describing some of the sensing systems with the most potential for damage detection, including frequency response, Lamb wave, acoustic emission and strain monitoring methods. In the literature it has been estimated that a SHM system for an aerospace vehicle would require between 100 and 1000 sensors, depending on its size and desired coverage area [29]. Sensing systems can generally be divided into two classes: passive or active sampling. Passive sampling systems are those that operate by detecting responses due to perturbations of ambient conditions without any artificially introduced energy. The simplest forms of a passive system are witness materials, which use sensors that intrinsically record a single value of maximum or threshold stress, strain or displacement. Examples of this can be phase change alloys that become magnetized beyond a certain stress level, shape memory alloys, pressure sensitive polymers, or extensometers. Another type of passive sensing is strain measurement by piezoelectric wafers. Lastly, several vibrational techniques can be performed passively, such as some accelerometers, ambient frequency response and acoustic emission with piezoelectric wafers. Active sampling systems are those that require externally supplied energy in the form of a stress or electromagnetic wave to properly function. A few strain-based examples of active systems include electrical and magnetic impedance measurements, eddy currents and optical fibers which require a laser light source. Active vibrational techniques include the transfer function modal analysis and Lamb wave propagation. Good references for selection of actuators for various active systems can be found in a review paper in the literature [164]. Passive techniques tend to be simpler to implement and operate within a SHM system and provide useful global damage

detection capabilities, however generally active methods are more accurate in providing localized information about a damaged area. A comparison of the sensing methods can be seen in **Table 6.1**. Sensor selection charts plotting size of detectable damage against sensor size and power requirement for various coverage areas, can be found in **Figure 6.1** and **Figure 6.2**. It can be seen that they are all generally capable of detecting the same size of damage and can be implemented with similar size and power sensors, however frequency response and Lamb wave techniques are the only ones that can offer full surface coverage for a 1 x 1 m plate. While some other methods, such as eddy currents, can offer better damage resolution, they are only capable of detecting damage directly below the sensor, which would drive the system to use either very large sensors or a large volume of sensors.

All of the aforementioned sensing systems have some merit for implementation in an SHM system. Frequency response methods can be used either actively or passively, Lamb wave methods are purely active and acoustic emission and strain measurements are typically passive methods. All of the methods presented in the present work utilize piezoelectric sensors since they are easy to integrate or embed into a structure, they are low power and fairly robust, making them a good choice for a composite structure. There are other sensors available for these methods, which could be suitable depending on the application or the material being monitored. Many of the other systems mentioned in this section however, require specialized sensors designed solely for their application, most notably eddy currents and optical fibers.

6.1.4 Computation

Several processing units are necessary to operate a SHM system. On the local level, a processor must interface with the sensors to acquire the data and convert the raw analog signals

to digital ones. If it is an active system, such as with Lamb wave methods, the processor must send instructions or waveforms to the actuator periodically. Data rates between 25 and 50 Megabytes per second would be necessary for each Lamb wave sensor collecting data in the system, or 0.5 to 1 Megabytes per second for acoustic emission sensors [29]. At these rates, it can be seen that a large data storage capacity would become necessary for continuous monitoring if the data is not immediately processed in a buffer and then overwritten, however a single Lamb wave test would only use 50 kilobytes. Once the information is collected, the useful, or "changed" data must be separated from the large quantity of collected data to send to the processing unit. Compression may be utilized at this step to condense the output signal for transmission. Local processing may also be necessary to compare data between neighboring sensor patches for damage verification. There are also global computational needs to use algorithms to assess the severity of damage, triangulate damage locations or make failure predictions, and to convey this information to the end-user.

6.1.5 Communication

Another important component of a SHM system is a communication system. This involves the transfer of data in one form or another between various components of the system. There are essentially four areas where the transfer of data is necessary: intra-patch, inter-patch, patch-processor and processor-operator. Intra-patch communications refers to the transfer of data, either analog or digital form, between various components within a local sensor patch. This might include the passing of data from the sensor to data acquisition board, an analog-to-digital converter, or possibly a local processor chip for preliminary data analysis. These transfers would most likely be across metallic wires or optical fibers since they would only be traveling a short

distance, on the order of a few centimeters to a meter at most, and there could be many sensors involved. The next category is inter-patch communications, which refers to the transfer of information between various patches in different regions. In some SHM schemes, it would be beneficial for local sensor sites to be able to communicate in order to compare or verify data and increase reliability. Inter-patch communication could also be a means to pass data down the line along a large structure, sacrificing speed for lower power requirements. Most of this category would be performed with low power wireless transfers over a few meters, so that the various patches could be installed and operate independently. Next, patch-processor communication is necessary to transfer the collected sensor data to a central processing unit. To maintain efficiency, only important data would be transferred to the central computer, which could be located with the vehicle avionics. Most likely a high-powered wireless method would be necessary to transfer the data to the computer which could be tens of meters away, unless the patches were to pass the information along in a data-bus fashion. Lastly, data must be passed between the processor and the end user to convey information about the state of the structure.

6.1.6 Power

Most of the components mentioned in the previous sections require power to function. Lamb wave actuators, for example, operating actuating at 15 kHz with 5 V peak-to-peak would draw 24 mW (using $P=2\pi fCV^2$). A low power micro-computer to process the data would likely draw about 10 mW, and a short range wireless device would require about 5 mW to function. This becomes difficult when there are many components distributed throughout the surface of the structure, some of which can even be embedded within the skin. Power could be supplied locally by batteries, or provided from within the vehicle via an electrical bus. Some researchers

have proposed systems where energy is transmitted by radio frequencies to inductive loops, or collected passively with energy harvesting devices to the local sensor and processing patches. Power systems for SHM systems are probably the least developed area currently.

6.1.7 Algorithms

Algorithms are probably the most essential component to a SHM system. They are necessary to decipher and interpret the collected data, and require an understanding of the operational environments and material thresholds. Examples of algorithms that have been mentioned in this thesis include codes that perform modal analysis and wavelet decomposition. Other algorithms that could be embedded into a SHM system include codes that interpret the sensor data to specify the damage size and location, codes that calculate the residual strength or stiffness of the structure, or codes that predict failure based upon the measured damage. The accuracy and robustness of the system is dependent on how well these codes are written.

6.1.8 Intervention

The last potential component of a SHM system is some form of intervention mechanism. Current intervention usually involves a mechanic performing a prescribed repair. Future advanced intervention systems mechanisms may use the collected damage detection data to mitigate further damage actively, or possibly even temporarily or permanently repair the damage site. Some proposed ways of achieving this intervention include the use of shape memory alloys to stiffen particular areas in the wake of a crack, or inserting epoxy reservoirs or duel phase

matrices into a composite to close punctures in the structure. These types of mechanisms are ideal for future SHM systems, but are not required for useful preliminary ones in the near future.

6.2 Recommendations of Implementation of SHMS in Composite Structures

The main focus of this thesis is to provide design recommendations and guidelines for the implementation of a structural health monitoring system in a composite structure. The previous sections of this chapter have explained the required components of SHM systems, and this section will propose an architecture to connect these components. In order for the system to be viable, the design must be based on the optimization of a cost function. Sensors and actuators would be chosen based upon the material to be monitored and the structural configuration, similar to the description in Chapter 4 for the optimization of Lamb wave sensors. A smart design will use several different sensing methods, taking advantage of both the strengths and weaknesses of each; for example certain methods work only in conducting materials and other in insulating ones, so potentially, damage to fibers could be differentiated from damaged matrix in a composite by using both concurrently. The trade between redundancy and reliability is essential since missed damage or false-positives could prove financially fatal to SHM systems. By using event-driven processing, such as a passive system triggering a dormant active one, a low duty cycle would save power and complexity. Further gains could be made by taking advantage of ambient conditions to provide power or actuation. As previously mentioned, good algorithms designed for the particular material being monitored is key. Lastly, it would be advantageous to design a system that was flexible enough that it could be retrofitted to existing aging systems as well as work on new structures.

A design proposed by the author would use relatively small (0.25 - 1.0 m^2) autonomous sensor patches as its key elements. These patches would include multiple piezoelectric sensors

around their perimeter, local wiring between the sensors (longest length of 0.5 m), a data acquisition/processing device (capable of sampling around 1 MHz), a rechargeable polymer battery with an inductive coil for power reception (50 mW required to power all components), and a short range wireless device (10 m transmission range). All of these components would be embedded deposited onto a conformable insulating polymer sheet with a thermoplastic adhesive backing so that it could easily be applied over any surface of a vehicle. Thermoplastic would be used to avoid the complexity of an autoclave cure, and so the patch could be removed if it were damaged or if the surface it was mounted over required repair. Other sensor types could possibly be deposited onto the polymer as well in certain regions, such as meandering wires for eddy current tests or differential parallel metal tracks for thermocouple readings. These patches would be generic so that they could be placed in any region of concern on a vehicle, and could even be placed on a dispenser like roll to be torn off and applied. Since thermoplastics are removable, patches could even be replaced if a section becomes damaged or is malfunctioning. Once attached to the structure, a neural network algorithm could be used for the sensors to learn the topology of the area of structure they are adhered over, to collect a small database of the undamaged state, and to discern where each patch was in relation to the others and in spatial coordinates of the structure. In operation the sensors would passively collect strain and acoustic emission data, passing their data along to their local processing units. When abnormal data is encountered, active transfer function frequency response and Lamb wave methods would be initiated, using the same piezoelectric sensors, to verify the presence of damage. Once damage is located within the patch region, the nearest neighbor patches would be contacted via a wireless connection to attempt to confirm the damage, and to establish the resulting effect of the damage on the structure as a whole. This compiled, consolidated and compressed data would then be

passed patch to patch to the central processing unit to be interpreted, and the damage type, severity and location would be indicated to the operator and ground crew on a computer terminal along with suggested actions. Separately, the individual patches might not have the capacity to behave intelligently, however collectively they would be able to make "smart" decisions. This system would function continuously during operation, and could also be automatically accessed by the operator or ground crew to perform a mid-air or ground inspection on demand. As a first step towards acceptance of such a system, the operator could rely on it only to speed ground inspections by using the in-situ sensor patches to replace tear-down component inspections. In that capacity, the central processor unit could be accessed via an ethernet connection to test each patch on the structure for damage prior to each flight.

6.3 Future of SHMS

Structural health monitoring systems will be an important aspect of future aerospace vehicles in order to reduce their life-cycle costs. They will be an essential part of Reusable Launch Vehicle (RLV) technology, which will require constant monitoring to eliminate the need for time-consuming inspections. While RLV projects may presently drive the funding for SHM since they are so critical to their feasibility, commercial and military aircrafts have just as much to benefit from SHM systems. To bring SHM systems to fruition, several areas in each of the components described above need to be researched further. Currently, there are a few papers in the literature that describe various types of architectural schemes. One particular thesis shows an economic study of life-cycle costs of an aircraft being monitoring via an internet-based SHM system [65]. In this study, sensors attached to the skin of the vehicle collect data about the health of the structure, which is then directly sent to the vendors of replacement parts via the internet to

allow them to stock and ship components properly. Other papers have looked at the value of combining two forms for NDE methods to increase reliability of damage detection, such as using eddy-current methods along with modal response methods [165]. A few companies are also working on concepts to integrate and attach sensor patches creatively such as the ones described in the proposed architecture in the previous section. A major enabling technology for SHM is Micro-Electro-Mechanical-Systems (MEMS). The miniaturization of each component would greatly reduce their weight and aspect ratio, and would also decrease the manufacturing times and costs. It has also been proven in the literature that for several applications that the sensor gains considerable sensitivity by reducing its scale [166]. Many companies have already developed various types of MEMS sensors, most notably a functional Lamb wave transducer and receiver fabricated as a MEMS device [167]. To decide between these architectural schemes, a SHM designer must compare the cost of development, the cost of implementation, the cost of operation, the impact to the production of the vehicle, the estimated savings in inspection and maintenance from traditional methods, the reliability and longevity of each system.

The next component that is currently being researched is the miniaturization and the computational devices. All of the large computer companies are working to shrink the size of processing chips, and others have been developing miniature analog-to-digital chips. There are also several researchers who are working on distributed arithmetic source coding that is more efficient to improve the speed and consolidation of data transfer within the shrunken chips [168, 169]. The area that has perhaps received the most attention has been wireless sensor communication [170-173]. Several companies, including Rockwell Collins, Boeing, and MTS Systems already have prototypes being produced for MEMS wireless devices that they propose to use to query embedded sensors remotely [174-177]. There are also a few university-led

initiatives that have used cellular-based wireless devices in civil SHM applications [178, 179]. Next, limited work can be found in the literature providing research into alternative power systems. MIT has been working with DARPA over the past several years to develop a MEMS based energy harvesting device, which extracts mechanical energy from ambient pressure variations and vibrations and converts it to electrical energy [180]. Other companies are working to develop radio-frequency transducers for wireless transmission of power to inductive loops [181]. Lastly, a few institutions have developed mechanisms for self-healing of polymer-matrix composites for possible damage intervention use, some by using pockets of uncured or two-phase resin in the polymer itself, and others by filling hollow fibers with uncured epoxy that cures upon being exposed to the external matrix [182].

Future SHM systems will incorporate all of the above mentioned technologies to provide reliable damage detection for aerospace vehicles. MEMS will be an integral part of each component, including the sensors, communication and power systems. These systems will be able to determine the integrity of the structure quickly and accurately, and make judgments as to what action should be taken. This information will be wirelessly transmitted to the operator and a ground station. If serious damage is detected, the SHM system will be able to intervene to prohibit the damage mode from further progression, and will attempt to seal the damage site to assist the pilot to a safe landing. At this point the system would have already contacted the repair technicians, and indicated where the damage is and how to fix it. Such a system will greatly reduce the life-cycle costs of aerospace vehicles by eliminating routine inspections, averting both underuse and overuse, and predicting failure in time for preventative care.

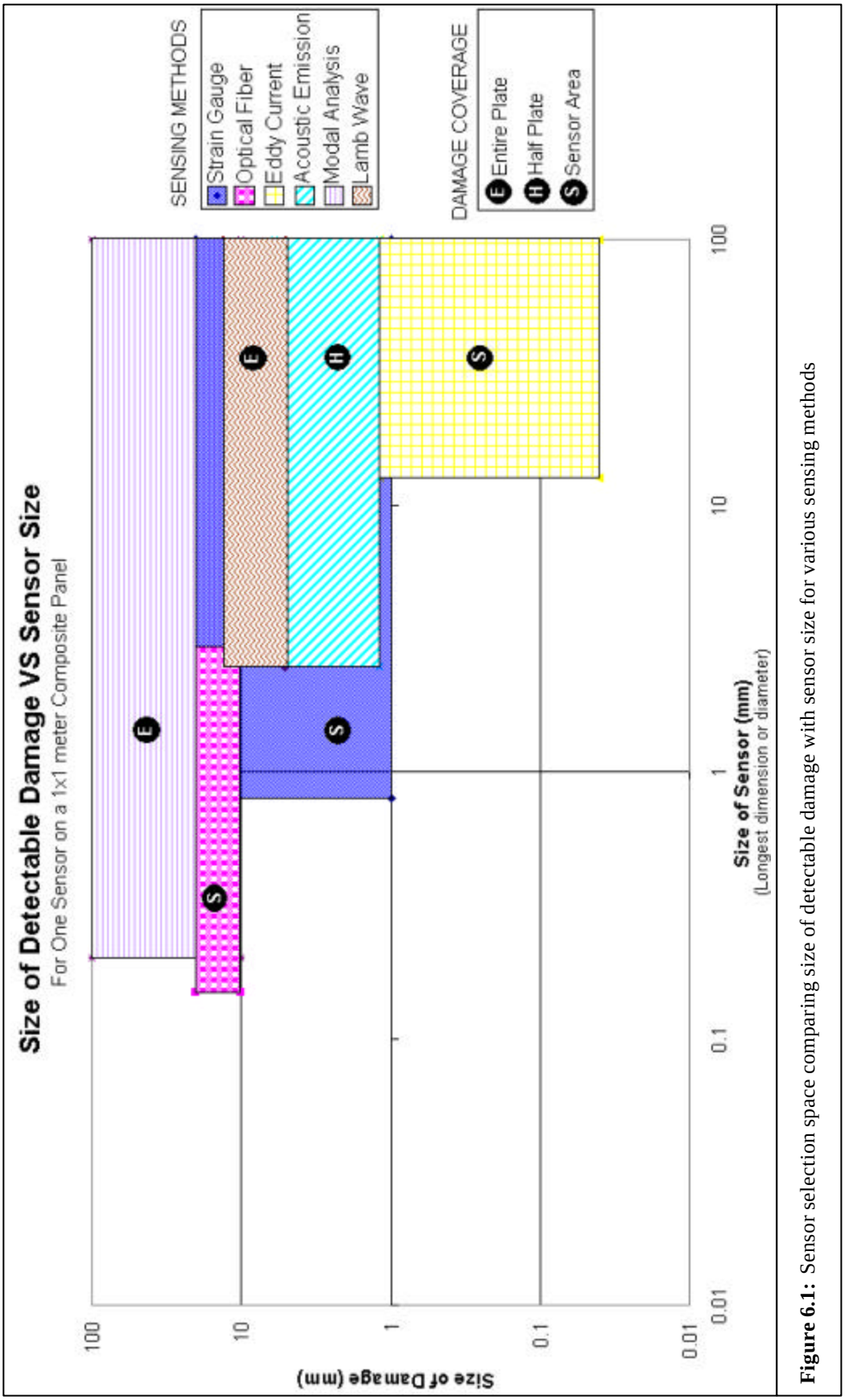

Figure 6.1: Sensor selection space comparing size of detectable damage with sensor size for various sensing methods

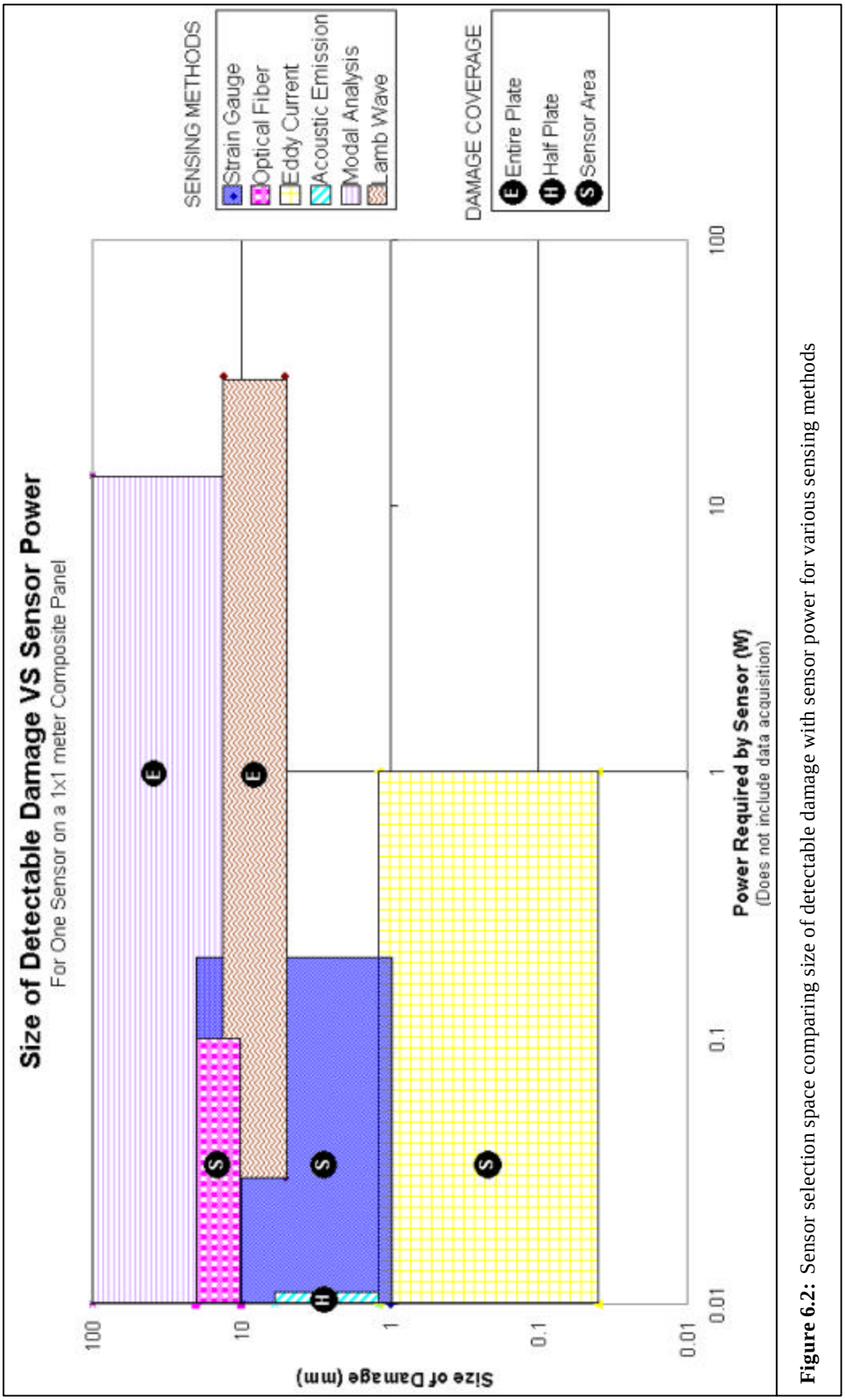

Figure 6.2: Sensor selection space comparing size of detectable damage with sensor power for various sensing methods

Table 6.1: Comparison of strengths, limitations and SHM implementation potential for various sensing systems

Method	Strengths	Limitations	SHM Potential
Visual	Inexpensive equipment Inexpensive to implement No data analysis Portable Simple procedure	Only surface damage Only large damage Human interpretation Can be time consuming	Currently none
X-radiography	Penetrates surface Small defects with penetrant No data analysis Permanent record of results Simple procedure	Expensive equipment Expensive to implement Human interpretation Can be time consuming Require access to both sides Safety hazard	Currently none
Strain gauge	Portable Embeddable Surface mountable Simple procedure Low data rates	Expensive equipment Expensive to implement Data analysis required Localized results	Lightweight Conformable Can be deposited Very low power draw Results for small area
Optical fibers	Inexpensive equipment Embeddable Quick scan of large area	Expensive to implement Data analysis required High data rates Accuracy in question	Lightweight Large area coverage Must be embedded Requires laser
Ultrasonic	Inexpensive to implement Portable Sensitive to small damage Quick scan of large area	Very expensive equipment Complex results Specialized software High data rates Couplant required Require access to both sides	Currently none
Eddy current	Inexpensive to implement Portable Surface mountable Sensitive to small damage	Expensive equipment Very complex results Specialized software Safety hazard Conductive material only	Lightweight Conformable Can be deposited Very high power draw Results for small area
Acoustic emission	Inexpensive equipment Inexpensive to implement Surface mountable Portable Quick scan of large area Sensitive to small events	Very complex results Very high data rates Specialized software	Lightweight Conformable Can be deposited No power required Results for large area Triangulation capable
Modal analysis	Inexpensive equipment Inexpensive to implement Surface mountable Portable Simple procedure Quick scan of large area	Complex results High data rates Specialized software Results are global	Lightweight Conformable Can be deposited Multi-purpose sensors Low power required Results for large area
Lamb waves	Inexpensive equipment Inexpensive to implement Surface mountable Portable Sensitive to small damage Quick scan of linear space	Very complex results Very high data rates Specialized software	Lightweight Conformable Can be deposited Medium power draw Linear scan results Triangulation possible

Chapter 7

CONCLUSIONS AND RECOMMENDATIONS

The previous chapters of this thesis have demonstrated the ability of piezoelectric sensors to detect damage in composite materials by various methods. Motivations for the application of structural health monitoring, its component requirements and the current state of SHM in industry have also been provided. This chapter draws conclusions from the analytical and experimental work presented in this thesis, and presents recommendations for further experimentation in this field. The following is a list of key contributions provided in this thesis, along with a summary of the other analytical and experimental results presented herein:

Key Contributions

- This thesis provides a thorough optimization study for the selection of Lamb wave propagation parameters. These include the choice of driving frequency, pulse shape, actuator geometry and sensor spacing. Signal decomposition and noise reduction are also discussed. The presented approach can be used to apply Lamb wave methods to detect damage in composite or metallic structures alike. A complete collection of these formulations is non-existent in the literature. (Section 4.3)

- An argument is presented using the finite element results for the modal analysis method that demonstrates the dependence of the frequency response of a structure on the damage type, location and orientation. Various combinations of damage would yield identical frequency shifts (or damage signatures), making model-dependent modal analysis methods impractical for SHM applications. (Section 3.5.1)

- A cohesive description of SHM components and their requirements is presented, currently not found in a single published paper in the literature. An SHM system architecture is proposed for implementation within a composite structure, with recommendations based upon the analytical and experimental results from this thesis. (Section 6)

Analytical Results

- Full Lamb wave derivation and solution for phase and group velocities commencing from original Lamb papers, which can be used to as a reference to replace many incorrect formulations in the literature. (Section 4.2.1)

- Direct comparison of damage sensitivities in identical finite element models solved by frequency response and Lamb wave techniques. (Section 4.6.2)

Experimental Results

- Frequency response experimental results presented for comparison with a much larger range of representative damage types in specimens than anywhere else in the literature. (Section 3.4.2)

- Detailed description of Lamb wave test setup, with explanations for parameter calculations. Mostly non-existent or arbitrary in literature. (Section 4.3)

- First published work to document experimental Lamb wave results for specimens with damage other than delamination, including matrix cracks, fiber fracture and through-holes. (Section 4.5.2)

- First published work to document experimental Lamb wave results for complex composite geometries. Results presented for 1-D application of Lamb wave tests in composite built up structure such as sandwich beams with various cores, rib-stiffened panels and a sandwich construction cylinder. New configurations of 2-D plate tests were also performed for Lamb wave techniques. (Section 4.5.2)

- Preliminary testing of acoustic emission methods and strain monitoring techniques for application in SHM system with frequency response and Lamb wave sensors. (Section 5.2)

General Results

- Economic and reliability motivations for SHM applications presented. (Section 2.3.1)

- Description of strengths, weaknesses, limitations and SHM applicability for frequency response and Lamb wave methods. Suggested roles for these methods within a SHM system. (Section 4.6.3)

- Thorough review paper of current SHM systems, and available components (Section 2.3.2)

7.1 Conclusions

This thesis presented an analytical and experimental study of various piezoelectric-based in-situ damage detection techniques as a basis for the health monitoring of composite materials. The main focus was placed on frequency response methods, which have traditionally received the most attention, and Lamb wave methods, which are now being heavily researched as having the most potential for damage detection in composite applications. For each of these methods, a thorough literature review was presented, followed by an analytical study to predict the theoretical sensitivity of each of these methods to representative damage. These studies were supported by finite element solutions for identical models using each method for comparison. Finally, each method was tested experimentally using a single set of specimens with several forms of representative damage. The strengths, weakness, and limitations of each method were explained and compared, and suggestions for implementation of these methods into a SHM system were given.

Using frequency response methods, good correlation was found between the model and the experimental results for low frequencies, however coalescing modes at higher frequencies made comparison impractical. In both the finite element models and experimental results there was strong correspondence between the extent of damaged and reduction in natural frequencies. Frequency response methods appear to be appropriate for detecting global changes in stiffness, for relatively large structures at a low power, or possibly even using ambient vibration energy. Not much information about the specifics of location or type of damage can be inferred by this method however, without the use of large stored models. Frequency response methods have a potentially useful role in a SHM system, by guiding other active sensor systems to regions of concern and monitoring the global decay of structural stiffness.

Using the models created for the frequency response methods, a finite element analysis was also performed for Lamb wave techniques. Lamb wave times of flight measurements were taken from the animations for comparison with experimental results. These experiments were setup using a series of optimization tools created using mathematical models developed and combined as a part of this thesis, and were performed on the narrow coupons from the previous frequency response tests. Similar tests were also performed on sandwich beams using cores of various densities and stiffness, plates with rib-stiffeners, 2-D plates and a composite micro-satellite. These tests demonstrated the feasibility of detecting several types of flaws in representative composite structures. The experimental procedure used in this thesis was also validated successfully by a "blind test" of several beam specimens. Lamb wave techniques have the potential to provide more information than frequency response methods since they are more sensitive to the local effects of damage to a material than the global response of a structure. The disadvantage of these methods is that they require an active driving mechanism to propagate the waves, however, Lamb wave methods have been found to be the most effective for the determination of the presence of damage in composite materials.

Furthermore this thesis described each component integral to a SHM system. This includes the sensors, processors, communication and power systems, algorithms, intervention systems and the architecture that binds them all together. A recommendation was provided for a feasible architecture for current implementation, and a prediction for the future of SHM systems is given. Structural heath monitoring systems are likely to be an important component in future designs of composite air and spacecraft to increase the feasibility of their missions and reduce their life-cycle costs, and in-situ piezoelectric-based NDE techniques will likely play a role in these systems.

7.2 Recommendations for Future Work

Much work still remains before current SHM systems can be relied upon to replace standard inspection and maintenance cycles. For frequency response methods, more experiments should be performed on built-up and larger structures to confirm the initial results. An experiment study paralleling the performed tests but varying the size of the damaged regions would also be useful in determining this method's sensitivity. For Lamb wave testing, further work lies ahead for different types of built-up structures other than the ones tested during the present research, including joined sections and tapers in laminate thickness. A more thorough investigation of 2-D sensing is necessary, as well as further investigation into the potential capabilities of "self-sensing" actuators. It would also be interesting to perform more experiments using one set of sensors to perform several types of tests, which should also be implemented on representative structures in future testing. Another possibility would be to test these methods on materials in use, since the present work only included newly manufactured specimens with artificially introduced damage, and did not account for the complexities inherent to retrofitting a system to an aging structure.

Beyond the methods examined in this thesis, there are also other useful methods that should be explored using similar procedures. This includes eddy current measurement, and several other electrical and magnetic impedance measurement methods. Another avenue of research could be pursuing all of the previously mentioned methods using new types of sensors, designed to be lightweight and conformable specifically for SHM applications. After good sensors and sensing systems have been developed, much work still remains on each of the other components of SHM systems. Testing the integration of these components will be an important

part of a successful program. Most directly, remotely controlling and accessing data from sensors via wireless connection and power still needs much attention. There are many components that have yet to be suitably developed for SHM applications, however the aerospace community has a present understanding of the need for SHM systems, and they will be a reality in the near future.

REFERENCES

1. Hall S.R. "The Effective Management and Use of Structural Health Data." *Proceedings of the 2nd International Workshop on Structural Health Monitoring*, 1999, 265-275.
2. Hall S.R. and T.J. Conquest. "The Total Data Integrity Initiative—Structural Health Monitoring, The Next Generation." *Proceedings of the USAF ASIP*, 1999. 2nd ed.
3. Bhat. N. "Delamination Growth in Graphite/Epoxy Composite Laminates Under Tensile Load." Massachusetts Institute of Technology, Cambridge, Ma, USA. 1993.
4. Wang S.S. "Delamination Crack Growth in Unidirectional Fiber-Reinforced Laminates under Static and Cyclic Loading." *Composite Material: Testing and Design*, ASTM STP (674), 1979, 642-663.
5. Bar-Cohen Y. "Emerging NDE Technologies and Challenges at the Beginning of the 3rd Millennium." *Materials Evaluation*, 1999.
6. Khan M.A.U. "Non-destructive Testing Applications in Commercial Aircraft Maintenance." *Proceedings of the 7th European Conference on Non-Destructive Testing*, v.4, 1999.
7. Chang FK. "Structural Health Monitoring: A Summary Report." *Proceedings of the 2nd International Workshop on Structural Health Monitoring*, Stanford, CA, September 8-10, 1999.
8. Oka K., Ohino H., Kurashima T., Matsumoto M., Kumagai H., Mita A. and K. Sekijima. "Fiber Optic Distributed Sensor for Structural Monitoring." *Proceedings of the 2nd International Workshop on Structural Health Monitoring*, 1999, 672-679.
9. Rogers A. "Distributed Optical-Fibre Sensing." *Measurement Science and Technology*, v.10, 1999, 75-99. Kim K.S., Kollar L. and G.S. Springer. "A Model of Embedded Fiber Optic Fabry-Perot Temperature and Strain Sensors." *Journal of Composite Materials*, v.27, 1993, 1618-1661.
10. Kollar L. and R.J. Steenkiste. "Calculation of the Stresses and Strains in Embedded Fiber Optic Sensors." *Journal of Composite Materials*, v.32, 1998, 1647-1679.
11. Todd M.D., Johnson G.A., Althouse B.A. and S.T. Vohra. "Flexural Beam-Based Fiber Bragg Grating Accelerometers." *IEEE Photonics Technology Letters*, v.10, 1998, 1605-1607
12. Parker T.R., Farhadiroushan M., Feced R. and V.A. Handerek. "Simultaneous Distributed Measurement of Strain and Temperature form Noise-Initiated Brillouin Scattering in Optical Fibers." *IEEE Journal of Quantum Electronics*, v.34, 1998, 645-659.
13. Kim K.S., Ismail Y. and G.S. Springer. "Measurement of Strain and Temperature with Embedded Intrinsic Fabry-Perot Optical Fiber Sensors." *Journal of Composite Materials*, v.27, 1993, 1663-1677.
14. Soloman S. Sensors Handbook. McGraw-Hill, New York, NY, 1998.
15. Bocherens E., Bourasseau S., Dewynter-Marty V., Py S., Dupont M., Ferdinand P. and H. Berenger. "Damage Detection in a Radome Sandwich Material with Embedded Fiber Optic Sensors." *Smart Materials and Structures*, v.9, 2000, 310-315.
16. Green A.K., Zaidman M., Shafir E., Tur M. and S. Gali. "Infrastructure Development for Incorporation Fibre-Optic Sensors in Composite Materials." *Smart Materials and Structures*, v.9, 2000, 316-321.
17. Steenkiste R.J., and L. Kollar. "Effect of Coating on the Stresses and Strains in an Embedded Fiber Optic Sensor." *Journal of Composite Materials*, v.32, 1998, 1680-1711.

18. Goldfine N., Schlicker D. and A. Washabaugh. "Surface-Mounted Eddy-Current Sensors for On-Line Monitoring of Fatigue Tests and for Aircraft Health Monitoring." *Proceedings of the 2nd Joint NASA/FAA/DoD Conference on Aging Aircraft*, 1998.
19. Goldfine N., Washbaugh A. and K. Walrath. "Conformable Eddy Current Sensors and Methods for Gas Turbine Inspection and Health Monitoring." *Gas Turbine Materials Technology*, 1999, 105-114.
20. Goldfine N. and V. Zilberstein. "Recent Applications of Meandering Winding Magnetometers to Materials Characterization." *Insight: Non-Destructive Testing and Condition Monitoring*, v.42, 2000, 154-165.
21. Goldfine N., Washbaugh A. and D. Schlicker. "High Resolutoin Inductive Array Imaging of Buried Objects." *SPIE AeroSense 2000*, Orlando, FL, April 2000.
22. Yentzer T., Zolberstein V., Goldfine N., Schlicker D. and D. Clark. "Anisotropic Conductivity Measurements for Quality Control of C-130/P-3 Propeller Blades Using MWM-Sensors with Grid Methods." *Proceedings of the 4nd Joint NASA/FAA/DoD Conference on Aging Aircraft*, 2000.
23. Goldfine N., Washbaugh A., Schlicker D., and V. Zilberstein. "Application of MWM-Array Eddy Current Sensor to Corrosion Mapping." *Proceedings of 4th International Aircraft Corrosion Workshop*, August 2000.
24. Mamishev A.V., Lesieutre B.C., and M. Zahn. "Optimization of Multi-Wavelength Interdigital Dielectrometry Instrumentation and Algorithms." *IEEE Transactions on Dielectrics and Electrical Insulation*, v.5, 1998, 408-420.
25. Zahn M. "Optical, Electrical and Electromechanical Measurement Methodologies of Fields, Charge and Polarization in Dielectrics." *IEEE Transactions on Dielectrics and Electrical Insulation*, v.5, 1998, 627-650.
26. Dowell M. and G. Sylvester. "Turbomachinery Prognostics and Health Management via Eddy Current Sensing: Current Developments." *General Dynamics Report*, 2000.
27. Aberg M. and P. Gudmundson. "Micromechanical Modeling of Transient Waves from Matrix Cracking and Fiber Fracture in Laminated Beams." *International Journal of Solids and Structures*, v.37, 2000, 4083-4102.
28. Zheng G.T., Buckley M.A., Kister G. and G.F. Fernando. "Blind Deconvolution of Acoustic Emission Signals for Damage Identification in Composites." *AIAA Journal*, v.39, 2001, 1198-1205.
29. Marantidis C., Van Way C.B. and J.N. Kudva. "Acoustic-Emission Sensing in an On-Board Smart Structural Health Monitoring System for Military Aircraft." *Proceedings of the SPIE Conference on Smart Structures and Integrated Systems*, v. 2191, 1994, 258-264.
30. Schoess J.N. and J.D. Zook. "Test Results of Resonant Integrated Microbeam Sensor (RIMS) for Acoustic Emission Monitoring." *Proceedings of the SPIE Conference on Smart Electronics and MEMS*, v.3328, 1998, 326-332.
31. Menon S. and J.N. Schoess. "Stress Wave Acoustics Analysis for the CH-46 Sea Knight Rotor System." *Honeywell Technology Center Report*, 1999.
32. Schoess J.N. "Development and Application of Stress-Wave Acoustic Diagnostics for Roller Bearings." *Honeywell Technology Center Report*, 1999.
33. Giurgiutiu V., Bao J. and W. Zhao. "Active Sensor Wave Propagation Health Monitoring of Beam and Plate Structures." Proceedings of the 8th International SPIE Symposium on Smart Structures and Materials, Newport Beach, CA, 2001.

34. Monkhouse R.S.C., Wilcox P.W., Lowe M.J.S., Dalton R.P., and P. Cawley. "The rapid Monitoring of Structures using Interdigital Lamb Wave Transducers." *Smart Materials and Structures*, v.9, 2000, 304-309.
35. Todoroki A., Tanaka Y. and Y. Shimamura. "Response Surface for Delamination Monitoring of Gr/Ep Composites Using Electric Resistance Change." *Proceedings of the International Workshop on Structural Health Monitoring*, 1999, 308-316.
36. Thompson L. and B. Westermo. "A New Strain Measurement Technology for Material Damage Assessment." *Proceedings of the SPIE Conference on Smart Structures*, v.2191, 1996, 380-391.
37. Monaco E., Franco F. and L. Lecce. "Structural Damage Identification using Magnetostrictive Actuators." *Proceedings of the SPIE Conference on Smart Structures and Integrated Systems*, v. 3668, 1999, 395-404.
38. Jain M.K., Schmidt S. and Ong K.G.. "Magnetoacoustic Remote Query Temperature and Humidity Sensors." *Smart Materials and Structures*, v.9, 2000, 502-510.
39. Emmerich H. and M. Schofthaler. "Magnetic Field Measurements with a Novel Surface Micromachined Magnetic-Field Sensor." *IEEE Transactions on Electron Devices*, v.47, 2000, 972-977.
40. Baglio S., Latorre L. and P. Nouet. "Development of Novel Magnetic Field Monolithic Sensors with Standard CMOS Compatible MEMS Technology." *Proceedings of the SPIE Conference on Smart Structures and Integrated Systems*, v. 3668, 1999, 417-424.
41. Sage I., Badcock R., Humberstone L., Geddes N., Kemp M. and G. Bourhill. "Triboluminescent Damage Sensors." *Smart Materials and Structures*, v.8, 1999, 504-510.
42. Javidinejad A. and S.P. Joshi. "Design and Structural Testing of Smart Composite Structures with Embedded Conductive Thermoplastic Film." *Smart Materials and Structures*, v.8, 1999, 585-590.
43. Tamiatto C., Krawczak P., Pabiot J. and F. Laurent. "Integrated Sensors for In-Service Health Monitoring of Glass/Resin Composites." *Journal of Advanced Materials*, v.30, 1998, 32-37.
44. Thompson L. and B. Westermo. "A New Strain Measurement Technology for Material Damage Assesment." *Proceedings of the SPIE Conference on Smart Structures and Integrated Systems*, v. 2191, 1994, 380-391.
45. Cao L., Kim T.S., Zhou J., Mantell S.C. and D.L. Polla. "Calibration Technique for MEMS Membrane Type Strain Sensors." *Proceedings of the IEEE*, 1999, 204-210.
46. Banaszak D., Dale G.A., and A.N. Watkins. "An Optical Technique for Detecting Fatigue Cracks in Aerospace Structures." *Proceedings of the IEEE*, 1999, 271-277.
47. http://www.faa.gov/avr/AFS/FARS/far-25.txt
48. http://www.airweb.faa.gov/Regulatory_and_Guidance_Library/rgAD.nsf/HomeFrame
49. Schmidt H.J., Schmidt-Bradecker B. and G. Tober. "Design of Modern Aircraft Structure and the Role of NDI." *Proceedings of the 7th European Conference on Non-Destructive Testing*, v.4, 1999.
50. Suresh S. Fatigue of Materials. 2nd Edition, Cambridge Press, 1998.
51. Amer KB. "A new philosophy of structural reliability, fail safe versus safe life," *Proceedings of the 44th Annual Forum of the American Helicopter Society*, 1988, 3-16.
52. Lee J, Harris B, Almond DP and F. Hammett. "Fibre Composite Fatigue-Life Determination," *Composites Part A-Applied Science and Manufacturing*, v.1, 1997, 5-15.

53. Nyman T. "Composite Fatigue Design Methodology: A Simplified Approach," *Composite Structures*, v.2, 1996, 183-194.
54. Radhakrishnan VM. "Endurance Diagram," *International Journal of Fatigue*, v.6, 1990, 513-517.
55. O'Brian TK. "Towards a Damage Tolerance Philosophy for Composite Materials and Structures," *Composite Materials: Testing and Design*, v.9, 1990, 7-33.
56. Shokrieh MM and LB Lessard. "Residual Fatigue Life Simulation of Laminated Composites," *Proceedings of the International Conference on Advanced Composites*, 1998, 79-86.
57. Michael J, Dickson B and T Cambell. "Analysis of Use of Damage Tolerance Criteria for Helicopter Design," *Proceedings of the 55th Annual Forum of the American Helicopter Society*, v.2, 1999, 1219-1231.
58. Talreja R. "Damage Mechanics and Fatigue Life Assessment of Composite Materials," *International Journal of Damage Mechanics*, v.8, 1999, 339-354.
59. http://www.faa.gov/avi/air/asc/20-107a.doc
60. Rouchon J. "Certification of Large Airplane Composite Structures." *ICAS Congress Proceedings*, v.2, 1990, 1439-1447.
61. Chaumette D. "Certification Problems for Composite Airplane Structures." *Proceedings of the 6th International European SAMPE Conference.* 1985, 19-28.
62. Smith PJ and RD Wilson "Damage Tolerant Composite Wing Panels for Transport Aircraft." NASA Technical Report CR-3951.
63. Ng K.W. "Integrated Diagnostics and Prognostics of Rotation Machinery." *Office of Naval Research Report.*
64. Bar-Cohen Y., Chang Z. and A. Mal. "Characterization of Defects in Composite Materials using Rapidly Acquired Leaky Lamb Wave Dispersion Data." *Proceedings of the 7th European Conference on Non-Destructive Testing*, v.3, 1998.
65. Wang J.M. "An Internet Based System to Monitor Aircraft's Health." S.M. thesis, Massachusetts Institute of Technology, June 2001.
66. Low, S. Jane's All the World's Aircrafts. 2001, 102-165.
67. Neumair M. "Requirements on Future Structural Health Monitoring Systems." *Proceedings of the 7th RTO Meetings*, May 1998.
68. Zimmerman D.C., Simmermacher T. and M. Kaouk. "Model Correlation and System Health Monitoring using Frequency Domain Measurements." *AIAA Journal*, 1995, 3318-3325.
69. Abdelghani M., Goursat M. and T. Biolchini. "On-Line Modal Monitoring of Aircraft Structures under Unknown Exication." *Mechanical Systems and Signal Processing*, v.13, 1999, 839-853.
70. Dalton R.P., Cawley P. and M.J.S. Lowe. "The Potential of Guided Waves for Monitoring Large Areas of Metallic Aircraft Fuselage Structure." *Journal of Nondestructive Evaluation*, v.20, 2001, 29-46.
71. Schoess J.N. "Distributed System Architecture Alternatives for Condition Based Maintenance (CBM)." *Honeywell Technology Center Report*, 1999.
72. Van Way C.B., Kudva J.N. and Schoess J.N. "Aircraft Structural Health Monitoring System Development—overview of the Air Force/Navy Smart Metallic Structures Program." *Proceedings of the SPIE Symposium on Smart Structures and Materials, San Diego*, CA, 1995.

73. Goldfine N., Schlicker D. and A. Washabaugh. "Surface-Mounded Eddy-Current Sensors for On-Line Monitoring of Fatigue Tests and for Aircraft Health Monitoring." *Proceedings of the 2nd Joint NASA/FAA/DoD Conference on Aging Aircraft*, 1998.
74. Zou Y., Tong L. and G.P. Steven. "Vibration-Based Model-Dependant Damage (Delamination) Identification and Health Monitoring for Composite Structures—A Review." *Journal of Sound and Vibration,* v.2, 2000, 357-378.
75. Zhang H., Schulz M.J. and F. Feruson. "Structural Health Monitoring Using Transmittance Functions." *Mechanical Systems and Signal Processing*, v.5, 1999, 765-787.
76. Dunne J.P., Pitt D.M. and D.A. Sofge. "Recent Advances in Active Damage Interrogation." Proceedings of the 42nd AIAA SDM Conference, Seattle, WA, 2001.
77. Deng X., Wang Q. and V. Giugiutiu." *Proceedings of the 6th International SPIE Symposium on Smart Structures and Materials*, Newport Beach, CA, 1999.
78. Lemistre M. and D. Balageas. "Structural Health Monitoring System based on Diffracted Lamb Wave Analysis by Multiresolution Processing." *Smart Materials and Structures*, v.10, 2001, 504-511.
79. Wang X. and G. Huang. "Elastic Wave Propagation Induced by Piezoelectric Actuators for Health Monitoring of Structures." *Journal of Intelligent Material Systems and Structures*, v.10, 1999.
80. Osmont D., Devillers D. and F. Taillade. "A Piezoelectric Based healther Monitoring System for Sandwich Plates Submitted to Damaging Impacts." *European Congress on Computational Methods in Applied Sciences and Engineering*, 2000.
81. Valdez S.H.D. and C. Soutis. "A Structural Health Monitoring System for Laminated Composites." *Proceedings of the 18th Biennial Conference on Mechanical Vibration and Noise*, 2001.
82. Valdez S.H.D. and C. Soutis. "Health Monitoring of Composites using Lamb Waves generated by Piezoelectric Devices." *Plastics, Rubber and Composites*¸v.29, 2000, 475-481.
83. Bar-Cohen Y. "NDE of Fiber Reinforced Composite Materials—A Review." *Materials Evaluation*, v.44, 1986, 446-454.
84. Doebling S.W., Farrar C.R., Prime M.B. and D.W. Shevitz. "Damage Identification and Health Monitoring of Structural and Mechanical Systems from Changes in their Vibration Characteristics: A Literature Review." *Los Alamos National Laboratory Technical Report*, LA-13070-MS, 1996.
85. Gadelrab R.M. "The Effect of Delamination on the Natural Frequencies of a Laminated Composite Beam." *Journal of Sound and Vibration*, v.197, 1996, 283-292.
86. Alampalli S. "Effects of Testing, Analysis, Damage, and Environment on Modal Parameter." *Mechanical Systems and Signal Processing*, v.14, 2000, 63-74.
87. Cawley P. and R.D. Adams. "A Vibration Technique for Non-Destructive Testing of Fibre Composite Structures." *Journal of Composite Materials*, v.13, 1979, 161-175.
88. Cawley P. and R.D. Adams. "The location of Defects in Structure form Measurements of Natural Frequencies." *Journal of Strain Analysis*, v.14, 1979, 49-57.
89. Narayana K.L. and C. Jebaraj. "Sensitivity Analysis of Local/Global Modal Parameters for Identification of a Crack in a Beam." *Journal of Sound and Vibration*, v.228, 1999, 977-994.

90. Parker B.E., Ware H.A., Wipf D.P., Tompkins W.R., Clark B.R., Larson E.C. and H.V. Poor "Fault Diagnostics using Statistical Changes in the Bispectral Domain." *Mechanical Systems and Signal Processing*, v.14, 2000, 561-570.
91. Park K.C. and G.W. Reich. "Model-Based Health Monitoring of Structural Systems: Progress, Potential and Challenges." ." *Proceedings of the 2nd International Workshop on Structural Health Monitoring*, 1999, 82-95.
92. Abdelghani M., Goursat M. and T. Biolchini. "On-Line Modal Monitoring of Aircraft Structures under Unknown Excitation." *Mechanical Systems and Signal Processing*, v.13, 1999, 839-853.
93. Sampaio R.P.C., Maia N.M.M. and J.M.M. Silva. "Damage Detection using the Frequency-Response-Function Curvature Method." *Journal of Sound and Vibration*, v.226, 1999, 1029-1042.
94. Chiu W.K., Galea S.C., Loss L.L. and N. Rajic. "Damage Detection in Bonded Repars using Piezoceramics." *Smart Materials and Structures*, v.9, 2000, 466-475.
95. Bedewi N.E. and D.N. Kung. "Effect of Fatigue Loading on the Modal Properties of Composite Structures and its Utilization for Prediction of Residual Life." *Composite Structures*, v.37, 1997, 357-371.
96. Valdes S.H.D. "Structural Integrity Monitoring of CFRP Laminates using Piezoelectric Devices." Ph.D. thesis, Imperial College of Science Technology and Medicine, September 2000.
97. Kaouk M. and D.C. Zimmerman. "Structural Damage Detection Using Measured Modal Data and No Original Analytical Model." *Proceedings of the International Modal Analysis Conference*, v.1, 1994, 731-737.
98. James G.H. and D.C. Zimmerman. "An Experimental Study of Frequency Response Function (FRF) Based Damage Assessment Tools." *Proceedings of the International Modal Analysis Conference*, v.1, 1998, 151-157.
99. Zimmerman D.C., Simmermacher T. and M. Kaouk. "Structural Damage Detection Using Frequency Response Functions." *Proceedings of the International Modal Analysis Conference*, v.1, 1995, 179-183.
100. Banks H.T. and P.R. Emeric. "Detection of Non-Symmetrical Damage in Smart Plate-Like Structures." *Journal of Intelligent Material Systems and Structures*, v.9, 1998, 818-828.
101. Mitchell K., Sana S., Balakrishnan V.S., Rao V.S., and H.J. Pottinger. "Micro Sensors for Health Monitoring of Smart Structures." *Proceedings of the SPIE Conference on Smart Electronics and MEMS*, v.3673, 1999, 351-358.
102. Purekar A.S. and D.J. Pines. "Detecting Damage in Non-Uniform Beams Using the Dereverberated Transfer Function Response." *Smart Materials & Structures*, v.9, 2000, 429-444.
103. Valdes S.H.D. and C. Soutis. "Delamination Detection in Composite Laminates from Variations of their Modal Characteristics." *Journal of Sound and Vibration*, v.1, 1999, 1-9.
104. Meirovitch L. *Elements of Vibration Analysis*. 2nd ed, McGraw-Hill, New York, NY, 1986.
105. Blevins R. *Formulas for Natural Frequency and Mode Shape*. Krieger Publishing Company, Malabar FL, 1995.
106. Jones, R. M. *Mechanics of Composite Materials*. 2nd ed, Taylor & Francis, Blacksburg, VA, 1999.
107. Bathe K.J., and E.L. Wilson. "Large Eigenvalue Problems in Dynamic Analysis." *Proceedings of the ASCE*, EM6, 1972, 1471-1485.

108. Whitney J. "Effective Elastic Constants of Bidirectional Laminates Containing Transverse Ply Cracks." *Journal of Composite Materials*, v.34, 2000, 954-978.
109. Tong J., Guild F.J., Ogin S.L. and P.A. Smith. "On Matrix Crack Growth in Quasi-Isotropic Laminates." *Composite Science and Technology*, v.57, 1997, 1527-1535.
110. Lagace P.A., Brewer J.C., and C. Varnerin. "TELAC Manufacturing Course Notes." TELAC Report 88-4B, Massachusetts Institute of Technology, 1990.
111. Avitabile P. "Modal Space — In Our Own Little World." *SEM Experimental Techniques*, 1998.
112. Viktorov I.A. *Rayleigh and Lamb Waves, Physical Theory and Applications*. Plenum Press, New York, 1967.
113. Nayfeh A.H. *Wave Propagation in Layered Anisotropic Media with Applications to Composites*. v.39, Elsevier, Amsterdam, 1995.
114. Lamb H. "On Waves in an Elastic Plate." *Proceedings of the Royal Society of London. Series A, Containing Papers of a Mathematical and Physical Character*, v.93, n.651, 1917, 293-312.
115. Worlton D.C. "Experimental Confirmation of Lamb Waves at Megacycle Frequencies." *Journal of Applied Physics*, v.32, 1961, 967-971.
116. Demer L.J. and L.H. Fentnor. "Lamb Wave Techniques in Nondestructive Testing." *International Journal of Nondestructive Testing*, v.1, 1969, 251-283.
117. White R.M. "Surface Elastic Waves." *Proceedings of the IEEE*, v.58, no.8, 1970.
118. Wenzel S.W. and R.M. White. "Silicon-Based Ultrasonic Lamb-Wave Multisensors." *IEEE Solid-State Sensor and Actuator Workshop*, 1988, 27-30.
119. Wenzel S.W. and R.M. White. "A Multisensor Employing an Ultrasonic Lamb-Wave Oscillator." *IEEE Transactions on Electronic Devices*, v.35 1988, 735-743.
120. Wenzel S.W., Martin B.A. and R.M. White. "Generalized Lamb-Wave Multisensor." *Proceedings of the IEEE Ultrasonics Symposium*, v.1, 1988, 563-567.
121. Grondel S., Assaad J., Delebarre C., Blanquet P. and e. Moulin "The Propagation of Lamb Waves in Multilayered Plates: Phase-Velocity Measurement." *Measurement Science and Technology*, v.10, 1999, 348-353.
122. Niethammer M. and L.J. Jacobs. "Time-Frequency Representation of Lamb Waves." *Journal of the Acoustic Society of America*, v.109, 2001, 1841-1847.
123. Valle C., Niethammer M. and L.J. Jacobs. "Crack Characterization using Guided Circumferential Waves." *Journal of the Acoustic Society of America*, v.110, 2001, 1282-1290.
124. Cho Y. "Lamb Wave Scattering Analysis for Reflector Characterization." *IEEE Transactions on Ultrasonics, Ferroelectrics, and Frequency Control*, v.44, 1997, 44-52.
125. Pagneux V. and A. Maurel. "Determination of Lamb Mode Eigenvalues." *Journal of the Acoustic Society of America*, v.110, 2001, 1307-1314.
126. Deutsch W.A.K. and K. Deutsch. "Defect Detection with Rayleigh and Lamb Waves Generated by a Self-Focusing Phased Array." *Proceedings of the 7th European Conference on Non-Destructive Testing*, v.3, 1998.
127. Lee Y.C. "Measuring Lamb Wave Dispersion Curves of a Bi-Layered Plate and its Applications on Material Characterization of Coating." *IEEE Transactions on Ultrasonics, Ferroelectrics, and Frequency Control*, v.48, 2001, 830-837.
128. Lee Y.C. "Measurements of Dispersion Curves Leaky Lamb Waves using a Lens-Less Line-Focus Transducer." *Ultrasonics*, v.39, 2001, 297-306.

129. Lemistre M and D. Balageas. "Structural Health Monitoring System based on Diffracted Lamb Wave Analysis by Multiresolution Processing." *Smart Materials and Structures*, v.10, 2001, 504-511.
130. Monkhouse R.S.C., Wilcox P.D. and P. Cawley. "Flexible Interdigital PVDF Transducers for the Generation of Lamb Waves in Structures." *Ultrasonics*, v.35, 1997, 489-498.
131. Wilcox P., Lowe M., and P. Cawley. "Lamb and SH Wave Transducer Arrays for the Inspection of Large Areas of Thick Plates." *Proceedings of the 15th World Conference on Non-Destructive Testing*, Rome, 2000.
132. Dalton R.P., Cawley P. and M.J.S. Lowe. "The potential of Guided Waves for Monitoring Large Areas of Metallic Aircraft Fuselage Structure." *Journal of Nondestructive Evaluation*, v.20, 2001, 29-46.
133. Saravanos D.A. and P.R. Heyliger. "Coupled Layerwise Analysis of Composite Beans with Embedded Piezoelectric Sensors and Actuators." *Journal of Intelligent Material Systems and Structures*, v.6, 1995, 350-362.
134. Saravanos D.A., Birman V. and D.A. Hopkins. "Detection of Delaminations in Composite Beams using Piezoelectric Sensors." *Proceedings of the 35th Structures, Structural Dynamics and Materials Conference of the AIAA*, 1994.
135. Percival W.J. and E.A. Birt. "A Study of Lamb Wave Propagation in Carbon-Fibre Composites." *Insight: Non-Destructive Testing and Condition Monitoring*, v.39, 1997, 728-735.
136. Birt E.A. "Damage Detection in Carbon-Fibre Composites using ultrasonic Lamb Waves." *Insight: Non-Destructive Testing and Condition Monitoring*, v.40, 1998, 335-339.
137. Badcock R.A. and E.A.Birt "The use of 0-3 Piezocomposite Embedded Lamb Wave Sensors for Detection of Damage in Advanced Fibre Composites." *Smart Materials and Structures*, v.9, 2000, 291-297.
138. Seale M.D., Smith B.T. and W.H. Prosser. "Lamb Wave Assessment of Fatigue and Thermal Damage in Composites." *Journal of the Acoustic Society of America*, v.103, 1998, 2416-2424.
139. Tang B. and E.G. Henneke. "Lamb Wave Monitoring of Axial Stiffness Reduction of Laminated Composite Plates." *Materials Evaluation*, v.47, 1989, 928-933.
140. Rose J.L., Hay T. and V.S. Agarwala. "Skin to Honeycomb Core Delamination Detection with Guided Waves." *4th Joint DOD/FAA/NASA Conference on Aging Aircraft*, 2000.
141. Kundu T., Potel C., and J.F. de Belleval. "Importance of Near Lamb Mode Imaging of Multilayered Composite Plates." *Ultrasonics*, v.39, 2001, 283-290.
142. Ishak S.I., Liu G.R., Lim S.P. and H.M. Shang. "Experimental Study on Employing Flexural Wave Measurements to Characterize Delamination in Beams." *Experimental Mechanics*, v.41, 2001 157-164.
143. Monnier T., Jayet Y., Guy P. and J.C. Baboux. "The Piezoelectric Implant Method: Implementation and Practical Applications." *Smart Materials and Structures*, v.9 2000, 267-272.
144. Rose J.L. and T. Hay. "Skin to Honeycomb Core Delamination Detection with Guided Waves." *Proceedings of the 15th World Conference on Non-Destructive Testing*, Rome, 2000.
145. Propser D. "Automated Detection of Wave Velocities in Concrete Bridge Decks." PhD thesis, Massachusetts Institute of Technology, June 2001.

146. Fripp M. “Distributed Structural Actuation and Control with Electrostrictors.” SM thesis, Massachusetts Institute of Technology, June 1995.
147. Lively P. “Dynamic Structural Shape Estimation using Integral Sensor Arrays.” SM thesis, Massachusetts Institute of Technology, June 2000.
148. Strang G. and T. Nguyen *Wavelets and Filter Banks.* Wellesley-Cambridge Press, Wellesley, Ma, 1996.
149. “The Composite Materials Handbook MIL-17 Vol. 1” Guidelines for Characterization of Structural Materials.” MIL-HDBK-1E, Department of Defense, 1999.
150. Kessler S.S., Spearing S.M., Atalla M.J., Cesnik C.E.S. and C. Soutis. “Structural Health Monitoring in Composite Materials using Frequency Response Methods.” *Proceedings of the SPIE International Symposium on Smart Strucutres and Material*, 2001.
151. Lind R., Kyle S. and M. Brenner. “Wavelet Analysis to Characterize Non-Linearities and Predict Limit Cycles of an Aeroelastic System.” *Mechanical Systems and Signal Processing*, v.15, 2001, 337-356.
152. Dunn C. “The Analysis, Design, Manufacture, and Testing of a Composite Micro-Satellite.” SM thesis, Massachusetts Institute of Technology, February 2001.
153. Anderson E.H. “Piezoceramic Induced Strain Actuation of One and Two Dimensional Structures.” PhD thesis, Massachusetts Institute of Technology, June 1989.
154. Kollar L. and R.J. Steenkiste. “Calculation of the Stresses and Strains in Embedded Fiber Optic Sensors.” *Journal of Composite Materials*, v.32, 1998, 1647-1679.
155. Rees D., Chiu W.K. and R. Jones. “A Numerical Study of Crack Monitoring in Patched Structures using a Piezo Sensor.” *Smart Materials and Structures*, v.1, 1992, 202-205.
156. Chiu W.K., Galea S.C., Koss L.L. and N. Rajic. “Damage Detection in Bonded Repairs using Piezoceramics.” *Smart Materials and Structures*, v.9, 2000, 466-475.
157. Hautamaki C., Zurn S., Mantell S.C. and D.L. Polla. “Experimental Evaluation of MEMS Strain Sensors Embedded in Composites.” *Journal of Microelectromechanical Systems*, v.8, 1999, 272-279.
158. Sung D.U., Kim C.G. and C.S. Hong. “Simultaneous Monitoring of Impact Locations and Damages in Composite Laminates using Piezoceramics Sensors.” *Proceedings of the 13th ICCM*, Beijing, 2001.
159. Benmadakhene S. and A. Laksimi. “Propagation Study of Acoustic Emission Waves in Composite Materials.” *Proceedings of the 13th ICCM*, Beijing, 2001.
160. Aberg M. and P. Gudmundson. “Micromechanical Modeling of Transient Waves from Matrix Cracking and Fiber Fracture in Laminated Beams.” *International Journal of Solids and Structures*, v.37, 2000, 4083-4102.
161. Seydel R.E. and F.K. Chang. “Implementation of a Real-Time Impact Identification Technique for Stiffened Composite Panels.” Proceedings of the 2nd International Workshop on Structural Health Monitoring, 1999, 225-233.
162. Noonan E.E., Protz C.S., Peles Y.P. and S.M. Spearing. "Structural Analysis of a Micro-Rocket Combustion Chamber." *Materials Research Society*, November 2001, Boston, MA.
163. Ikegami R. “Structural Health Monitoring: Assessment of Aircraft Customer Needs.” *Proceedings of the International Workshop on Structural Health Monitoring*, 1999, 12-23.
164. Huber J.E., Fleck N.A. and M.F. Ashby. “The Selection of Mechanical Actuators based on Performance Indices.” *Proceedings of the Royal Society of London*, 1997, 2185-2205.
165. Horn D. and W.R. Mayo. “NDE Reliability Gains from Combining Eddy-Current and Ultrasonic Testing.” *NDT&E International*, v.33, 2000, 351-362.

166. Schoess J.N., Arch D. and Yang W. "MEMS Sensing and Control: An Aerospace Perspective." *Honeywell Technology Center Report*, 2000.
167. Luginbuhl P., Collins S.D., Racine G.A., Gretillat M.A., de Rooij N.F., Brooks, K.G. and N. Setter. "Ultrasonic Flexural Lamb-Wave Actuators based on PZT Thin Film." *Sensors and Actuators A*, v.64, 1998, 41-49.
168. Yuan L., Sana S., Pottinger H.J. and V.S. Rao. "Distributed Arithmetic Implementation of Multivariable Controllers for Smart Structural Systems." *Smart Materials and Structures*, v.9, 2000, 401-412.
169. Pradhan S.S. and K. Ramchandran. "Distributed Source Coding: Symmetric Rates and Applications to Sensor Networks." *Proceedings of the IEEE*, 2000, 363-372.
170. Das N.K., Khorrami F. and S. Nourbakhsh. "A New Integrated Piezoelectric-Dielectric Microstrip Antenna for Dual Wireless Actuation and Sensing Functions." *Proceedings of the SPIE Symposium on Smart Electronics and MEMS*, San Diego, CA, 1998.
171. Porret A.S., Melly T., Enz C.C. and E.A. Vittoz. "Design of Hih-Q Varactors for Low-Power Wireless Applications using a Standard CMOS Process." *IEEE Journal of Solid-State Circuits*, v.35, 2000, 337-345.
172. van den Boom T., Tebmann D., Lerch R., vom Boegel G., Hammerschmidt D., Amelung J., Hosticka B. and P. Mahdavi. "Romote CMOS Pressure Sensor Chip with Wireless Power and Data Transmission." *Proceedings of the IEEE International Solid-State Circuits Conference*, 2000, 186-187.
173. Rabaey J., Ammer J., da Silva J.L. and D. Patel. "Ad-hoc Wireless Networking of Ubiquitous Low-Energy Sensor/Monitor Nodes." *Proceedings of the IEEE*, 2000, 9-12.
174. Britton C.L., Warmack R.J., Smigh S.F., Oden P.I. and G.M. Brown. "MEMS Sensors and Wireless Telemetry for Distributed Systems." *Proceedings of the SPIE Symposium on Smart Electronics and MEMS*, San Diego, CA, 1998.
175. Britton C.L., Warmack R.J., Smigh S.F., Oden P.I. and G.M. Brown. "Battery-Powered, Wireless MEMS Sensors for High-Sensitivity Chemical and Biological Sensing." *Proceedings of the IEEE*, 1999, 359-368 .
176. Krantz D., Belk J., Dubow J., Hautamaki C., Matell S., Polla D. and S. Zurn. "Applied Research in Remotely-Queried Embedded Microsensors." *Proceedings of the SPIE Symposium on Smart Electronics and MEMS*, San Diego, CA, 1998.
177. Varadan V.K., Teo P.T., Jose K.A. and V.V. Varadan. "Design and Development of a Smart Wireless System for Passive Temperature Sensors." *Smart Materials and Structures*, v.9, 2000, 379-388.
178. Mitchell K., Sana S., Valakrishnan V.S., Rao V.S. and H.J. Pottinger. "Micro Sensors for Health Monitoring of Smart Structure." *Proceedings of the SPIE Symposium on Smart Electronics and MEMS*, Newport Beach, CA, 1999.
179. Gilbert R.W., Bond L.J. and Skorpik J.R. "Smart Multi-Sensor Radio Frequency Tags for Propulsion Systems." *Pacific Northwest National Laboratory Report*, 2000.
180. Pulitzer S.W. "Feasibility Assessment and Design of Micro Hydraulic Solid State Transducers." S.M. thesis, Massachusetts Institute of Technology, June 1998.
181. Spillman W.B. and S. Durkee. "Non-Contact Power/Interrogation System for Smart Stuctures." *Proceedings of the SPIE Symposium on Smart Structures and Materials*, San Diego, CA, 1994.
182. Bleay S.M, Loader C.B., Hawyes V.J., Humberstone L. and P.T. Curtis. "A smart Repair System for Polymer Matrix Composites." *Composites Part A*, v.32, 2001, 1767-1776.

APPENDIX A

Mathematica ä Code for Phase and Group Velocities

```
(* CLPT code to determine material properties for laminate*)

layup={90, 45, -45, 0};
sym=1;
El=21500000*6912;
Et=1460000*6912;
vlt=.3;
vtl=Et/El*vlt;
G=810000*6912;
t=.005*.0254;
rho=.055*27680;
ply=Length[layup];

q=IdentityMatrix[3]*0;
q[[1,1]]=El/(1-vlt*vtl);
q[[2,2]]=Et/(1-vlt*vtl);
q[[1,2]]=(Et*vlt)/(1-vlt*vtl);
q[[2,1]]=q[[1,2]];
q[[3,3]]=G;

QBAR=IdentityMatrix[3]*0;

For[z=1,z<=ply,z++,
        x=layup[[z]]*\[Pi]/180;
        a={{Cos[x]*Cos[x],Sin[x]*Sin[x],Cos[x]*Sin[x]},{Sin[x]*Sin[x],
    Cos[x]*Cos[x],-Cos[x]*Sin[x]},{-2*Cos[x]*Sin[x],2*Cos[x]*Sin[x],
    Cos[x]*Cos[x]-Sin[x]*Sin[x]}};
        b=Transpose[a];
        Q=b.q.a;
        QBAR=QBAR+Q;]
QBAR=2*QBAR;
A=QBAR/ply/2;
As=Inverse[A];
Es11=As[[1,1]];
Es22=As[[2,2]];
Es33=As[[3,3]];
Es12=As[[1,2]];
E11=Es11^-1;
E22=Es22^-1;
G=Es33^-1;
v=-Es12*E11;
t=ply*2*t;
(*Compute phase velocity*)

n=0;
x=Table[{j,j},{j,1,3000}]*0;
```

```
y=Table[{j,j},{j,1,3000}]*0;
For[w=20000, w<1520000, w=w+500,
n=n+1;
d=(w*t)/2*Sqrt[((2rho(1+v))/E11)];
z=(1-2*v)/(2-2*v);
a=E11/(2rho(1+v)*L^2);
h=Tan[Sqrt[(1-a)]*d]/Tan[Sqrt[(z-a)]*d]+(2a-1)^2/(4a*Sqrt[(1-a)]*Sqrt[(z-a)]);
x[[n,2]]=N[Re[L/. FindRoot[h==0,{L,1000,100,4000}]]];
x[[n,1]]=N[w]/2/Pi/1000;];

(*Compute group velocity*)

n=0;
For[i=1,i<2999,i++,
        n=n+1;
        f=(x[[i+1,1]]+x[[i,1]])/2;
        cp=(x[[i+1,2]]+x[[i,2]])/2;
        g=(x[[i+1,2]]-x[[i,2]])/(x[[i+1,1]]-x[[i,1]]);
        cg=cp/(1-f/cp*g);
        y1[[n,1]]=f;
        y1[[n,2]]=cg;]

(*Approximated phase and group velocities from exponencial regression*)

n=0;
For[i=1,i<2999,i++,
        n=n+1;
        f=x[[n,1]]*1000;
        cp=3.4378*f^0.4989;
        g=1.7151*f^(-0.5011);
        cg=cp/(1-f/cp*g);
        y2[[n,1]]=x[[n,1]];
        y2[[n,2]]=cg;]

(*Plotting functions*)

one=ListPlot[x, PlotLabel→"Lamb Wave Phase Velocity for AS4/3501-6 [90/+45/-45/0]s",
PlotRange→{{0,100},{0,2000}}, FrameLabel→{"Frequency (kHz)","Group Velocity  (m/s)"}]
two=ListPlot[y1, PlotLabel→"Lamb Wave Group Velocity for AS4/3501-6 [90/+45/-45/0]s",
PlotRange→{{0,100},{0,2000}}, FrameLabel→{"Frequency (kHz)","Phase Velocity  (m/s)"}];
three=ListPlot[y2, PlotLabel→"Lamb Wave Group Velocity for AS4/3501-6 [90/+45/-45/0]s",
PlotRange→{{0,100},{0,2000}}, FrameLabel→{"Frequency (kHz)","Phase Velocity  (m/s)"}];
Show[one,two,three]
```

APPENDIX B

Lamb Wave Derivations

Phase Velocity Derivation

From Lamb's original work [114], he presents the anti-symmetric solution to the wave equation in a thin solid medium as:

$$\frac{\tanh\, bf}{\tanh\, af} = \frac{\left(x^2 + b^2\right)^2}{4x^2 a\, b}$$

where these terms are defined as:

$$a = \sqrt{x^2 - h^2}\,, b = \sqrt{x^2 - k^2}$$

$$h^2 = \frac{rw^2}{l + 2m}, k^2 = \frac{rw^2}{m}, x^2 = \frac{w^2}{c_{phase}^2}, f = \frac{t}{2}$$

$$m = \frac{\mathrm{E}}{2(1+n)}, \quad l = \frac{\mathrm{E}n}{(1-2n)(1+n)}$$

The hyperbolic terms can be eliminated by using the identity:

$$\tanh(iz) = i\tan(z) \qquad \frac{\tanh\, bf}{\tanh\, af} = \frac{\tanh\sqrt{h^2 - x^2}\, fi}{\tanh\sqrt{k^2 - x^2}\, fi} = \frac{\tan\sqrt{h^2 - x^2}\, f}{\tan\sqrt{k^2 - x^2}\, f}$$

Substituting into both sides and collecting like terms the equation becomes:

$$\frac{\tan\sqrt{1 - \frac{m}{rc_{phase}^2}}\sqrt{\frac{r}{m}}\frac{wt}{2}}{\tan\sqrt{\frac{m}{l+2m} - \frac{m}{rc_{phase}^2}}\sqrt{\frac{r}{m}}\frac{wt}{2}} = \frac{4\frac{1}{c_{phase}^2} - 4\frac{1}{m} + \frac{r^2}{m^2}c_{phase}^2}{4\sqrt{1 - \frac{r}{l+2m}c_{phase}^2}\sqrt{1 - \frac{r}{m}c_{phase}^2}}$$

Now, by collecting the terms into the following non-dimensional parameters, the equation given in Viktorov [112] is recovered (note that ξ is a different variable than the one used by Lamb):

$$x^2 = \frac{m}{(l+2m)}, \; z^2 = \frac{m}{rc_{phase}^2}, \bar{\mathrm{d}} = \frac{wt}{2}\sqrt{\frac{r}{m}}$$

$$\frac{\tan(\bar{\mathrm{d}}\sqrt{1 - z^2})}{\tan(\bar{\mathrm{d}}\sqrt{x^2 - z^2})} + \frac{(2z^2 - 1)^2}{4z^2\sqrt{1 - z^2}\sqrt{x^2 - z^2}} = 0$$

This is the solution as presented in Chapter 4 that was numerically solved in **Appendix A**.

Group Velocity Derivation

The group velocity of a traveling elastic wave is defined as:

$$c_{group} = \frac{\partial w}{\partial k}$$

where the wavenumber k is defined as:

$$k = \frac{w}{c_{phase}}$$

Direct differentiation of this equality with respect to k yields the classical form:

$$c_{group} = c_{phase} + \frac{\partial c_{phase}}{\partial k} k$$

Alternatively, a more practical form can be reached by differentiating with respect to w:

$$c_{group} = \frac{c_{phase}}{1 - \frac{w}{c_{phase}} \cdot \frac{\partial c_{phase}}{\partial w}}$$

This equation, which relies only on the frequency and phase velocity (which is also a function of frequency), can be implemented as part as a numerical solution as seen in **Appendix A**, or can be used to solve for the group velocity directly if the phase velocity equation is exponentially regressed (approximately a square root relationship) for a range of frequencies.

Optimal Actuator Size Derivation

The out of plane displacement of an elastic wave traveling in a solid medium follows the proportionality:

$$W \propto \sin ka$$

where $2a$ is the length of the actuator in the direction of propagation. The maximum displacement is achieved were the derivative is zero:

$$a \cos ka = 0$$

for which the solution is:

$$ka = (2n+1)\frac{p}{2} \quad \text{for n} = 0,1,2...$$

manipulating this equality yields:

$$2a = (n+\frac{1}{2})\frac{2p}{k}$$

where the wavenumber k is defined again as:

$$k = \frac{w}{c_{phase}} = \frac{2pf}{c_{phase}}$$

Substituting this into the previous equality yields the practical form of this equation:

$$2a = (n+\frac{1}{2})\frac{c_{phase}}{f} \quad \text{for n} = 0,1,2...$$

where f is the frequency in Hertz. From this equation, the actuator dimensions can be optimized as discussed in Chapter 4.

APPENDIX C

ABAQUS® Codes for Frequency Response and Lamb Wave Models

```
*HEADING
Control Model for Frequency Response
*NODE
1,0,0,0
8,0,0.7,0
21,0,2,0
211,1,0,0
218,1,0.7,0
231,1,2,0
841,4,0,0
848,4,0.7,0
861,4,2,0
1261,6,0,0
1268,6,0.7,0
1281,6,2,0
2101,10,0,0
2108,10,0.7,0
2121,10,2,0
*NGEN, NSET=N1
1,8,1
*NGEN,NSET=N2
8,21,1
*NGEN,NSET=N3
211,218,1
*NGEN,NSET=N4
218,231,1
*NGEN,NSET=N5
841, 848, 1
*NGEN,NSET=N6
848, 861, 1
*NGEN,NSET=N7
1261, 1268, 1
*NGEN,NSET=N8
1268, 1281, 1
*NGEN,NSET=N9
2101, 2108, 1
*NGEN,NSET=N10
2108, 2121, 1
*NFILL,NSET=CLAMPED1
N1, N3, 10, 21
*NFILL,NSET=CLAMPED2
N2, N4, 10, 21
*NFILL,NSET=BOTTOM1
N3, N5, 30, 21
*NFILL,NSET=BOTTOM2
N4, N6, 30, 21
*NFILL,NSET=DELAM
N5, N7, 20, 21
*NFILL,NSET=UNDELAM
N6, N8, 20, 21
*NFILL,NSET=TOP1
N7, N9, 40, 21
*NFILL,NSET=TOP2
N8, N10, 40, 21
*NSET,NSET=CLAMPED
CLAMPED1,CLAMPED2
```

```
*NSET,NSET=UNDAMAGED
BOTTOM1,BOTTOM2,TOP1,TOP2,UNDELAM,CLAMPED
*NSET,NSET=ALL1
UNDAMAGED,DELAM
*NCOPY,OLD SET=ALL1 ,CHANGE NUMBER=10000 ,NEW SET=ALL2 ,SHIFT
0,0,0.0
0,0,0,1,0,0,0
*MPC
TIE,ALL2,ALL1
*ELEMENT,TYPE=S9R5
1,1,43,45,3,22,44,24,2,23
10001,10001,10043,10045,10003,10022,10044,10024,10002,10023
*ELGEN,ELSET=SPECIMEN1
1,10,2,1,50,42,10
*ELGEN,ELSET=SPECIMEN2
10001,10,2,1,50,42,10
*SHELL SECTION,OFFSET=SNEG,ELSET=SPECIMEN1,COMPOSITE
.005,,LAMINA,  0.
.005,,LAMINA,+45.
.005,,LAMINA,-45.
.005,,LAMINA, 90.
*SHELL SECTION,OFFSET=SPOS,ELSET=SPECIMEN2,COMPOSITE
.005,,LAMINA, 90.
.005,,LAMINA,-45.
.005,,LAMINA,+45.
.005,,LAMINA,  0.
**defined 90 degrees rotated
*MATERIAL,NAME=LAMINA
*ELASTIC,TYPE=LAMINA
21.5E6, 1.46E6, 0.3, 0.81E6, 0.46E6, 0.46E6
*DENSITY
 0.0001417
*BOUNDARY
CLAMPED, ENCASTRE
*STEP, PERTURBATION
*FREQUENCY, EIGENSOLVER=SUBSPACE
50,
*RESTART,WRITE,OVERLAY
*END STEP
**-------
```

```
*HEADING
Center Delamination Model for Frequency Response
*NODE
1,0,0,0
21,0,2,0
211,1,0,0
231,1,2,0
946,4.5,0,0
966,4.5,2,0
1156,5.5,0,0
1176,5.5,2,0
2101,10,0,0
2121,10,2,0
*NGEN, NSET=N1
1,21,1
*NGEN,NSET=N2
211,231,1
*NGEN,NSET=N3
946, 966, 1
*NGEN,NSET=N4
1156, 1176, 1
*NGEN,NSET=N5
2101, 2121, 1
*NFILL,NSET=CLAMPED
N1, N2, 10, 21
*NFILL,NSET=BOTTOM
N2, N3, 35, 21
*NFILL,NSET=DELAM
N3, N4, 10, 21
*NFILL,NSET=TOP
N4, N5, 45, 21
*NSET,NSET=UNDAMAGED
BOTTOM,TOP,CLAMPED
*NCOPY,OLD SET=UNDAMAGED, CHANGE NUMBER=10000, NEW SET=UNDAMAGED2, SHIFT
0,0,0.0
0,0,0,1,0,0,0
*NCOPY,OLD SET=DELAM ,CHANGE NUMBER=10000 ,NEW SET=DELAM2 ,SHIFT
0,0,0.0
0,0,0,1,0,0,0
*MPC
TIE,UNDAMAGED2,UNDAMAGED
*ELEMENT,TYPE=S9R5
1,1,43,45,3,22,44,24,2,23
10001,10001,10043,10045,10003,10022,10044,10024,10002,10023
*ELGEN,ELSET=SPECIMEN1
1,10,2,1,50,42,10
*ELGEN,ELSET=SPECIMEN2
10001,10,2,1,50,42,10
*SHELL SECTION,OFFSET=SNEG,ELSET=SPECIMEN1,COMPOSITE
.005,,LAMINA,  0.
.005,,LAMINA,+45.
.005,,LAMINA,-45.
.005,,LAMINA, 90.
*SHELL SECTION,OFFSET=SPOS,ELSET=SPECIMEN2,COMPOSITE
.005,,LAMINA, 90.
.005,,LAMINA,-45.
```

```
.005,,LAMINA,+45.
.005,,LAMINA,  0.
**defined 90 degrees rotated
*MATERIAL,NAME=LAMINA
*ELASTIC,TYPE=LAMINA
21.5E6, 1.46E6, 0.3, 0.81E6, 0.81E6, 0.46E6
*DENSITY
 0.0001417
*BOUNDARY
CLAMPED, ENCASTRE
*STEP, PERTURBATION
*FREQUENCY, EIGENSOLVER=SUBSPACE
50,
*RESTART,WRITE,OVERLAY
*END STEP
**-------
```

```
*HEADING
Control Model for Lamb wave
*NODE
1,0,0,0
21,0,2,0
211,1,0,0
231,1,2,0
946,4.5,0,0
966,4.5,2,0
1156,5.5,0,0
1176,5.5,2,0
2101,10,0,0
2121,10,2,0
*NGEN, NSET=N1
1,21,1
*NGEN,NSET=N2
211,231,1
*NGEN,NSET=N3
946, 966, 1
*NGEN,NSET=N4
1156, 1176, 1
*NGEN,NSET=N5
2101, 2121, 1
*NFILL,NSET=CLAMPED
N1, N2, 10, 21
*NFILL,NSET=BOTTOM
N2, N3, 35, 21
*NFILL,NSET=DELAM
N3, N4, 10, 21
*NFILL,NSET=TOP
N4, N5, 45, 21
*NSET,NSET=ALL
BOTTOM,TOP,DELAM,CLAMPED
*ELEMENT,TYPE=S9R5
1,1,43,45,3,22,44,24,2,23
*ELGEN,ELSET=SPECIMEN
1,10,2,1,50,42,10
*NSET, NSET=EDGE1,GENERATE
232,294,1
*NSET, NSET=EDGE2,GENERATE
295,357,1
*NSET, NSET=CORRECT1,GENERATE
232,274,21
252,294,21
*NSET, NSET=CORRECT2,GENERATE
295,337,21
315,357,21
*SHELL SECTION,ELSET=SPECIMEN,COMPOSITE
.005,,LAMINA,  0.
.005,,LAMINA,+45.
.005,,LAMINA,-45.
.005,,LAMINA, 90.
.005,,LAMINA, 90.
.005,,LAMINA,+45.
.005,,LAMINA,-45.
.005,,LAMINA,  0.
```

```
**defined 90 degrees rotated
*MATERIAL,NAME=LAMINA
*ELASTIC,TYPE=LAMINA
21.5E6, 1.46E6, 0.3, 0.81E6, 0.46E6, 0.46E6
*DENSITY
 0.0001417
*BOUNDARY
CLAMPED, ENCASTRE
*AMPLITUDE,NAME=HANNING,INPUT=waveform2.inp,DEFINITION=TABULAR,TIME=TOTAL
TIME,VALUE=RELATIVE
*STEP,INC=500
*DYNAMIC,DIRECT,NOHAF
1E-6,0.5E-3
*CLOAD,AMPLITUDE=HANNING
EDGE1,5,1
CORRECT1,5,-0.5
EDGE2,5,-1
CORRECT2,5,0.5
*NODE PRINT,FREQUENCY=500
U3
*EL PRINT, FREQUENCY=0
*PRINT,FREQUENCY=500
*END STEP
**-------
```

```
*HEADING
Center Delamination Model for Lamb wave
*NODE
1,0,0,0
21,0,2,0
211,1,0,0
231,1,2,0
946,4.5,0,0
966,4.5,2,0
1156,5.5,0,0
1176,5.5,2,0
2101,10,0,0
2121,10,2,0
*NGEN, NSET=N1
1,21,1
*NGEN,NSET=N2
211,231,1
*NGEN,NSET=N3
946, 966, 1
*NGEN,NSET=N4
1156, 1176, 1
*NGEN,NSET=N5
2101, 2121, 1
*NFILL,NSET=CLAMPED
N1, N2, 10, 21
*NFILL,NSET=BOTTOM
N2, N3, 35, 21
*NFILL,NSET=DELAM
N3, N4, 10, 21
*NFILL,NSET=TOP
N4, N5, 45, 21
*NSET,NSET=UNDAMAGED
BOTTOM,TOP,CLAMPED
*NCOPY,OLD SET=UNDAMAGED, CHANGE NUMBER=10000, NEW SET=UNDAMAGED2, SHIFT
0,0,0.0
0,0,0,1,0,0,0
*NCOPY,OLD SET=DELAM ,CHANGE NUMBER=10000 ,NEW SET=DELAM2 ,SHIFT
0,0,0.0
0,0,0,1,0,0,0
*MPC
TIE,UNDAMAGED2,UNDAMAGED
*ELEMENT,TYPE=S9R5
1,1,43,45,3,22,44,24,2,23
10001,10001,10043,10045,10003,10022,10044,10024,10002,10023
*ELGEN,ELSET=SPECIMEN1
1,10,2,1,50,42,10
*ELGEN,ELSET=SPECIMEN2
10001,10,2,1,50,42,10
*NSET, NSET=EDGE1,GENERATE
232,294,1
*NSET, NSET=EDGE2,GENERATE
295,357,1
*NSET, NSET=CORRECT1,GENERATE
232,274,21
252,294,21
*NSET, NSET=CORRECT2,GENERATE
```

```
295,337,21
315,357,21
*SHELL SECTION,OFFSET=SNEG,ELSET=SPECIMEN1,COMPOSITE
.005,,LAMINA,  0.
.005,,LAMINA,+45.
.005,,LAMINA,-45.
.005,,LAMINA, 90.
*SHELL SECTION,OFFSET=SPOS,ELSET=SPECIMEN2,COMPOSITE
.005,,LAMINA, 90.
.005,,LAMINA,+45.
.005,,LAMINA,-45.
.005,,LAMINA,  0.
**defined 90 degrees rotated
*MATERIAL,NAME=LAMINA
*ELASTIC,TYPE=LAMINA
21.5E6, 1.46E6, 0.3, 0.81E6, 0.46E6, 0.46E6
*DENSITY
 0.0001417
*BOUNDARY
CLAMPED, ENCASTRE
*AMPLITUDE,NAME=HANNING,INPUT=waveform2.inp,DEFINITION=TABULAR,TIME=TOTAL
TIME,VALUE=RELATIVE
*STEP,INC=500
*DYNAMIC,DIRECT,NOHAF
1E-6,0.5E-3
*CLOAD,AMPLITUDE=HANNING
EDGE1,5,1
CORRECT1,5,-0.5
EDGE2,5,-1
CORRECT2,5,0.5
*NODE PRINT,FREQUENCY=500
U3
*EL PRINT, FREQUENCY=0
*PRINT,FREQUENCY=500
*END STEP
**-------
```

```
*HEADING
High Density Al Beam for Lamb wave
*NODE
1,0,0,0
21,0,2,0
211,1,0,0
231,1,2,0
946,4.5,0,0
966,4.5,2,0
1156,5.5,0,0
1176,5.5,2,0
2101,10,0,0
2121,10,2,0
*NGEN, NSET=N1
1,21,1
*NGEN,NSET=N2
211,231,1
*NGEN,NSET=N3
946, 966, 1
*NGEN,NSET=N4
1156, 1176, 1
*NGEN,NSET=N5
2101, 2121, 1
*NFILL,NSET=CLAMPED
N1, N2, 10, 21
*NFILL,NSET=BOTTOM
N2, N3, 35, 21
*NFILL,NSET=DELAM
N3, N4, 10, 21
*NFILL,NSET=TOP
N4, N5, 45, 21
*NSET,NSET=ALL
BOTTOM,TOP,DELAM,CLAMPED
*ELEMENT,TYPE=S9R5
1,1,43,45,3,22,44,24,2,23
*ELGEN,ELSET=SPECIMEN
1,10,2,1,50,42,10
*NSET, NSET=EDGE1,GENERATE
232,294,1
*NSET, NSET=EDGE2,GENERATE
295,357,1
*NSET, NSET=CORRECT1,GENERATE
232,274,21
252,294,21
*NSET, NSET=CORRECT2,GENERATE
295,337,21
315,357,21
*SHELL SECTION,ELSET=SPECIMEN,COMPOSITE
.005,,LAMINA,  0.
.005,,LAMINA,+45.
.005,,LAMINA,-45.
.005,,LAMINA, 90.
.005,,LAMINA, 90.
.005,,LAMINA,+45.
.005,,LAMINA,-45.
.005,,LAMINA,  0.
```

```
.375,,HDA, 90.
.375,,HDA, 90.
.005,,LAMINA,  0.
.005,,LAMINA,+45.
.005,,LAMINA,-45.
.005,,LAMINA, 90.
.005,,LAMINA, 90.
.005,,LAMINA,+45.
.005,,LAMINA,-45.
.005,,LAMINA,  0.
**defined 90 degrees rotated
*MATERIAL,NAME=LAMINA
*ELASTIC,TYPE=LAMINA
21.5E6, 1.46E6, 0.3, 0.81E6, 0.46E6, 0.46E6
*DENSITY
 0.0001417
*MATERIAL,NAME=HDA
*ELASTIC,TYPE=ISOTROPIC
100000,0.3
*DENSITY
 0.000003
*BOUNDARY
CLAMPED, ENCASTRE
*AMPLITUDE,NAME=HANNING,INPUT=waveform3.inp,DEFINITION=TABULAR,TIME=TOTAL
TIME,VALUE=RELATIVE
*STEP,INC=500
*DYNAMIC,DIRECT,NOHAF
1E-6,0.5E-3
*CLOAD,AMPLITUDE=HANNING
EDGE1,5,1
CORRECT1,5,-0.5
EDGE2,5,-1
CORRECT2,5,0.5
*NODE PRINT,FREQUENCY=500
U3
*EL PRINT, FREQUENCY=0
*PRINT,FREQUENCY=500
*END STEP
**-------
```

```
*HEADING
High Density Al Beam w/Delam for Lamb wave
*NODE
1,0,0,0
21,0,2,0
211,1,0,0
231,1,2,0
946,4.5,0,0
966,4.5,2,0
1156,5.5,0,0
1176,5.5,2,0
2101,10,0,0
2121,10,2,0
*NGEN, NSET=N1
1,21,1
*NGEN,NSET=N2
211,231,1
*NGEN,NSET=N3
946, 966, 1
*NGEN,NSET=N4
1156, 1176, 1
*NGEN,NSET=N5
2101, 2121, 1
*NFILL,NSET=CLAMPED
N1, N2, 10, 21
*NFILL,NSET=BOTTOM
N2, N3, 35, 21
*NFILL,NSET=DELAM
N3, N4, 10, 21
*NFILL,NSET=TOP
N4, N5, 45, 21
*NSET,NSET=UNDAMAGED
BOTTOM,TOP,CLAMPED
*NCOPY,OLD SET=UNDAMAGED, CHANGE NUMBER=10000, NEW SET=UNDAMAGED2, SHIFT
0,0,0.0
0,0,0,1,0,0,0
*NCOPY,OLD SET=DELAM ,CHANGE NUMBER=10000 ,NEW SET=DELAM2 ,SHIFT
0,0,0.0
0,0,0,1,0,0,0
*MPC
TIE,UNDAMAGED2,UNDAMAGED
*ELEMENT,TYPE=S9R5
1,1,43,45,3,22,44,24,2,23
10001,10001,10043,10045,10003,10022,10044,10024,10002,10023
*ELGEN,ELSET=SPECIMEN1
1,10,2,1,50,42,10
*ELGEN,ELSET=SPECIMEN2
10001,10,2,1,50,42,10
*NSET, NSET=EDGE1,GENERATE
232,294,1
*NSET, NSET=EDGE2,GENERATE
295,357,1
*NSET, NSET=CORRECT1,GENERATE
232,274,21
252,294,21
*NSET, NSET=CORRECT2,GENERATE
```

```
295,337,21
315,357,21
*SHELL SECTION,OFFSET=SNEG,ELSET=SPECIMEN1,COMPOSITE
.005,,LAMINA,  0.
.005,,LAMINA,+45.
.005,,LAMINA,-45.
.005,,LAMINA, 90.
.005,,LAMINA, 90.
.005,,LAMINA,+45.
.005,,LAMINA,-45.
.005,,LAMINA,  0.
*SHELL SECTION,OFFSET=SPOS,ELSET=SPECIMEN2,COMPOSITE
.75,,HDA, 90.
.005,,LAMINA,  0.
.005,,LAMINA,+45.
.005,,LAMINA,-45.
.005,,LAMINA, 90.
.005,,LAMINA, 90.
.005,,LAMINA,+45.
.005,,LAMINA,-45.
.005,,LAMINA,  0.
**defined 90 degrees rotated
*MATERIAL,NAME=LAMINA
*ELASTIC,TYPE=LAMINA
21.5E6, 1.46E6, 0.3, 0.81E6, 0.46E6, 0.46E6
*DENSITY
 0.0001417
*MATERIAL,NAME=HDA
*ELASTIC,TYPE=ISOTROPIC
100000,0.3
*DENSITY
 0.000003
*BOUNDARY
CLAMPED, ENCASTRE
*AMPLITUDE,NAME=HANNING,INPUT=waveform3.inp,DEFINITION=TABULAR,TIME=TOTAL
TIME,VALUE=RELATIVE
*STEP,INC=500
*DYNAMIC,DIRECT,NOHAF
1E-6,0.25E-3
*CLOAD,AMPLITUDE=HANNING
EDGE1,5,1
CORRECT1,5,-0.5
EDGE2,5,-1
CORRECT2,5,0.5
*NODE PRINT,FREQUENCY=250
U3
*EL PRINT, FREQUENCY=0
*PRINT,FREQUENCY=250
*END STEP
**-------
```

```
*HEADING
Plate with Composite Stiffener (2 Layers) for Lamb wave
*NODE
1,0,0,0
101,0,10,0
4546,4.5,0,0
4646,4.5,10,0
5556,5.5,0,0
5656,5.5,10,0
10101,10,0,0
10201,10,10,0
*NGEN, NSET=N1
1,101,1
*NGEN,NSET=N3
4546, 4646, 1
*NGEN,NSET=N4
5556, 5656, 1
*NGEN,NSET=N5
10101, 10201, 1
*NFILL,NSET=BOTTOM
N1, N3, 45, 101
*NFILL,NSET=DELAM
N3, N4, 10, 101
*NFILL,NSET=TOP
N4, N5, 45, 101
*ELEMENT,TYPE=S9R5
1,1,203,205,3,102,204,104,2,103
*ELGEN,ELSET=SPECIMEN
1,50,2,1,50,202,50
*ELSET,ELSET=NORMAL,GENERATE
1,1250,1
1501,2500,1
*ELSET,ELSET=STIFFEN,GENERATE
1251,1500,1
*NSET, NSET=EDGE1
49,50,51
*NSET, NSET=EDGE2
554,555,556
*ELSET,ELSET=SPECIMEN
NORMAL,STIFFEN
*NCOPY, OLD SET=DELAM, CHANGE NUMBER=20000, NEW SET=DELAM2, SHIFT
0,0,0.0
0,0,0,1,0,0
*ELEMENT,TYPE=S9R5
21251,24546,24748,24750,24548,24647,24749,24649,24547,24648
*ELGEN,ELSET=STIFFEN2
21251,50,2,1,5,202,50
*NSET,NSET=DELAM_BL,GENERATE
4546,4590,1
4647,4691,1
4748,4792,1
4849,4893,1
4950,4994,1
5051,5095,1
5152,5196,1
5253,5297,1
```

5354,5398,1
5455,5499,1
5556,5600,1
*NSET,NSET=DELAM_BM,GENERATE
4591,4601,1
4692,4702,1
4793,4803,1
4894,4904,1
4995,5005,1
5096,5106,1
5197,5207,1
5298,5308,1
5399,5409,1
5500,5510,1
5601,5611,1
*NSET,NSET=DELAM_BR,GENERATE
4602,4646,1
4703,4747,1
4804,4848,1
4905,4949,1
5006,5050,1
5107,5151,1
5208,5252,1
5309,5353,1
5410,5454,1
5511,5555,1
5612,5656,1
*NSET,NSET=DELAM_TL,GENERATE
24546,24590,1
24647,24691,1
24748,24792,1
24849,24893,1
24950,24994,1
25051,25095,1
25152,25196,1
25253,25297,1
25354,25398,1
25455,25499,1
25556,25600,1
*NSET,NSET=DELAM_TM,GENERATE
24591,24601,1
24692,24702,1
24793,24803,1
24894,24904,1
24995,25005,1
25096,25106,1
25197,25207,1
25298,25308,1
25399,25409,1
25500,25510,1
25601,25611,1
*NSET,NSET=DELAM_TR,GENERATE
24602,24646,1
24703,24747,1
24804,24848,1
24905,24949,1

```
25006,25050,1
25107,25151,1
25208,25252,1
25309,25353,1
25410,25454,1
25511,25555,1
25612,25656,1
*MPC
TIE,DELAM_TL,DELAM_BL
TIE,DELAM_TR,DELAM_BR
TIE,DELAM_TM,DELAM_BM
*SHELL SECTION,ELSET=SPECIMEN,COMPOSITE
.005,,LAMINA,  0.
.005,,LAMINA,+45.
.005,,LAMINA,-45.
.005,,LAMINA, 90.
.005,,LAMINA, 90.
.005,,LAMINA,-45.
.005,,LAMINA,+45.
.005,,LAMINA,  0.
**defined 90 degrees rotated
*MATERIAL,NAME=LAMINA
*ELASTIC,TYPE=LAMINA
21.5E6, 1.46E6, 0.3, 0.81E6, 0.46E6, 0.46E6
*DENSITY
 0.0001417
*SHELL SECTION,ELSET=STIFFEN2,COMPOSITE,OFFSET=SNEG
.005,,LAMINA,  0.
.005,,LAMINA,+45.
.005,,LAMINA,-45.
.005,,LAMINA, 90.
.005,,LAMINA, 90.
.005,,LAMINA,+45.
.005,,LAMINA,-45.
.005,,LAMINA,  0.
.005,,LAMINA,  0.
.005,,LAMINA,+45.
.005,,LAMINA,-45.
.005,,LAMINA, 90.
.005,,LAMINA, 90.
.005,,LAMINA,+45.
.005,,LAMINA,-45.
.005,,LAMINA,  0.
**defined 90 degrees rotated
*AMPLITUDE,NAME=HANNING,INPUT=waveform2.inp,DEFINITION=TABULAR,TIME=TOTAL
TIME,VALUE=RELATIVE
*STEP,INC=500
*DYNAMIC,DIRECT,NOHAF
1E-6,0.5E-3
*CLOAD,AMPLITUDE=HANNING
EDGE1,5,1
EDGE2,5,-1
*NODE PRINT,FREQUENCY=500
U3
*PRINT,FREQUENCY=500
*END STEP
```

```
*HEADING
Plate with Composite Stiffener (Delam) for Lamb wave
*NODE
1,0,0,0
101,0,10,0
4546,4.5,0,0
4646,4.5,10,0
5556,5.5,0,0
5656,5.5,10,0
10101,10,0,0
10201,10,10,0
*NGEN, NSET=N1
1,101,1
*NGEN,NSET=N3
4546, 4646, 1
*NGEN,NSET=N4
5556, 5656, 1
*NGEN,NSET=N5
10101, 10201, 1
*NFILL,NSET=BOTTOM
N1, N3, 45, 101
*NFILL,NSET=DELAM
N3, N4, 10, 101
*NFILL,NSET=TOP
N4, N5, 45, 101
*ELEMENT,TYPE=S9R5
1,1,203,205,3,102,204,104,2,103
*ELGEN,ELSET=SPECIMEN
1,50,2,1,50,202,50
*ELSET,ELSET=NORMAL,GENERATE
1,1250,1
1501,2500,1
*ELSET,ELSET=STIFFEN,GENERATE
1251,1500,1
*NSET, NSET=EDGE1
49,50,51
*NSET, NSET=EDGE2
554,555,556
*ELSET,ELSET=SPECIMEN
NORMAL,STIFFEN
*NCOPY, OLD SET=DELAM, CHANGE NUMBER=20000, NEW SET=DELAM2, SHIFT
0,0,0.0
0,0,0,1,0,0
*ELEMENT,TYPE=S9R5
21251,24546,24748,24750,24548,24647,24749,24649,24547,24648
*ELGEN,ELSET=STIFFEN2
21251,50,2,1,5,202,50
*NSET,NSET=DELAM_BL,GENERATE
4546,4590,1
4647,4691,1
4748,4792,1
4849,4893,1
4950,4994,1
5051,5095,1
5152,5196,1
5253,5297,1
```

```
5354,5398,1
5455,5499,1
5556,5600,1
*NSET,NSET=DELAM_BM,GENERATE
4591,4601,1
4692,4702,1
4793,4803,1
4894,4904,1
4995,5005,1
5096,5106,1
5197,5207,1
5298,5308,1
5399,5409,1
5500,5510,1
5601,5611,1
*NSET,NSET=DELAM_BR,GENERATE
4602,4646,1
4703,4747,1
4804,4848,1
4905,4949,1
5006,5050,1
5107,5151,1
5208,5252,1
5309,5353,1
5410,5454,1
5511,5555,1
5612,5656,1
*NSET,NSET=DELAM_TL,GENERATE
24546,24590,1
24647,24691,1
24748,24792,1
24849,24893,1
24950,24994,1
25051,25095,1
25152,25196,1
25253,25297,1
25354,25398,1
25455,25499,1
25556,25600,1
*NSET,NSET=DELAM_TM,GENERATE
24591,24601,1
24692,24702,1
24793,24803,1
24894,24904,1
24995,25005,1
25096,25106,1
25197,25207,1
25298,25308,1
25399,25409,1
25500,25510,1
25601,25611,1
*NSET,NSET=DELAM_TR,GENERATE
24602,24646,1
24703,24747,1
24804,24848,1
24905,24949,1
```

```
25006,25050,1
25107,25151,1
25208,25252,1
25309,25353,1
25410,25454,1
25511,25555,1
25612,25656,1
*MPC
TIE,DELAM_TL,DELAM_BL
TIE,DELAM_TR,DELAM_BR
*SHELL SECTION,ELSET=SPECIMEN,COMPOSITE
.005,,LAMINA,  0.
.005,,LAMINA,+45.
.005,,LAMINA,-45.
.005,,LAMINA, 90.
.005,,LAMINA, 90.
.005,,LAMINA,-45.
.005,,LAMINA,+45.
.005,,LAMINA,  0.
**defined 90 degrees rotated
*MATERIAL,NAME=LAMINA
*ELASTIC,TYPE=LAMINA
21.5E6, 1.46E6, 0.3, 0.81E6, 0.46E6, 0.46E6
*DENSITY
 0.0001417
*SHELL SECTION,ELSET=STIFFEN2,COMPOSITE,OFFSET=SNEG
.005,,LAMINA,  0.
.005,,LAMINA,+45.
.005,,LAMINA,-45.
.005,,LAMINA, 90.
.005,,LAMINA, 90.
.005,,LAMINA,+45.
.005,,LAMINA,-45.
.005,,LAMINA,  0.
.005,,LAMINA,  0.
.005,,LAMINA,+45.
.005,,LAMINA,-45.
.005,,LAMINA, 90.
.005,,LAMINA, 90.
.005,,LAMINA,+45.
.005,,LAMINA,-45.
.005,,LAMINA,  0.
**defined 90 degrees rotated
*AMPLITUDE,NAME=HANNING,INPUT=waveform2.inp,DEFINITION=TABULAR,TIME=TOTAL
TIME,VALUE=RELATIVE
*STEP,INC=500
*DYNAMIC,DIRECT,NOHAF
1E-6,0.5E-3
*CLOAD,AMPLITUDE=HANNING
EDGE1,5,1
EDGE2,5,-1
*NODE PRINT,FREQUENCY=500
U3
*PRINT,FREQUENCY=500
*END STEP
**-------
```

```
*HEADING
Tube without damage for Lamb wave
*NODE, SYSTEM=C
1,10,60,0
101,10,120,0
10101,10,60,10
10201,10,1200,10
100000,0,0,0
100001,0,0,10
*NGEN,LINE=C,SYSTEM=C,NSET=N1
1,101,1,100000
*NGEN,LINE=C,SYSTEM=C,NSET=N2
10101,10201,1,100001
*NFILL,NSET=ALL
N1,N2,100,101
*ELEMENT,TYPE=S9R5
1,1,203,205,3,102,204,104,2,103
*ELGEN,ELSET=SPECIMEN
1,50,2,1,50,202,50
*ELSET,ELSET=NORMAL,GENERATE
1,1250,1
1501,2500,1
*ELSET,ELSET=SIDES,GENERATE
1251,1274,1
1301,1324,1
1351,1374,1
1401,1424,1
1451,1474,1
1277,1300,1
1327,1350,1
1377,4000,1
1427,1450,1
1477,1500,1
*ELSET,ELSET=DAMAGE,GENERATE
1275,1475,50
1276,1476,50
*NSET, NSET=EDGE1
49,50,51
*NSET, NSET=EDGE2
554,555,556
*ELSET,ELSET=LAMINATE
NORMAL,SIDES,DAMAGE
*SHELL GENERAL SECTION,ELSET=LAMINATE,COMPOSITE,ORIENTATION=SECORI
.005,,LAMINA,  0.
.005,,LAMINA,+47.
.005,,LAMINA,-47.
.005,,LAMINA,  0.
.5,,LDA,0.
.5,,LDA,0.
.005,,LAMINA,  0.
.005,,LAMINA,+47.
.005,,LAMINA,-47.
.005,,LAMINA,  0.
*ORIENTATION,SYSTEM=CYLINDRICAL,NAME=SECORI
0.,0.,0., 0.,0., 1.
1, 0.
```

```
*MATERIAL,NAME=LAMINA
*ELASTIC,TYPE=LAMINA
21.5E6, 1.46E6, 0.3, 0.81E6, 0.46E6, 0.46E6
*DENSITY
 0.0001417
*MATERIAL,NAME=LDA
*ELASTIC,TYPE=ISOTROPIC
1000,0.3
*DENSITY
 0.0000015
*AMPLITUDE,NAME=HANNING,INPUT=waveform3.inp,DEFINITION=TABULAR,TIME=TOTAL
TIME,VALUE=RELATIVE
*STEP,INC=500
*DYNAMIC,DIRECT,NOHAF
1E-6,0.1E-3
*CLOAD,AMPLITUDE=HANNING
EDGE1,5,1
EDGE2,5,-1
*NODE PRINT,FREQUENCY=100
U3
*EL PRINT, FREQUENCY=0
*PRINT,FREQUENCY=100
*END STEP
**-------
```

```
*HEADING
Tube with damage for Lamb wave
*NODE, SYSTEM=C
1,10,60,0
101,10,120,0
10101,10,60,10
10201,10,120,10
100000,0,0,0
100001,0,0,10
*NGEN,LINE=C,SYSTEM=C,NSET=N1
1,101,1,100000
*NGEN,LINE=C,SYSTEM=C,NSET=N2
10101,10201,1,100001
*NFILL,NSET=ALL
N1,N2,100,101
*ELEMENT,TYPE=S9R5
1,1,203,205,3,102,204,104,2,103
*ELGEN,ELSET=SPECIMEN
1,50,2,1,50,202,50
*ELSET,ELSET=NORMAL,GENERATE
1,1250,1
1501,2500,1
*ELSET,ELSET=SIDES,GENERATE
1251,1274,1
1301,1324,1
1351,1374,1
1401,1424,1
1451,1474,1
1277,1300,1
1327,1350,1
1377,4000,1
1427,1450,1
1477,1500,1
*ELSET,ELSET=DAMAGE,GENERATE
1275,1475,50
1276,1476,50
*NSET, NSET=EDGE1
49,50,51
*NSET, NSET=EDGE2
554,555,556
*ELSET,ELSET=LAMINATE
NORMAL,SIDES
*SHELL GENERAL SECTION,ELSET=LAMINATE,COMPOSITE,ORIENTATION=SECORI
.005,,LAMINA,  0.
.005,,LAMINA,+47.
.005,,LAMINA,-47.
.005,,LAMINA,  0.
.5,,LDA,0.
.5,,LDA,0.
.005,,LAMINA,  0.
.005,,LAMINA,+47.
.005,,LAMINA,-47.
.005,,LAMINA,  0.
*SHELL GENERAL SECTION,ELSET=DAMAGE,COMPOSITE,ORIENTATION=SECORI
.005,,LAMINA, 90.
.005,,LAMINA,+47.
```

```
.005,,LAMINA,-47.
.005,,LAMINA, 90.
.5,,LDA,0.
.5,,LDA,0.
.005,,LAMINA,  0.
.005,,LAMINA,+47.
.005,,LAMINA,-47.
.005,,LAMINA,  0.
*ORIENTATION,SYSTEM=CYLINDRICAL,NAME=SECORI
0.,0.,0., 0.,0., 1.
1, 0.
*MATERIAL,NAME=LA MINA
*ELASTIC,TYPE=LAMINA
21.5E6, 1.46E6, 0.3, 0.81E6, 0.46E6, 0.46E6
*DENSITY
 0.0001417
*MATERIAL,NAME=LDA
*ELASTIC,TYPE=ISOTROPIC
1000,0.3
*DENSITY
 0.0000015
*AMPLITUDE,NAME=HANNING,INPUT=waveform3.inp,DEFINITION=TABULAR,TIME=TOTAL
TIME,VALUE=RELATIVE
*STEP,INC=500
*DYNAMIC,DIRECT,NOHAF
1E-6,0.1E-3
*CLOAD,AMPLITUDE=HANNING
EDGE1,5,1
EDGE2,5,-1
*NODE PRINT,FREQUENCY=100
U3
*EL PRINT, FREQUENCY=0
*PRINT,FREQUENCY=100
*END STEP
**-------
```

**waveform2.inp

0,0,0.000001,-1.73543E-05,0.000002,-0.000138186,0.000003,-0.000462743
0.000004,-0.001084883,0.000005,-0.002089044,0.000006,-0.003547406,0.000007,-0.005517317
0.000008,-0.008039016,0.000009,-0.011133725,0.00001,-0.014802145,0.000011,-0.019023382
0.000012,-0.023754348,0.000013,-0.028929646,0.000014,-0.034461957,0.000015,-0.040242921
0.000016,-0.046144516,0.000017,-0.052020915,0.000018,-0.057710789,0.000019,-0.063040035
0.00002,-0.067824875,0.000021,-0.071875286,0.000022,-0.074998694,0.000023,-0.077003888
0.000024,-0.077705064,0.000025,-0.076925951,0.000026,-0.074503925,0.000027,-0.07029406
0.000028,-0.064173012,0.000029,-0.056042691,0.00003,-0.045833629,0.000031,-0.033507986
0.000032,-0.019062124,0.000033,-0.002528702,0.000034,0.016021779,0.000035,0.036479995
0.000036,0.058697448,0.000037,0.082486747,0.000038,0.107622546,0.000039,0.133843147
0.00004,0.160852752,0.000041,0.188324361,0.000042,0.215903278,0.000043,0.243211198
0.000044,0.269850821,0.000045,0.295410938,0.000046,0.319471929,0.000047,0.341611591
0.000048,0.361411231,0.000049,0.378461921,0.00005,0.392370839,0.000051,0.402767598
0.000052,0.409310466,0.000053,0.411692388,0.000054,0.409646704,0.000055,0.402952491
0.000056,0.39143941,0.000057,0.374992011,0.000058,0.353553391,0.000059,0.327128145
0.00006,0.29578456,0.000061,0.259655985,0.000062,0.218941346,0.000063,0.173904785
0.000064,0.124874394,0.000065,0.072240042,0.000066,0.016450326,0.000067,-0.04199137
0.000068,-0.102531633,0.000069,-0.164572577,0.00007,-0.227478127,0.000071,-0.290580957
0.000072,-0.353190005,0.000073,-0.414598487,0.000074,-0.47409228,0.000075,-0.530958609
0.000076,-0.584494889,0.000077,-0.634017639,0.000078,-0.67887133,0.000079,-0.718437052
0.00008,-0.752140893,0.000081,-0.7794619,0.000082,-0.799939525,0.000083,-0.813180439
0.000084,-0.818864618,0.000085,-0.81675062,0.000086,-0.806679957,0.000087,-0.788580507
0.000088,-0.762468903,0.000089,-0.728451848,0.00009,-0.686726344,0.000091,-0.637578796
0.000092,-0.581383008,0.000093,-0.518597076,0.000094,-0.4497592,0.000095,-0.375482468
0.000096,-0.296448669,0.000097,-0.213401186,0.000098,-0.127137076,0.000099,-0.038498407
0.0001,0.051637026,0.000101,0.142365504,0.000102,0.232767587,0.000103,0.321918585
0.000104,0.40889917,0.000105,0.492805999,0.000106,0.572762211,0.000107,0.647927667
0.000108,0.717508806,0.000109,0.780767988,0.00011,0.837032206,0.000111,0.885701056
0.000112,0.926253869,0.000113,0.958255905,0.000114,0.981363528,0.000115,0.995328311
0.000116,1,0.000117,0.995328311,0.000118,0.981363528,0.000119,0.958255905
0.00012,0.926253869,0.000121,0.885701056,0.000122,0.837032206,0.000123,0.780767988
0.000124,0.717508806,0.000125,0.647927667,0.000126,0.572762211,0.000127,0.492805999
0.000128,0.40889917,0.000129,0.321918585,0.00013,0.232767587,0.000131,0.142365504
0.000132,0.051637026,0.000133,-0.038498407,0.000134,-0.127137076,0.000135,-0.213401186
0.000136,-0.296448669,0.000137,-0.375482468,0.000138,-0.4497592,0.000139,-0.518597076
0.00014,-0.581383008,0.000141,-0.637578796,0.000142,-0.686726344,0.000143,-0.728451848
0.000144,-0.762468903,0.000145,-0.788580507,0.000146,-0.806679957,0.000147,-0.81675062
0.000148,-0.818864618,0.000149,-0.813180439,0.00015,-0.799939525,0.000151,-0.7794619
0.000152,-0.752140893,0.000153,-0.718437052,0.000154,-0.67887133,0.000155,-0.634017639
0.000156,-0.584494889,0.000157,-0.530958609,0.000158,-0.47409228,0.000159,-0.414598487
0.00016,-0.353190005,0.000161,-0.290580957,0.000162,-0.227478127,0.000163,-0.164572577
0.000164,-0.102531633,0.000165,-0.04199137,0.000166,0.016450326,0.000167,0.072240042
0.000168,0.124874394,0.000169,0.173904785,0.00017,0.218941346,0.000171,0.259655985
0.000172,0.29578456,0.000173,0.327128145,0.000174,0.353553391,0.000175,0.374992011
0.000176,0.39143941,0.000177,0.402952491,0.000178,0.409646704,0.000179,0.411692388
0.00018,0.409310466,0.000181,0.402767598,0.000182,0.392370839,0.000183,0.378461921
0.000184,0.361411231,0.000185,0.341611591,0.000186,0.319471929,0.000187,0.295410938
0.000188,0.269850821,0.000189,0.243211198,0.00019,0.215903278,0.000191,0.188324361
0.000192,0.160852752,0.000193,0.133843147,0.000194,0.107622546,0.000195,0.082486747
0.000196,0.058697448,0.000197,0.036479995,0.000198,0.016021779,0.000199,-0.002528702
0.0002,-0.019062124,0.000201,-0.033507986,0.000202,-0.045833629,0.000203,-0.056042691
0.000204,-0.064173012,0.000205,-0.07029406,0.000206,-0.074503925,0.000207,-0.076925951
0.000208,-0.077705064,0.000209,-0.077003888,0.00021,-0.074998694,0.000211,-0.071875286
0.000212,-0.067824875,0.000213,-0.063040035,0.000214,-0.057710789,0.000215,-0.052020915

0.000216,-0.046144516,0.000217,-0.040242921,0.000218,-0.034461957,0.000219,-0.028929646
0.00022,-0.023754348,0.000221,-0.019023382,0.000222,-0.014802145,0.000223,-0.011133725
0.000224,-0.008039016,0.000225,-0.005517317,0.000226,-0.003547406,0.000227,-0.002089044
0.000228,-0.001084883,0.000229,-0.000462743,0.00023,-0.000138186,0.000231,-1.73543E-05
0.000232,0

**waveform3.inp

0,0,1.00E-06,-0.000649117,0.000002,-0.0049212,0.000003,-0.01514773
0.000004,-0.031377012,0.000005,-0.050922949,0.000006,-0.068587453,0.000007,-0.077553522
0.000008,-0.070806382,0.000009,-0.042823068,0.00001,0.008801004,0.000011,0.08213177
0.000012,0.170373223,0.000013,0.262221889,0.000014,0.343129972,0.000015,0.39734353
0.000016,0.41043122,0.000017,0.371909312,0.000018,0.277520806,0.000019,0.130751752
0.00002,-0.056734615,0.000021,-0.265908746,0.000022,-0.472401373,0.000023,-0.649519053
0.000024,-0.771851307,0.000025,-0.818956919,0.000026,-0.778578036,0.000027,-0.648876837
0.000028,-0.439316056,0.000029,-0.169994099,0.00003,0.130530119,0.000031,0.428662135
0.000032,0.689994866,0.000033,0.883750313,0.000034,0.986818058,0.000035,0.986818058
0.000036,0.883750313,0.000037,0.689994866,0.000038,0.428662135,0.000039,0.130530119
0.00004,-0.169994099,0.000041,-0.439316056,0.000042,-0.648876837,0.000043,-0.778578036
0.000044,-0.818956919,0.000045,-0.771851307,0.000046,-0.649519053,0.000047,-0.472401373
0.000048,-0.265908746,0.000049,-0.056734615,0.00005,0.130751752,0.000051,0.277520806
0.000052,0.371909312,0.000053,0.41043122,0.000054,0.39734353,0.000055,0.343129972
0.000056,0.262221889,0.000057,0.170373223,0.000058,0.08213177,0.000059,0.008801004
0.00006,-0.042823068,0.000061,-0.070806382,0.000062,-0.077553522,0.000063,-0.068587453
0.000064,-0.050922949,0.000065,-0.031377012,0.000066,-0.01514773,0.000067,-0.0049212
0.000068,-0.000649117,0.000069,0

APPENDIX D

MATLAB ä Code for Data Analysis by Wavelet Decomposition

```
% **Generic MATLAB code for wavelet analysis**%


% Open LabView data files and assign variables
clear
file1
filea=w;
file2
fileb=w;
file3
filec=w;
file4
filed=w;

% Perform wavelet decomposition with Morlet mother wavelet, ignore first 116 microseconds
f1= cwt(filea(116:600),1:1:64,'morl');
f2= cwt(fileb(116:600),1:1:64,'morl');
f3= cwt(filec(116:600),1:1:64,'morl');
f4= cwt(filed(116:600),1:1:64,'morl');

% Set first and last point to zero for energy plots
e=size(f1,2);
f1(32,1)=0;
f2(32,1)=0;
f3(32,1)=0;
f4(32,1)=0;
f1(32,e)=0;
f2(32,e)=0;
f3(32,e)=0;
f4(32,e)=0;

% Plotting setup
x1=1:1:600;
x2=116:1:600;
z=x2*0;

% Plots of voltage data
figure
title('Unfiltered Voltage Data of Ao Lamb Waves from PZT Sensors')
plot(x1,filea,'-', x1,fileb,'--',x1,filec,':',x1,filed,'*')
axis([0 600 -.01 .01])
ylabel('Volts (V)')
xlabel('Time (microseconds)')
```

```
% Plots of wavelet coefficient energy
figure
subplot(4,1,1)
fill(x2,abs(f1(32,:)'),z)
axis([116 600 0 .05])
ylabel('Dataset 1')
title('Wavelet Coefficient Magnitudes for 15 kHz Signal Content')
subplot(4,1,2)
fill(x2,abs(f2(32,:)'),z)
axis([116 600 0 .05])
ylabel(' Dataset 2')
subplot(4,1,3)
fill(x2,abs(f3(32,:)'),z)
axis([116 600 0 .05])
ylabel(' Dataset 3')
subplot(4,1,4)
fill(x2,abs(f4(32,:)'),z)
axis([116 600 0 .05])
ylabel(' Dataset 4')
xlabel('Time (microseconds)')
```

APPENDIX E

LabViewä Codes for Experimental Procedures

Arbitrary Function Generator VI

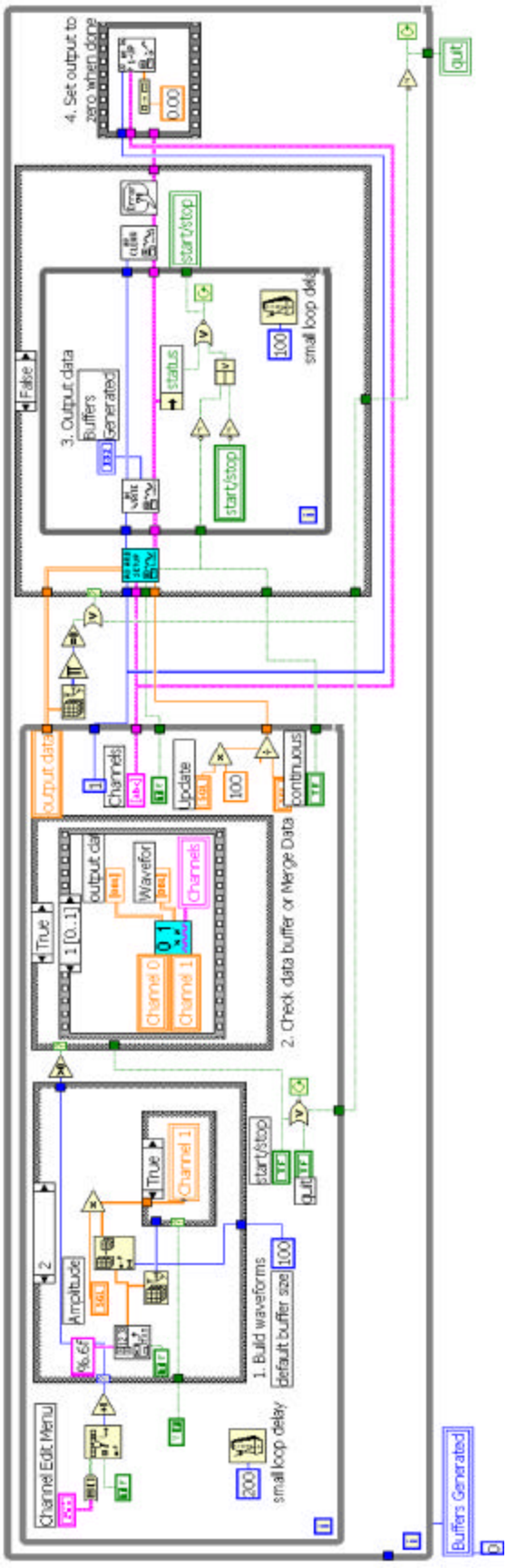

Lamb Wave Data Acquisition VI

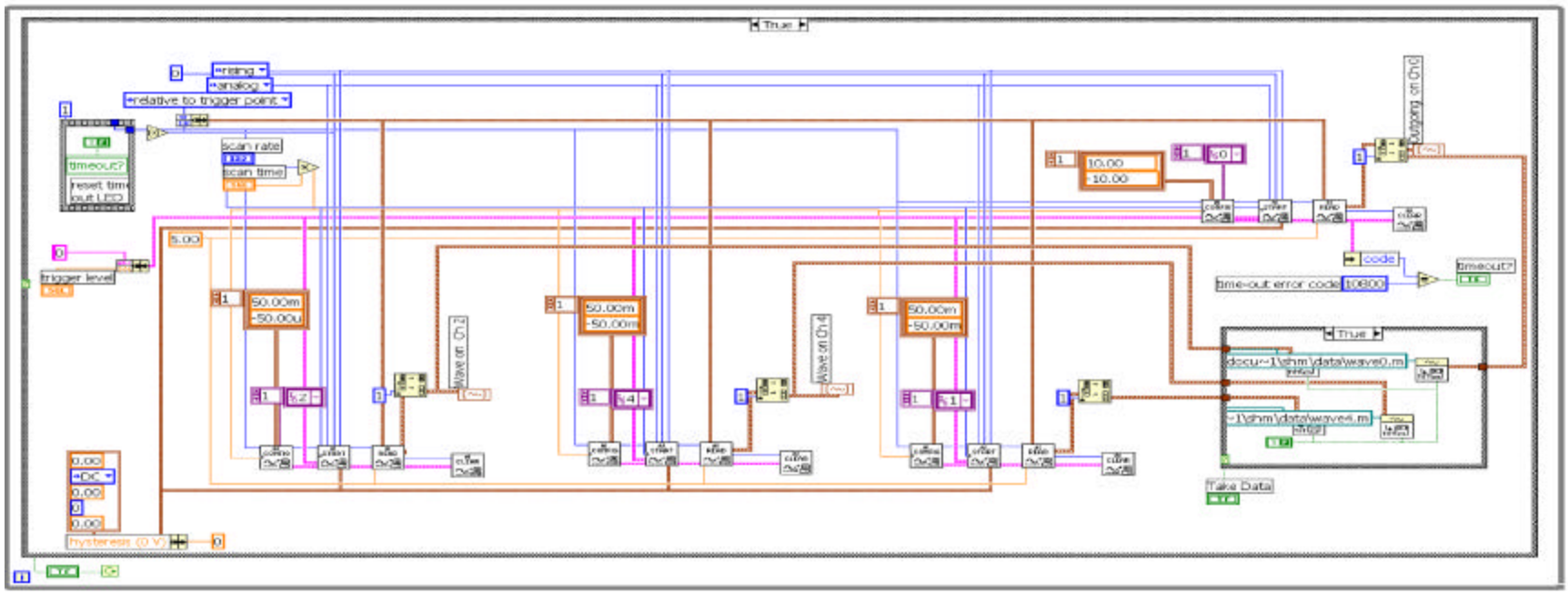

Acoustic Emission Pencil Break VI

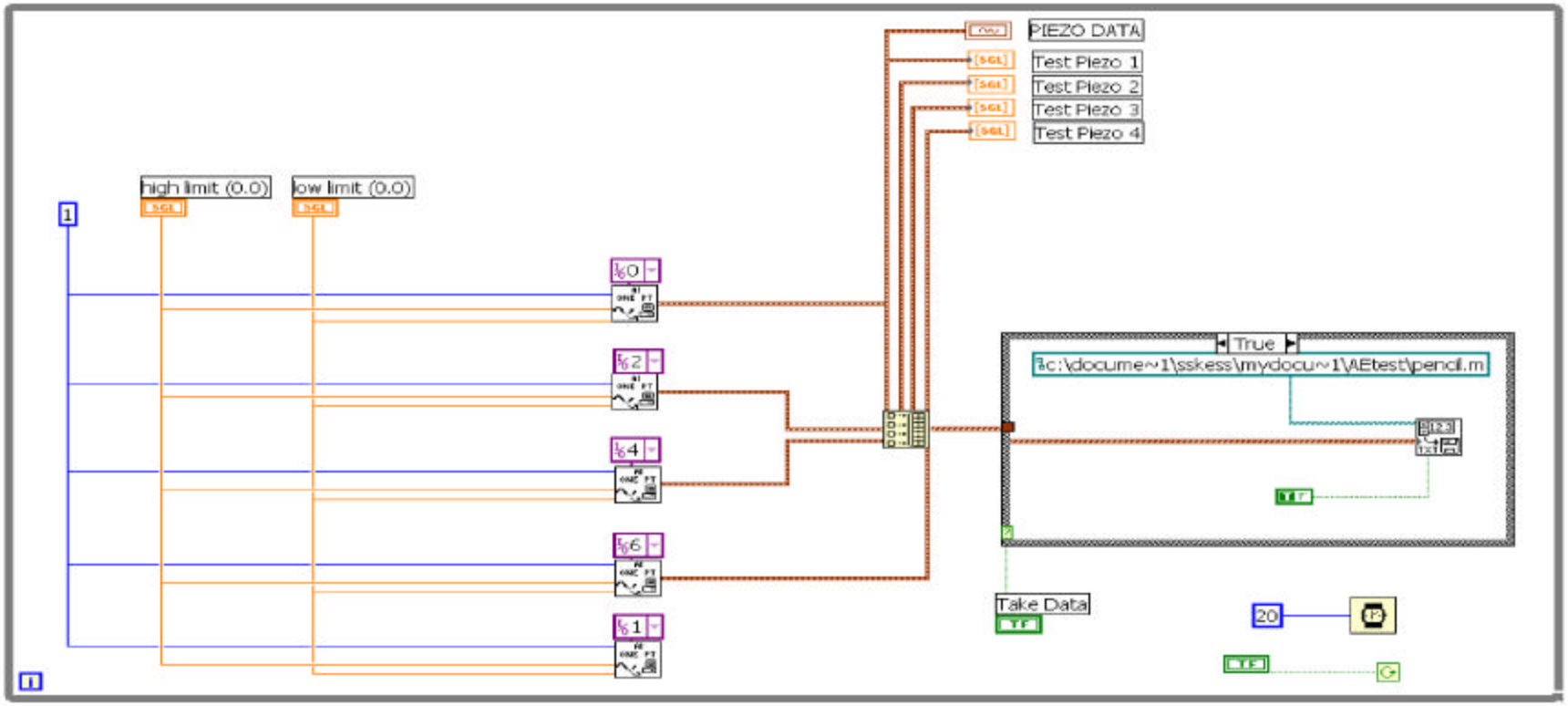

Narrow Coupon Tensile Test VI